Université de Montréal

Dynamiques hydrologiques d'un petit bassin versant arctique, rivière Niaqunguk, Iqaluit, Nunavut

Par Gabriel Chiasson-Poirier

Département de géographie
Faculté des arts et des sciences

Mémoire présenté
En vue de l'obtention du grade de maîtrise
en géographie

Mai 2019

Université de Montréal
Faculté des études supérieur et postdoctorales

Mémoire intitulé :

Dynamiques hydrologiques d'un petit bassin versant arctique, rivière Niaqunguk, Iqaluit, Nunavut

Par Gabriel Chiasson-Poirier

a été évalué par un jury composé de :

François Courchesne, président du jury
Jan Franssen, directeur de recherche
Daniel Fortier, membre du jury
Oliver Sonnentag, membre du jury

Résumé

Même si des avancées importantes ont été réalisées au cours des dernières années quant à la compréhension des dynamiques hydrologiques des environnements de pergélisol, un manque de connaissances limite toujours notre capacité à prédire précisément les impacts dynamiques hydrologiques des bassins versants Arctique. Ce mémoire se divise selon deux principales études effectuées respectivement à l'échelle d'une pente et à l'échelle du bassin versant de la rivière Niaqunguk, près d'Iqaluit, Nunavut, ont été réalisées. La première étude démontre que les dynamiques de drainage d'une pente sont intrinsèquement liées aux patrons de dégel de la couche active du pergélisol. Les connaissances développées à l'échelle de la pente ont été essentielles à la compréhension des dynamiques émergentes à l'échelle du bassin versant. Quatre périodes hydrologiques distinctes correspondant au début de la fonte des neiges, à la récession de la fonte, au débit de base et aux crues estivales ont été délimitées selon les caractéristiques physicochimiques de l'eau échantillonnée dans le bassin versant de la rivière Niaqunguk. Les principaux processus associés à ces périodes sont respectivement la contribution de la fonte des neiges, la distinction entre la contribution des neiges résiduelles et des lacs, les écoulements à travers la portion minérale de la couche active et les écoulements en surface à travers la microtopographie de la couche organique. Globalement, cette recherche propose des connaissances fondamentales qui sont essentielles à la compréhension des dynamiques hydrologiques en milieu de pergélisol. De plus, elle fournit des connaissances significatives pour une exploitation durable de la rivière comme source d'eau potable.

Mots-clés : Arctique, hydrologie, pergélisol, couche active, écoulements souterrains, lacs, écoulements de surface

Abstract

Despite recent advances in the hydrological knowledge of permafrost regions, precise predictions or modelling of hydrological dynamics in Arctic watersheds remains difficult. In this master thesis a combination of field measurements, chemistry and statistical analysis were conducted at the hillslope scale and at watershed scale within the Niaqunguk River catchment, to improve our understanding of the processes controlling the water delivery to rivers in permafrost landscape. The first study show that hillslope drainage dynamics were intrinsically linked to permafrost active layer thawing patterns. The microtopography of the surficial organic layer has a great influence on the distribution across the hillslope, by first enhancing the accumulation of water in surficial depressions, which in return enhance localized thaw and the accumulation of water in subsurface depressions. The second study conducted at the watershed scale allowed to delineated, based on the particularities of the water chemistry along the river network, four distinct periods, corresponding respectively to early snowmelt, snowmelt recession, baseflow and summer rainfall events. Since dominant hydrological processes within the watershed changed from one period to another, this period division is relevant the understand the behaviour of the river system. The primary processes associated with each of the four periods were: snowmelt contributions, the distinction between late lying snowpack melt and lake contributions, subsurface flows through mineral deposits and surface flows through the organic layer. Fundamental hydrological knowledge generated in this research will greatly help to improve our ability to predict the response of Arctic hydrological systems to climate changes, but is also indispensable for a sustainable management of a future exploitation of the Niaqunguk River as a potable water for the City of Iqaluit.

Keywords : Arctic, hydrology, active layer, subsurface flows, lakes, surface flows

Table des matières

Liste des tableaux

Liste des figures

Liste des sigles et abréviations

µS/cm	Microsiemens par centimètre (microsiemens per centimeter)
$^{0}/_{00}$	Pour mille (permille)
AEM	Cartes de vecteur de valeurs propres (asymmetric Eigenvector Maps)
ANOVA	Analyse de variance univariée (univariate analysis of variance)
AOV	Analyse de variance (analysis of variance)
asl	Au-dessus du niveau marin actuel (above sea level)
CRVE	Erreur par validation croisée (cross-validation error)
DA	Indice de superficie de drainage (drainage are index)
DD	Indice de densité de drainage (drainage density index)
DEM	Modèle d'élévation numérique (digital elevation model)
DOC	Carbone organique dissout (dissolved organic carbon)
Drift-SE	Indice d'accumulation de neige exposée au Sud (south-exposed drift areas index)
DTW	Indice de zone riveraine (depth-to-water or riparian area index)
EC	Conductivité électrique de l'eau (water electrical conductivity)
GMWL	Droite météorique globale (global meteoric water line)
GW1 - 4	Numérotation des piézomètres d'échantillonnage (groundwater sampling piezometers)
L/s	Débit d'eau en litre par seconde (discharge in liter per second)
LAKE	Indice de lac (proportion of lake areas index)
LMWL	Droite météorique locale (local meteoric water line)
m^3/s	Débit d'eau en mètre cube par seconde (discharge in meter cube per second)
mg L^{-1}	Milligramme par litre (milligrams per litre)
Mg^{2+}	Magnésium (magnesium)
MRT	Arbre de régression multivarié (multivariate regression tree)
PC	Composante principale (principal component)
PCA	Analyse en composante principale (principal component analysis)
PVC	PolyVinyl Chloride
R^2	Coefficient non ajusté de détermination (unadjusted coefficient of determination)
R^2_a	Coefficient ajusté de détermination (adjusted coefficient of determination)
RDA	Analyse de redondance (redundancy analysis)
SD	Écart-type (standard déviation)
SpC	Conductivité spécifique de l'eau (water specific conductance)
UCA	Indice de zone de drainage en amont (upslope contributing area index)
VSMOW	Eau océanique moyenne normalisée de Vienne (vienna standard mean ocean water)
WLAFT	Niveau d'eau au-dessus du plafond de gel (water level above frost table)
WLRGS	Niveau d'eau relatif à la surface du sol (water level relative to ground surface)
$\delta^{18}O$	Delta dix-huit oxygène ou ratio isotopique $^{18}O/^{16}O$ (stable oxygen isotopes)
δD	Delta deutérium ou ratio isotopique $^{2}H/^{1}H$ (stable deuterium isotopes)

Remerciements

Oufff. Ça fait assez bizarre d'être rendu à cette étape après trois années de maîtrise et quatre années à travailler sur ce projet. C'est la fin d'une grande aventure pour moi et d'une étape très importante de ma vie. Jamais je n'aurais cru qu'un jour j'allais m'impliquer autant dans un projet que je l'avais fait dans le sport par le passé. Je me trompais et ce mémoire en témoigne.

Cette aventure n'aurait toutefois jamais été possible sans mon directeur. Mes premiers remerciements vont donc à Jan. Quelle aventure! Merci d'avoir cru en moi, en ma passion, et ce, même si j'étais parfois un peu brouillon. Merci de m'avoir gardé une place pour ce beau projet même si je partais au loin en échange. Sans votre dévouement, je n'aurais probablement pas passé à travers toutes les embuches de ce projet. Merci d'avoir été disponible pour répondre à mes questions ou me rassurer, et ce, à toutes heures, en vacances et le dimanche matin. Je ne suis pas seulement devenu un meilleur étudiant ou chercheur à travers ce projet, je suis devenu une meilleure personne et vous y êtes pour beaucoup. Vous m'avez souvent offert la bière, dans les bons et les moments difficiles de cette aventure, j'espère qu'il y en aura d'autres, mais à partir de maintenant, la bière est sur moi, no kidding.

Un merci spécial à Daniel Fortier et à toute l'équipe du Géocryolab, vous m'avez transmis tôt au baccalauréat votre passion pour la géomorphologie et je ne suis pas certain que mon parcours se serait poursuivi jusqu'ici sans vous. Merci à François Girard, de m'avoir parlé dans le casque un jour dans le corridor et de m'avoir dit d'arrêter de niaiser, car tu pensais que j'avais beaucoup de potentiel, ça a certainement été un élément déclencheur pour moi. Pour son aide avec mes projets électroniques, mes analyses et pour son soutien moral, un énorme merci à Michel Sliger. Pour ces conseils, ces révisions et ces « toujours en forme, toujours content », un très grand merci à Christophoros Papas, j'espère qu'on courra d'autres marathons ensemble après la maîtrise, sas efcharisto. Merci au meilleur partner de bureau et de maîtrise, Antoine Prince, sans tes nombreux coups de main, la maîtrise aurait été beaucoup plus ardue.

Je dois aussi remercier mes parents, mais seulement parce que je suis obligé, sans blague, vous êtes incroyable. Merci à mon père pour ses très nombreux conseils et corrections de mes

textes. Merci à ma mère pour ses conseils philosophiques, dont je cherche toujours le sens, mais qui ont dû aider un peu. Merci aussi pour la journée de travail à coller des piézomètres, je ne sais pas si vous méritez une maîtrise aussi, mais certainement 3 crédits. Merci à Gaëlle et Karine, je suis conscient de tout le soutien que vous m'avez apporté durant cette aventure.

Ce mémoire ne reflète qu'une petite partie de tout le travail de terrain qui a été réalisé lors de trois campagnes de collecte de données dans le bassin versant de la rivière Niaqunguk. Je tiens donc à souligner le travail exceptionnel de Marc-Oliver Gaudreault, le meilleur assistant de terrain, en tout cas selon moi. Merci pour ton dévouement et ton soutien, j'espère que tu iras loin. Merci aussi à Keegan Smith, je me sens privilégié, d'avoir partagé des moments incroyables avec toi à Iqaluit. Merci aussi à Tommy Tremblay, Michael Bakaic, Anika Bychok, Hannah Boomer, Louis-Gabriel Pouliot, Gillian Thiel, Bridget Rusk et Jessica Peters, votre aide et vos conseils m'ont grandement marqué. Un immense merci aussi a Scott Lamoureux et Mélissa Lafrenière pour leur aide au cours de ce projet. Merci aussi à Naomie Short, de Ressources Naturelles Canada, de nous avoir permis d'accéder au modèle d'élévation numérique pour la région de bassin versant de la rivière Niaqunguk.

Chapitre 1 - Introduction générale

Bien qu'important dans les basses latitudes, le réchauffement climatique se répercute beaucoup plus durement sur la région Boréal-Arctique, comme en témoigne l'augmentation, de deux fois supérieure à celles du Sud, des températures de l'air en Arctique au cours des 30 dernières années (ACIA, 2013). Les impacts de cette hausse des températures sont particulièrement importants à l'égard du cycle hydrologique des régions arctiques. D'ailleurs, Bring et al. (2016) mentionnent que des changements importants aux dynamiques naturelles des écosystèmes d'eau douce de l'Arctique sont déjà en trait se produire ou se produiront dans un avenir rapproché. Ces changements toucheront différentes composantes du cycle de l'eau en Arctique. Une des composantes fortement impactée sera les précipitations, pour lesquelles une hausse de la quantité totale annuelle a été observée, ceci associé au constat que les précipitations sous forme liquide devraient augmenter par rapport aux précipitations sous forme neigeuse (Bintanja, 2018). Nous constatons aussi que les eaux stockées sous forme de neige ou de glace sont sujettes à une fonte accrue, alors qu'une fonte plus tôt au printemps, une durée réduite du couvert terrestre de neige et une diminution de la superficie de la couverture des glaces de mer sont attendues (Hinzman et al., 2013). Pour leur part, (Walvoord and Kurylyk, 2016) ont démontré que la couche active du pergélisol ou couche superficielle sujette au gel/dégel saisonnier a déjà et devrait continuer de s'approfondir. Bien qu'il ne soit pas directement associé au cycle hydrologique, l'approfondissement de la couche active permettra un plus grand stockage de l'eau et une augmentation potentielle des écoulements d'eau supra-pergélisol ou des dans la couche superficielle du sol, au-dessus du plafond de gel . Enfin, tous ces changements ont déjà mené à une augmentation des débits annuels et des débits de base des rivières Arctiques, une augmentation qui devrait aussi s'amplifier au cours des prochaines décennies (Déry, 2008; St. Jacques and Sauchyn, 2009). Même si d'importantes avancées ont été réalisées au cours des dernières années à l'égard de la compréhension des dynamiques hydrologiques en Arctique, il demeure que nous pouvons difficilement prédire et modéliser, avec précision, les impacts concrets des changements climatiques sur les processus hydrologiques des bassins versants Arctique.

En modifiant les dynamiques naturelles de toutes les grandes sphères environnementales (atmosphère, biosphère, hydrosphère, cryosphère) de l'Arctique, les changements climatiques ont plusieurs répercutions sur les pratiques traditionnelles des communautés de la région Boréal-Arctique (AMAP, 2013). Par exemple, la modification des débits des rivières entraine du même coup une modification des nutriments qu'elles transportent ou des habitats qu'elles offrent, qui peuvent ne plus corresponde aux besoins de poissons traditionnellement pêchés par les communautés boréales-arctiques, comme l'ombre de l'Arctique. Des processus comme la fonte de la glace souterraine ou l'augmentation des profondeurs de dégel sont reliés au réchauffement du pergélisol conséquence des changements climatiques, ils amplifient les risques pour les infrastructures (routes, bâtiments) et augmente les coûts d'entretien que doivent débourser les communautés pour le maintien d'infrastructure sécuritaire (de Grandpré et al., 2012). En plus des impacts liés aux changements climatiques, la ville d'Iqaluit, capital du Nunavut doit aussi faire face à un « boom » démographique, comme en témoigne le taux annuel d'accroissement de sa population de 3%, le plus élevé au Nunavut (*Iqaluit General Plan*, 2010). Cette augmentation de la population et l'insuffisance de leur source d'eau actuelle (lac Geraldine) ont amené les dirigeants de la ville à identifier la rivière Niaqunguk (communément nommée Apex) comme source supplémentaire d'eau potable (*Iqaluit Sustainable Community Plan*, 2014). Toutefois, cette rivière connait régulières des périodes d'étiage pour lesquelles le débit demeure considérablement bas (< 1 m^3/s) et ce, pour des périodes prolongées (plus d'un mois) (Water Office Canada, 2019). Ces périodes d'étiage reflètent la nécessité de développer une connaissance adéquate des dynamiques hydrologiques dans le bassin versant de la rivière Naqunguk, afin de déterminer si son exploitation est durable. La présente recherche s'inscrit d'ailleurs dans un projet multi-institutionnel, regroupant les universités de Queen's, Montréal, Guelph et Carleton, qui visent à identifier les sources en eau qui alimentent la rivière Niqunguk tout au long de sa saison de débit, ainsi que les impacts potentiels des changements climatiques sur l'hydrologie de cette rivière.

L'hydrologie en milieu périglaciaire se distingue d'abord des autres grandes régions morphogénétiques par l'influence du pergélisol ou couche du sol perpétuellement gelé sur les mouvements et stockage de l'eau dans la partie terrestre de son cycle (Woo, 2012). L'on considère généralement que le plafond de gel du pergélisol constitue une couche relativement

imperméable qui agit comme aquitar sur les eaux souterraines, de sorte que les écoulements et le stockages des eaux souterraines sont limités à la partie dégelée de la couche-active (Carey and Woo, 2005). Plusieurs études effectuées au cours de la deuxième moitié du dernier siècle ont permis d'améliorer de façon significative notre connaissance des dynamiques hydrologiques en milieux de pergélisol. Parmi celles-ci, l'étude pionnière de Woo et Steer (1983), qui à l'aide d'un réseau de piézomètres et de mesures de profondeur de la couche active effectuées sur deux pentes près de Resolute, au Nunavut, a déterminé que les profondeurs de dégel de la couche active n'évoluaient pas de manière uniforme durant l'été et que les patrons d'écoulement souterrains dans la couche dégelée du sol évoluaient en fonction de l'hétérogénéité du plafond de gel. Soulignons aussi la première étude isotopique réalisée en Arctique par Obradovic et Sklash (1986) dans le bassin de la rivière Niaqunguk, qui a suggéré qu'une proportion de 40 à 50% de l'hydrographe de crue printanière de la rivière était composée de « vieilles eaux » ou d'eaux stockées dans le bassin versant préalablement à l'évènement de pluie ou de fonte des neiges. Les données générées dans le deuxième article de ce mémoire suggèrent toutefois que cette proportion pourrait être gonflée par la contribution de l'eau stockée dans les lacs du bassin versants.

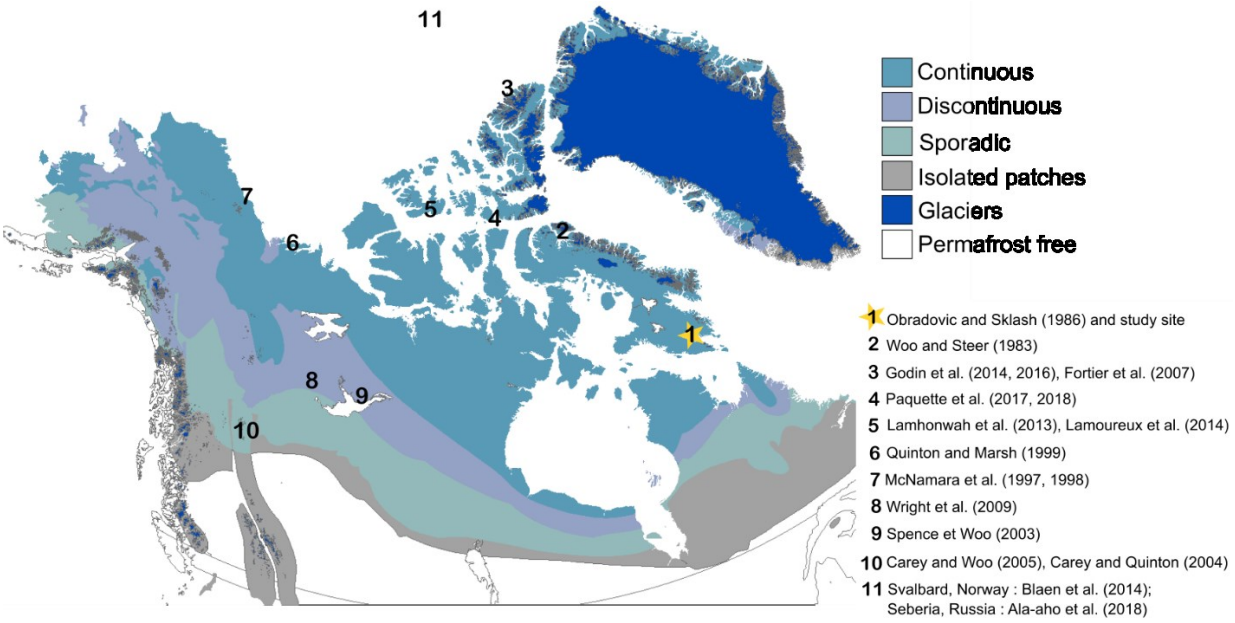

Figure I. Distribution du pergélisol en Amérique du nord et emplacement d'études portant sur diverses dynamiques hydrologiques en lien avec ce mémoire, modifié de Brown et al. (1997).

Depuis les années 80, plusieurs autres études utilisant des mesures terrain, des analyses géochimiques, mais aussi de nouvelles techniques comme la modélisation ou l'expérimentation en laboratoire ont contribué à nos connaissances sur les processus hydrologiques dans divers milieux pergélisolés (Figure I). Bien que ces différentes études aient été réalisées dans différents types d'environnements (ex : plaines, montagnes, plateaux, forêt boréale ou toundra), où l'entendu du pergélisol peut aussi varier (ex : continu, discontinu, sporadique et isolé), elles mettent toutefois de l'avant des concepts permettant de mieux comprendre les dynamiques hydrologiques des bassins versants de l'Arctique. Récemment, Wright et al. (2009) ont démontré, par modélisation que les écoulements souterrains dans la couche active du pergélisol étaient grandement influencés par les dépressions se formant dans le plafond de gel, et que les écoulements étaient dirigés vers les dépressions en période de déficit en saturation, tandis qu'en période de pluie les dépressions dans le plafond de gel débordaient pour générer du ruissèlement vers le bas de la pente. Ces observations renvoient au concept de « *fill-and-spill* » ou de remplissage-déversement développé décrit d'abord par Spence et Woo (2003), aujourd'hui communément utilisé pour expliquer le ruissèlement de surface sur les pentes des basses comme des hautes latitudes (Coles and McDonnell, 2018; Tromp-van Meerveld and McDonnell, 2006). Ce concept propose qu'en période plus sèche, les dépressions dans la couche délimitant les écoulements souterrains ou dans la microtopographie de surface favorisent le stockage de l'eau et limite la connectivité entre l'amont et l'aval, jusqu'à ce qu'un certain niveau de saturation soit atteint, ainsi lorsque la capacité maximale de stockage est atteinte, l'eau se déverse vers l'aval. En lien avec les observations faites par Wright et al. (2009), le concept de « *fill-and-spill* » pourrait donc être en partis applicables pour expliquer les dynamiques d'écoulement dans la couche active des environnements de pergélisol. Pour leur part, Quinton and Marsh, (1999) ont réalisé une conceptualisation du drainage typique des pentes de la grande zone écologique de la Toundra arctique, qui se base sur leur structure physique typique, composée d'une couche de matériel minéral plus fin (basse conductivité hydraulique) et d'une couverture de dépôt organique (haute conductivité hydraulique), démontrant ainsi que la quantité de ruissèlement généré sur ces pentes est liée à la position de la nappe d'eau supra-pergélisol relativement à ces deux couches. Carey and Woo (2001) ont nommé cette dynamique le « *two-layer flow system* » ou l'écoulement à deux vitesses, en fonction de la position de la nappe souterraine par rapport à

la couche minérale (écoulement lent) ou couche organique de surface (écoulement rapide). D'autres études, comme celles de Blaen et al., (2014), de Carey and Quinton (2004), de McNamara et al. (1997), ont établi que la proportion des vieilles eaux ou les eaux stockées dans le bassin versant préalablement à l'évènement de pluie ou de fonte des neige, contribuant à l'hydrographe de crue des rivières arctique, durant la période de fonte des neiges, était beaucoup moins importante que celle estimée par Obradovic et Sklash (1986). Toutefois, ces dernières études et d'autres (Ala-aho et al., 2018; Lamhonwah et al., 2017; Tetzlaff et al., 2015), ont démontré que la contribution des vieilles eaux ou des eaux stockés dans le bassin versant à l'hydrographe des rivières avait tendance à augmenter au cours de l'été arctique en raison, notamment, de l'augmentation de la profondeur de dégel de la couche active, ce qui qui augmente du même coup la capacité de stockage du sol.

Pour leur part, Bring et al. (2016), Walvoord et Kurylyk (2016), mentionnent qu'une augmentation de la capacité de stockage de l'eau dans le sol, qu'une modification de la connectivité entre les nappes d'eau souterraine supra-pergélisol et une augmentation de la contribution des eaux souterraines supra-pergélisol figurent parmi des modifications de dynamiques hydrologiques en milieux de pergélisol sont suggérées dans le contexte des changements climatiques. En favorisant la thermo-érosion, l'eau peut aussi agir comme accélérateur de l'érosion des paysages pergélisolés et bouleverser les dynamiques hydrologiques de certaines régions arctiques (Fortier et al., 2007; Godin et al., 2016, 2014). Des répercussions envisageables de ces ruptures d'équilibre sont une augmentation des taux d'érosion et des changements de flux hydrologiques et élémentaires vers les eaux de surface (Lamoureux et al., 2014; Wrona et al., 2016). Nous devons admettre que, malgré les avancées récentes des connaissances sur l'hydrologique Arctique, la projection des impacts des changements climatiques sur les dynamiques hydrologiques des rivières en milieu de pergélisol demeure limitées, en raison notamment d'un manque de connaissances sur les interactions entre les processus contrôlants d'écoulement à différentes échelles spatiales (ex : pente, tronçon, sous-bassin et bassin versant), ainsi que leurs liens avec les conditions d'humidité dans le bassin versant (Bring et al., 2016).

Trois nouveaux paradigmes ont été récemment proposés pour les études hydrologiques et la compréhension des dynamiques émergentes à l'échelle d'un bassin versant : (1) d'abord, au lieu de se concentrer sur la caractérisation de plus en plus poussée

des hétérogénéités du paysage (modèles calibrés à très fine résolution), il est suggéré d'explorer les interactions entre les processus qui sous-tendent la complexité des dynamiques qui émergent à l'échelle d'un bassin versant (McDonnell et al., 2007), (2) ensuite, la saisonnalité constitue une signature hydrologique importante pour la comparaison de bassins, ceci en ciblant les oscillations récurrentes d'année en année ou annuelles–et spécifiques à certaines périodes, et en fournissant des indications importantes sur l'échelle temporelle des processus d'écoulement et leur lien avec conditions saisonnières d'humidité spécifiques à une certaine région (Ali et al., 2014), (3) finalement, la caractérisation des processus nichés à certaines échelles spatiales (ex : pente, tronçon, sous-bassin et bassin versant) en utilisant des mesures terrains ou des analyses géochimiques pourraient aussi permettre de comprendre les dynamiques qui émergent à l'échelle d'un bassin versant (McNamara et al., 1998, 1997).

Des processus analytiques développés dans des environnements non-pergélisolés ou encore, dans des domaines d'étude autres que l'hydrologie, présentent un potentiel fort intéressant pour répondre trois paradigmes mentionnés ci-haut. Comme les dynamiques hydrologiques observées à plus grande échelle résultent souvent d'une combinaison linéaire de plusieurs processus s'opérant à échelle plus fine (McDonnell et al., 2007), de plus en plus d'études utilisent des analyses statistiques avancées permettant de refléter la complexité des réseaux hydrologiques (Ali et al., 2010; Ali et Roy, 2010; Anderson et al., 2010; Haught et Van Meerveld, 2011). Legendre and Legendre (2012) soulignent d'ailleurs que les analyses statiques sont une partie importante de la méthodologie des études écologiques, et ce depuis longtemps. Des écologistes (Blanchet et al., 2008; Borcard and Legendre, 2002; Dray et al., 2006) ont d'ailleurs récemment développé une nouvelle famille d'analyse statistique, nommée « *Eigenfunctions analysis* » ou analyses par fonctions de valeurs propres, pour investiguer les structures spatiales présentes dans des systèmes complexes. En effet, les « *Eigenfunctions* » peuvent être utilisées comme variables explicatives spatiales lors d'analyse canonique de la variance présente pour une ou des variables étudiées et ainsi permettre de cerner l'échelle de la connectivité hydrologique ou des contrôles spatiaux qui sont les plus significatifs pour explique la dynamique à l'étude. Ali et al. (2010) soulignent d'ailleurs le grand potentiel des « *Eigenfunctions analysis* » asymétriques ou AEM qui sont adaptées aux réseaux influencés par des processus directionnels, pour l'étude des dynamiques à l'intérieur d'un réseau fluvial.

Ce mémoire cherche à améliorer nos connaissances quant aux dynamiques hydrologiques en région de pergélisol, ou plus précisément, d'identification les processus et caractéristiques du paysage qui contrôlent les mouvements de l'eau au cours de la période de dégel de la couche active du pergélisol. Dans un l'objectif ultime d'aider à prédire les impacts qu'auront les changements climatiques sur les rivières de l'Arctique. Dans une perspective d'application plus locales et court terme, elle vise aussi à fournir des informations concrètes sur la distribution spatiale et les processus qui contrôlent les sources en eaux pour la rivière Niaqunguk, ceci afin d'aider les acteurs en place dans leur processus décisionnel sur la mise en place d'un projet d'exploitation de l'eau de la rivière. Les études présentées dans ce mémoire reposent sur une combinaison entre (1) des mesures ont été réalisées dans le bassin versant de la rivière Niaqunguk, tout près d'Iqaluit, au Nunavut (63º 45' N, 68º 75' W), lors des saisons printanière et estivale de 2016 et 2017 et (2) des analyses statiques permettant de répondre aux objectifs du mémoire en se basant sur les paradigmes et concepts hydrologiques mentionnés plus haut. Ce mémoire se divise quatre chapitres. Un premier chapitre d'introduction (le présent chapitre), un deuxième et un troisième chapitres présentés sous forme d'articles scientifiques réalisés à la suite de deux campagnes terrain de collecte de données et d'un quatrième chapitre qui propose une brève discussion et présente les conclusions générales issues des principaux résultats et retombées de ce travail de recherche. Les chapitres deux et trois, qui constituent le coeur du présent mémoire, proposent une description détaillée des processus hydrologiques contrôlant les écoulements et la contribution de différentes sources d'eau, ainsi que leurs liens avec les conditions en humidité, et ce, respectivement aux échelles spatiales ; (i) d'une pente et (ii) du bassin versant de la rivière Niaqunguk. Ces articles sont intitulés ;

(i) How active layer thaw impact the hillslope-stream connections in the Niaqunguk River watershed, Iqaluit, Nunavut (Chapter 2).

(ii) Detailed geochemical and streamflow monitoring to understand the evolution of water sources and dominant hydrological processes from the spring freshet to the baseflow season of the Niaqunguk River, near Iqaluit, Nunavut (Chapter 3).

Chapitre 2 - Article 1

Titre : *How active layer thaw impact the hillslope-stream connections in the Niaqunguk River watershed, Iqaluit, Nunavut*

Auteurs : Gabriel Chiasson-Poirier, Jan Franssen, Daniel Fortier, Scott Lamoureux, Mélissa Lafrenière, Tommy Tremblay et Jamal Shirley

Le premier article de ce mémoire a déjà été soumis à la revue Water Resources Research, suite aux commentaires des réviseurs un deuxième manuscrit de l'étude a été produit, celui présenté dans ce mémoire. Ce deuxième manuscrit n'avait pas encore été resoumis pour publication au moment du dépôt de ce mémoire.

Cette étude démontre que les dynamiques de drainage d'une pente sont intrinsèquement liées aux patrons de dégel de la couche active du pergélisol. Elle relève aussi le rôle très important de la microtopographie de la couche de dépôt organique de surface qui recouvre une couche minérale, une structure typique des environnements arctiques. Les dépressions en surface associées aux hétérogénéités de l'épaisseur de la couche organique peuvent favoriser le stockage de l'eau en surface et limiter la contribution des écoulements de surface aux périodes de pluie ou de saturation importantes. Elle influence aussi la répartition de l'eau qui en retour entraine une hétérogénéité des profondeurs de dégel à l'échelle de la pente en raison de la plus grande conductivité thermique des dépôts saturés. L'évolution temporelle et spatiale de la topographie du plafond de gel joue aussi un rôle très important au fur et à mesure de la période de dégel de la couche active.

La méthodologie de collecte de données sur le terrain a été élaborée de façon conjointe entre Gabriel Chiasson-Poirier et Jan Franssen. Les analyses et la rédaction ont été réalisées par Gabriel Chiasson-Poirier sous la supervision de Jan Franssen. Daniel Fortier, Scott Lamoureux, Mélissa Lafrenière, Tommy Tremblay et Jamal Shirley ont aussi contribué de manière significative à cette étude, soit par leurs conseils, en donnant accès à leur laboratoire ou en permettant l'emprunt de leur matériel scientifique.

Référence: Chiasson-Poirier, G., Franssen, J., Fortier, D., Lamoureux, S., Lafrenière, M., Tremblay, T., Shirley, J., How active layer thaw impact the hillslope-stream connections in the Niaqunguk River watershed, Iqaluit, Nunavut. En preparation.

Abstract

In Arctic environments the hydrological processes remain fairly uncertain due to pronounced spatiotemporal variation in the active layer thaw depth (i.e., frost table depth). Advanced understanding of how physical controls on hillslope drainage change during the active layer thawing period is therefore required to adequately model hydrological connections in permafrost-affected environments. This research investigates hillslope-stream hydrological connections and shed light on how active layer and frost table topography influence fluxes of water across an Arctic hillslope. Our experimental design combined field measurements of hydro-physical conditions (i.e., discharge, frost table depths and saturations of the thawed portion of the active layer) of a hillslope-stream sequence together with hydrochemistry analysis of different water sources (i.e., groundwater, stream, lake) within this hydrological system. Research were conducted within sub-catchment of the Niaqunguk River watershed, Iqaluit, Nunavut. The dataset covers a period of two months (i.e., July – August) of the 2016 summer. Our results revealed positive feedback between subsurface flows and frost table progression. Such feedback can be initiated by hillslope surface characteristics that govern surficial runoff and distribution of water across hillslope early after snowmelt, when active layer remained entirely frozen. Moreover, our analysis highlighted the development of potential buffering zone for hillslope subsurface drainage on lower permafrost hillslope, enhanced by the formation of ridge in the frost table. This spatiotemporal pattern is partly explained by the topographic setting of the analysed hillslope that maintained high active layer saturation conditions during dryer periods and thus low magnitude late-summer rainfall event allowed the reactivation of hillslope-stream connexions via surficial drainage through the organic layer. In addition, the analysis of water chemistry suggested a transition from a system dominated by water contributions via organic flow paths during the early summer to a dominance of contributions via mineral flow path latter during summer. These findings enhance our understanding of Arctic hillslope hydrological processes and highlight that hydrological association to hillslope drainage may be greatly related to inter and intra annual variation in wetness condition.

2.1 Introduction

In the context of a climate-driven permafrost degradation, multiple changes to Arctic freshwater hydrological processes have been observed and/or suggested. Even if the spatial distribution needs to be refining, there is a scientific consensus on the recent increase of Arctic rivers discharge following total annual precipitation (Smith et al., 2007; St. Jacques and Sauchyn, 2009; Walsh et al., 2011). In the Arctic, similarly to other environments, for rain or other water sources to get from hillslope to the lakes or rivers, runoff must be generated from the slope and conveyed down to reach the surface water. However, the permafrost, particularity of Arctic environment, greatly influence slope runoff and water storage (Hinzman et al., 1991; Woo and Steer, 1982). The frost table of the seasonally thawed active layer serves as an impermeable boundary; thus, the depth of thawing front is a key factor to understand how water is routed from hillslope recharge areas to lakes and streams (Wright et al., 2009). However, the dynamics of groundwater fluxes and their interaction with surface runoff remain difficult to predict due to uncertainties related to spatiotemporal variation of thaw depths (i.e., frost table depths). While studies using sophisticated instruments and elaborate field research designs have been conducted to understand the role of bedrock topography or other subsurface impeding layers on hillslope drainage in southern watersheds (Ali et al., 2011; van Meerveld et al., 2015), there is still a lack of studies on dynamics of permafrost hillslope soil drainage and subsurface flow within the active layer (Hinzman et al., 2013; Walvoord and Kurylyk, 2016). Furthermore, recent research investigating shallow groundwater flow processes in permafrost environments has been mainly therotical and there is a need to validate these results with field observations (Bring et al., 2016).

Active-layer thickness varies both spatially and temporally in response to many climatological parameters, as well as physical, hydrological, and thermal properties of the surface soil layers (Akerman and Johansson, 2008; Nelson et al., 1998). Even within small areas, thaw depths may vary substantially, emphasizing the importance of localized processes on active layer thawing dynamics (Gao et al., 2016). Subsurface flows or wetness conditions can influence the local variation in active layer depth, by enhancing the transfer of thermal energy

via heat advection (Carey and Quinton, 2005a; de Grandpré et al., 2012; Hayashi et al., 2007). In turn, heterogeneity in the frost table due to differential localized thaw can impact the patterns of surface soil moisture distribution (Guan et al., 2010; Williams et al., 2013). The pioneering study of Woo et Steer (1983) analyzed hillslope drainage dynamics and active layer thaw depths by monitoring the groundwater levels in a network of piezometers installed on two hillslopes near Resolute, Nunavut. The authors observed changes in runoff flow patterns due to the deepening of the frost table during the active layer thaw and thus a seasonal evolution of the water storage capacity. They highlighted the need for improving our knowledge of the interaction between these two processes. Wright et al. (2009) more recently, greatly improved our understanding on the role of active layer development on runoff generation. They observed that soil saturation patterns were partly controlled by subsurface lateral flow converging to frost table depressions. They also simulated that frost table depressions had to first be filled, before water spill over frozen ridges and generate flow downslope.

Many processes controlling the movement of water on Arctic tundra hillslopes have been well studied, such as for example the study of Quinton and Marsh (Quinton and Marsh, 1999) that provided a conceptual model for runoff generation developed for hillslopes characterized by a surficial organic layer (high hydraulic conductivity) and an underlying mineral layer (low hydraulic conductivity). Water table position with respect to these two layers (i.e., organic and mineral) will result in downslope runoff of different importance. This two-layer flow system was also observed by Carey and Woo (2001), who concluded that water table elevation is controlled by multiple factors (e.g., thawing depths, hillslope structure), and that during summer, quickflow (i.e., water table within the surface organic layer) is largely dependent on antecedent wetness condition. On hillslopes with thick organic cover, overland flow is rarely observed due to the high infiltration capacity of the organic matter. Thus, the entire active layer saturation can lead to quick downslope water delivery through preferential overland flow paths (Woo and Steer, 1982). Subsurface drainage controlled by the frost table topography acting as an impeding layer, proposed by Wright et al. (2009) can be compared to the fill and spill mechanism which is well detailed for multiple environments/conditions (Ali et

al., 2011; Brannen et al., 2015; Coles and McDonnell, 2018; Spence and Woo, 2003; Tromp-van Meerveld and McDonnell, 2006). This hillslope drainage process can be related to either an impeding layer (i.e., bedrock, active layer frost table, surficial frozen soil or low conductivity layer) or to soil saturation conditions that led to fill and spill mechanism whether over surficial microtopography or at basin scales. While modelling (hillslope scale) or chemical (catchment scale) studies have been conducted, there is a lack of field-based measurements on how this process controls the transfer of water on Arctic tundra hillslopes.

Emerging trends in experimental designs developed to understand how upland water transit through hillslope to stream is to combine physical and hydrologic characterizations with chemical monitoring of stream water and potential water sources (Coles and McDonnell, 2018; Jencso et al., 2010; Tetzlaff et al., 2014). Applied to permafrost environment, Bolduc et al. (Bolduc et al., 2018) used natural tracers to identify lateral hillslope contributions to river baseflow, they related the contribution to either surface or subsurface water source based on their isotopic signature and enrichment of depletion of the river water downstream of the identified connection. Koch et al. (2014) in a conducted within a boreal catchment of the Alaskan discontinuous permafrost zone showed using permeability test, active layer depth measurements and end-member model, that on hillslopes characterized by a two layers flow system, the position of the thaw front relative to these two layers is a key driver of the hydrological processes occurring on the hillslope. When the frost table stand in the mineral layer, but relatively close to the organic layer, depression that forms in the frost table topography must be filled to allow the water table to reach the surficial organic layer and generated lateral hillslope drainage. One of the oldest known isotopic and geochemical study conducted in Arctic was by Obradovic and Sklash (1986) within the same catchment where this study is conducted (Niaqunguk River watershed), the authors found that stormflow events consisted of 40-50% of old water and that proportion of old water to the entire river hydrograph ranged between 50-60%. They related these proportions to a displacement of stored pre-event water. These results differ from numerous recent studies that suggested a more important contribution of new or event water to the hydrograph of continuous permafrost rivers (Blaen et al., 2014; Cooper et al., 1993; McNamara et al., 1997). The latter

studies thus identify a significant contribution of pre-event or enriched waters to stormflow generated by summer rainfall events, attributable to a deepening of the active layer and a mixing between stored (older water) and event water (Tetzlaff et al., 2015). Combining multiple hydrometric and active layer thaw measurements with stream and water sources sampling present a great potential to elucidate controls on water storage and contributions.

Here, we instrumented a hillslope-stream sequence draining into a headwater tributary of the Niaqunguk River, where subsurface flows are constrained by the presence of a frost table. We also developed a water sampling design to confirm potential hillslope-stream hydrological connections. Our aim is to provide a better characterization of how active layer and evolution of the frost table topography can influence fluxes of suprapermafrost groundwater and hillslope runoff production during the Arctic summer. This knowledge is essential to assess how the terrestrial landscape is hydrologically connected with Arctic river systems, and to determine the impacts of climate-related changes on permafrost hydrology. Specific research objectives were to: (i) Map across a hillslope the evolution of saturation and thawing conditions, as well as the resulting water/frost table topography; (ii) Identify rupture in chemical and isotopic time series of the stream water just downstream and lake water upstream of the hillslope, suggesting a contribution of hillslope runoff to the stream; and finally (iii) Combine geochemical and/or isotopic tracer analyses with the mapping of the hillslope spatiotemporal patterns to assess how changes in frost table topography interact with the hillslope structure to control the water transfer from the hillslope to the stream.

2.2 Site description

The Niaqunguk River is a fourth-order stream located northeast of the City of Iqaluit, Nunavut (63° 45’ N, 68° 33’ W) and draining an area of 58 km^2. The Niaqunguk watershed is situated in a region of continuous permafrost. Studies conducted in the southern portion of the watershed indicate that active layer thickness is varying between 1 m and 2 m under different types of natural ground (LeBlanc et al., 2015). An end moraine forms the eastern border of the watershed and a wide variety of Quaternary deposits (e.g., till blanket and

veneer, glaciofluvial deposits, boulder fields) are found throughout the watershed (Hodgson, 2005). Streamflow in the Niaqunguk River usually begins in May and ends in October, with peak annual discharge typically observed in June during the spring freshet. (Kjikjerkovska, 2016). Mean precipitation for the months of July and August are 52 and 70 mm, respectively; mean annual total precipitation is 404 mm with snow accounting for 57% (1973-2010; Environment Canada, station #2402596).

We focus our water sampling design and hillslope characterization within the drainage area (0.41 km^2) of a head-water tributary centrally located within the Niaqunguk watershed and approximately 6 km northeast of the Iqaluit airport (Figure 1a). The terrain is of moderate relief with local elevations ranging from 163 m above sea level (asl) at the subwatershed outlet to 230 m asl on the eastern boundary of the subwatershed. Chiasson-Poirier et al. (2016) identified nine distinct surficial geologic unit types within the subwatershed (i.e., Well-drained boulder field, Boulder-sand-organic, Glaciofluvial outwash and veneer, Organic, Alluvial, Till blanket and veneer) (Figure 1b). They also highlighted the great agreement between location of important topographic flow accumulation, streams and the boulder, sand and organic unit type. This latter unit can be distinguished from the well-drained boulder field unit-type by the presence of a mineral matrix covering/surroundings and the presence of boulders, with an important cover of organic matter. Due to wetter conditions vegetation (i.e., grass, sedge and moss) is also denser on these deposit areas than on surrounding till or bedrock. These boulders, sand and organic unit-types are likely to be hydrologically important to understand landscape contributions to surficial water. The configuration of hydrogeomorphological landscape elements within our subwatershed study area is also typical of that observed throughout the Niaqunguk watershed.

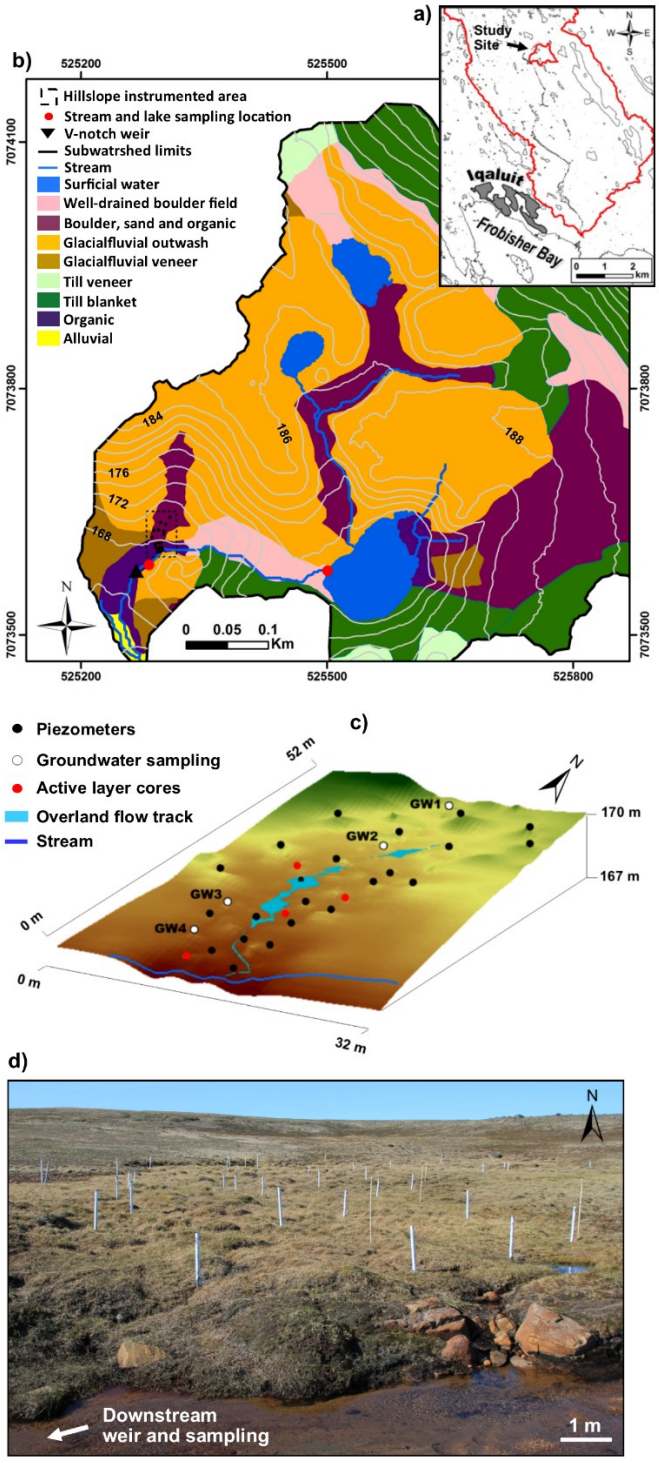

Figure 1. a) Localization of the subwatershed study site in the Niaqunguk River watershed, b) surficial deposits, hydrological network and topography of the subwatershed study area, as well as the location of the instrumented hillslope and water sampling sites, c) instrumented hillslope area showing key measurements/monitoring points, including; piezometer locations, active layer cores, and groundwater sampling piezometers location, d) downslope photography from the hillslope instrumented area.

To characterize the evolution of hillslope saturation and thaw conditions, we instrumented (i.e., piezometers and frost table depth measurements) the lower portion of a convergent (i.e., bowl-shaped) hillslope situated within the studied subwatershed (see Figure 1c and d). The instrumented hillslope is adjacent to the north (i.e., right) bank of the downstream section of the principal stream draining the subwatershed, and just downstream (200 m) of the largest lake connected to the surficial drainage network of the subwatershed (see Figure 1b). The instrumented area has a 5% gradient and an irregular surface micro-topography, due to accumulation of organic material of varying thickness with the presence of turf hummocks. Inter-hummock areas are characterized by thin organic cover or bare mineral deposits. Turf hummocks differs from mineral earth hummocks described by Quinton and Marsh (1998) and consists of an accumulation of organic material capped by living vegetation, such as sedges and grass (O. van Everdingen, 1998). Turf hummock dimensions can vary greatly; here hummock sizes varied between small (i.e., diameter: <20 cm; height: <20 cm) and large (i.e., width: ~1 m; height: ~50 cm).

Active layer cores (4) were sampled across the hillslope study area (see Figure 1c) at the end of the monitoring period (August 25) and particle size analysis was performed using the dry-sieving and hydrometer methods (ASTM D6913M-17, 2017). Active layer cores description and statistics are presented in Table I. Thickness of the surficial organic cover varied greatly across the hillslope which is reflected by our coring that showed surficial organic layer < 1 cm in some areas and > 20 cm under turf hummocks. Textural groups are varying between slightly gravelly muddy sand and gravelly sand, while variations in gravel, sand or silt contents are greater between the coring sites than between depths at each of the core sites. For coring sites 1, 2 and 3 there is a slight decrease of sand content and increase of silt content with depths. Active layer cores thus show that the hillslope is comprised of two main and distinct layers; a surficial organic layer of varying thickness and an underlying mineral layer with slight variation in texture. Using a handheld concrete core drill, frozen active layer cores were extracted adjacent to the hillslope study area (between depths of 50 to 115 cm below the ground surface), so as not to interfere with the routing of flow in the study site. Saturation conditions, vegetation, deposits and slopes at the coring locations were comparable to the adjacent locations on the instrumented hillslope. No ice-rich transient layer was observed, but

rather ice-content proportions consistent with porosity values of fine-grained sand, which confirmed that frost table acted as an impeding layer for subsurface flows (Chiasson-Poirier et al., 2016).

Table I. Characteristics of the sampled active layer cores, cores number (1 to 4) refer respectively to the downslope to upslope location of the cores illustrated on Figure 1c.

AL cores	Depth (cm)	Textural group	D50 (µm)	D10 (µm)	% gravel	% sand	% silt
1	0 - 18	Organic	-	-	-	-	-
	18 - 40	Slightly Gravelly Sand	239	65	1.9	89.0	9.1
	40 - 61	Slightly Gravelly Muddy Sand	228	52	1.6	83.0	15.0
	61 - 80	Slightly Gravelly Muddy Sand	143	47	1.6	76.0	24.0
2	0 - 20	Slightly Gravelly Sand	260	76	4.0	90.0	6.0
	20 - 37	Gravelly Sand	247	70	6.0	87.0	7.0
	37 - 58	Slightly Gravelly Muddy Sand	198	61	2.0	87.0	11.0
	58 - 78	Gravelly Muddy Sand	238	59	8.3	80.2	11.5
3	0 - 20	Organic	-	-	-	-	-
	20 - 38	Slightly Gravelly Sand	253	84	3.0	92.0	5.0
	38 - 62	Gravelly Sand	304	85	6.0	87.0	7.0
4	0 - 20	Slightly Gravelly Muddy Sand	129	50	1.0	73.0	26.0
	20 - 40	Slightly Gravelly Muddy Sand	110	50	0.3	71.0	28.0
	40 - 58	Slightly Gravelly Muddy Sand	137	53	0.4	80.0	19.0
	58 - 78	Slightly Gravelly Sand	188	63	0.5	90.0	9.0
	78 - 93	Slightly Gravelly Muddy Sand	175	57	1.0	85.0	13.0

2.3 Methods

2.3.1 Field measurements

Hillslope saturation conditions were monitored using a network of 24 drive-point piezometers installed from the toe of the hillslope (at the streambank) to 50 m upslope, corresponding to the upper limit of the footslope section, and were distributed across a roughly 25 m wide area (see Figure 1). The installation covered an area of approximately 711 m^2 (i.e., 1 piezometer per 29 m^2). Piezometers were constructed of schedule 80 polyvinyl chloride (PVC) tubing (3.7cm in diameter) with solid PVC drive point fitted to the bottom. Each had a screen length

of 14cm at the bottom end of the tube and 20 holes of 1 cm in diameter, Nitex® nylon 50 μ m mesh was fitted to the interior of the screened section of the piezometer to prevent the infiltration of fine sediments. Piezometers were installed on July 8, 2016 and were thereafter routinely advanced to frost table depth using a hammer. We used this approach to measure vertical hydraulic head at the frost table and to avoid the anticipated dewatering of the piezometers due to deepening of the frost table during active layer thaw. Here piezometers were preferred over wells to ensure that we were capturing water level elevation related to the active layer saturation and to prevent filling of wells by overland flows.

Hillslope architecture was taken into consideration during piezometer placement such that piezometers were only installed in areas of thin (<10 cm) organic cover. We assumed here that the two layers flow system described by Quinton and Marsh (Quinton and Marsh, 1999) was most likely to influence the hillslope drainage, since the hillslope was characterized by a highly permeable surficial organic layer overlaying a much less permeable mineral layer. Due to the high heterogeneity in the thickness of surficial organic layer and since no significantly lower conductivity layer was observed within the mineral layer (see table I), here we assume that vertical hydraulic head measured in our shallow piezometers reflected the local water table height and it position relative to the surface of the mineral layer (i.e., below: slower subsurface drainage; above: surficial pounding water or quickflow through the organic layer). Punctual water level measurements were routinely (i.e., 2 times per week) conducted and always before the repositioning of the piezometer to the frost table depth.

Thaw conditions were characterized between piezometer sites using a graduated metal rod that was advanced into the soil until refusal, assumed frost table depth as measured depths increased for all sites throughout the monitoring period. At piezometers sites to prevent soil disturbance, thaw depths were established by subtracting the piezometer length above ground surface from the total length of the piezometer, after the advancement of the piezometers to frost table depth. This gave us routine measurements (i.e., 10 measurements events between July 8 and August 19) of frost table depths at 70 points across the instrumented hillslope.

The position and elevation of each piezometer site and frost-table measurement point were surveyed using a total station (Model TC805 manufactured by Leica Geosystems, Saint-Gall, Suisse, relative to the local datum accuracy $\pm$1cm) and referenced to a local datum. Water levels relative to ground surface (WLRGS) or the piezometer water level above frost table (WLAFT) were computed from the surface and frost table elevation surveyed at each piezometer site. Nearest neighbour’s interpolations (ArcGIS 10.5, Natural Neighbor interpolation tool) of WLRGS, WLAFT and frost table

depths were used to infer the evolution of saturation and thaw condition across the instrumented area. While water and frost tables elevations were derived from ground surface topography to investigated relations between hillslope drainage dynamics and active layer thaw.

Daily rainfall records were obtained from the Iqaluit Airport meteorological station (Environment Canada, station #2402596, 4km south-west of our studied hillslope). Daily mean air temperatures were measured at the hillslope site with a shielded temperature-sensor (Onset, UA-001 temperature logger, Bourne, United-States, accuracy $\pm$0.5 ^{o}C). Streamflow of the tributary stream located at the base of the instrumented hillslope was monitored at a V-notch weir (α = 5^{o}) installed in the stream 10 m downstream of the hillslope (Figure 1b). Stage upstream the weir and atmospheric pressure at the site were recorded at 15-minute intervals, using a pair of pressure sensor-loggers (Onset, U20 water level loggers; accuracy $\pm$0.5 cm), and absolute water levels obtained by subtracting atmospheric pressure from total pressure recorded by the submerged pressure transducer. Stream discharge was computed from upstream water stage using the Kindsvater-Shen equation (USBR, 2001). To prevent submergence of the weir mouth downstream, the weir was installed just upstream of a natural drop in the tributary channel, also creating ideal conditions from pounding water upstream the weir. Water was close to the weir height the day following the most important rainfall event that occurred in July, otherwise water never circumvented the weir. Hydrometeorological conditions were monitored from July 6 to August 26 which delineate the start (day 1; D-1) and end (day 52; D-52) of the monitoring period.

2.3.2 Water sampling design and analysis

To identify potential water contributions from the hillslope to the adjacent tributary, water samples were collected from the stream (i.e., 10 m downstream of the hillslope) and from the stream source (i.e., the lake 200 m upstream of the hillslope) (see Figure 1b). To characterize the chemical signature of potential hillslope contributions, water was also sampled from four groundwater piezometers (i.e., GW1 - GW4) installed respectively along an upslope-downslope transect (see Figure 1c). To assess the signature of potential water contributions via surface runoff, surficial water present on the hillslope was also sampled at approximately 20 m upslope and 15 m along the slope (see Figure 1c). Water was either pounded or connected to the stream downslope via overland flow depending of wetness conditions. Water samples from the stream, lake and hillslope groundwater piezometers were collected twice weekly from July 7 (D2: Sampling Day 2) to August 25 (D51: Sampling Day 51). Surficial water on the hillslope was only sampled between August 14 and 25, connexions of water downslope via overland flow slowly decreased from the first

sampled day to become disconnected/pounded approximately on D45 and was reactivated on the last two sampled days. Surface water samples were collected using 1-L high-density polyethylene bottles, water in piezometers was sampled using bailer samplers. Samples were filtered using either a reusable polysulfone vacuum filtration unit with 0.22-µm PVDF filter membranes (Isotopes analysis) or a Millipore glass filtration unit and 0.47µm glass fibre filters (DOC concentration measurements) and separated into respectively 25-ml high-density polyethylene scintillation vials or sterile 40 mL amber EPA vials. Samples were kept refrigerated until analysis at the FaBRECC laboratory at Queen's University.

Water electrical conductivity (EC) was measured in-situ during sampling using a YSI PRO30 (YSI Inc., Yellow Springs, OH). Stable isotopes composition (oxygen - $\delta^{18}O$ and hydrogen - δD) from collected samples was analyzed with a liquid water isotope analyzer (Los Gatos Research, Mountain View, CA) and reported in parts per thousand (‰) relative to VSMOW (Vienna Standard Mean Ocean Water). The uncertainty ranges of this instrument are ±0.2‰ for $\delta^{18}O$ and ±0.8‰ for δD, respectively. Dissolve organic carbon (DOC) concentrations were determined by high-temperature combustion on a Shimadzu (TOC-V) organic carbon analyzer (Shimadzu TMN-1). Concentrations was calculated as the means of between three injections with standard deviation <0.1% and coefficient of variation always <2%. Besides identifying potential rupture in stream-lake chemistry associated to hillslope contributions, these analyses will also provide indications of the dominant water sources and the evolution of water pathways that occurred in the subwatershed during the monitoring period (Tetzlaff et al., 2015).

2.3.3 Statistical analysis

A useful approach to detect ruptures in multivariate time series (e.g., multiple water chemical parameters) is to associate ordination and clustering results (Legendre and Legendre, 2012, chapter 12 - detection of discontinuities in multivariate series). To identify how the chemistry of the stream water differed from the upstream lake water or how groundwater chemistry differed along the hillslope (GW1 - GW4) we then used principal component analysis (PCA) which included the following chemical variables; EC, DOC concentrations, oxygen ($\delta^{18}O$) and deuterium (δD) isotopes measured for sampling dates S2 to S51 (n= 18). Clustering methods (Unconstrained Ward minimum variance clustering or Chronological clustering by Multivariate Regression Tree) were subsequently used to identify significant discontinuities in chemical time series and therefore identify periods with distinct chemical signatures. The advantage combining ordination in two-dimensional space with clustering analysis is that one allows to visually identify similarities between

dates and sites in the reduced-spaced ordination (only the first two PC axes were retained here) and the second is used to confirmed the significance of delineations between dates that may not be clear on the ordination and to compensate for errors related to misrepresentation of object clusters in the reduced space that may by distinct in higher dimensions (Legendre and Legendre, 2012).

Ward minimum variance clustering defines groups in such a way that the within-group sum of squares is minimized based on the Euclidian distance between sites. Chronological clustering by Multivariate Regression Tree (MRT) was only used if groups formed by unconstrained Ward clustering were not in coherent chronological order. The ultimate objective of MRT is to build a nested sequence of individual groups or sub-trees that are as homogeneous as possible (Ali et al., 2010). All sampling dates are first labelled upon their chronological order (explanatory variable) and a recursive search is then conducted to find the explanatory variable (or sampling date) that splits the chemical variables measured at the different sites into the two most dissimilar subsets. The optimal number of groups for the MRT tree is determined from a cross-validation procedure. This procedure is necessary to avoid an oversized, over-fitted tree with very few elements in each terminal node (Breiman et al., 1984). For cross-validation purposes, a portion of the data is removed and kept for the validation, the cross-validation is then repeated n number of times (n = 1000). For each simulation, the k models corresponding to the number of tree divisions (k = 7) are tested for the smallest cross-validation error (CRVE) or the smallest deviation from the predicted and real values of the validation data. The optimal tree size corresponds to the model or number of divisions having the smallest cross-validation error.

Here the purpose of using either ward clustering or MRT in addition of PCA analysis to analyze the surface water (stream and lake) or groundwater (GW1-GW4) chemical time series is to (1) determine if chemical time series of the different water source are characterized by similar discontinuities or (2) to identify non-arbitrary periods on which further statistical analysis can be conducted to identify significant differences between sampling sites. For each significant period identifying the groundwater time series, we tested for differences between groundwater sampling sites (GW1 - GW4), for each chemical variable using a univariate analysis of variance (ANOVA). Principal component analysis, Ward clustering and multivariate regression tree were computed using the functions rda(), h.clust() and mv.part() of the R packages vegan, stats and mv.part (Oksanen et al., 2018; R Core Team, 2017; Therneau and Atkinson, 2014).

2.4 Results

2.4.1 Hydrometeorological conditions

The instrumented portion of the hillslope and its entire upslope contributing area were entirely snow-free on the first day of our study (July 6 - D1). Some isolated snow patches were still present in other portions of the subwatershed (<5% coverage). There were five significant rain events that generated a total of 172 mm of rainfall during the study period; 126 mm of which occurred during the month of July 2016 (Figure 2). The most important rainfall event (i.e., 80 mm; July 21-22) contributed to significantly higher than normal monthly total precipitation observed for the month of July; mean July precipitation is 53 mm (1981 - 2010; Environment Canada). The July 21-22 event caused a considerable runoff response with discharge reaching a peak of 30 L/s in the tributary stream adjacent to the hillslope. Following this event, the streamflow decreased to approximately 1 L/s during an extended rain-free period that lasted until August 10. A series of rainfall events between July 13 and 20 with total rainfall of 37 mm caused a peak discharge of 14 L/s in the adjacent tributary. We observed a similar amplitude of stormflow response in the tributary following a rainfall event on July 10 (9 mm), and a rainfall event on August 10 (15 mm); stormflow volumes calculated using the constant discharge method were 900 m^3 and 990 m^3 respectively. Daily air temperatures were consistently below 10 ^{O}C during the multiple rainfall events of July and generally warmer (> 10 ^{O}C) during the rain-free periods of early-to-mid August.

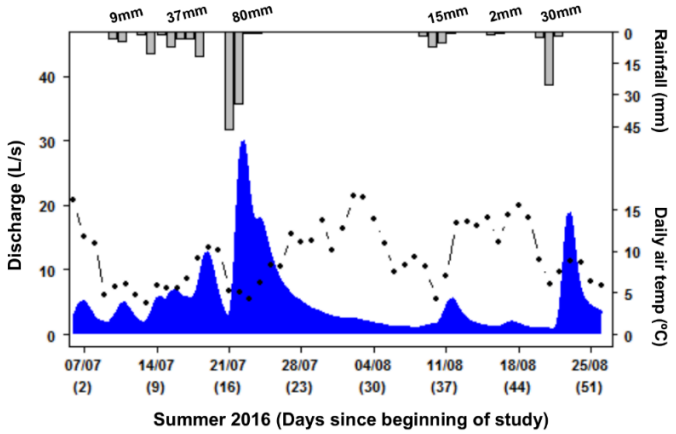

Figure 2. Discharge of the tributary adjacent to the hillslope as measured at the downstream weir (see Figure 1b). Grey bars indicated daily rainfalls measured at Iqaluit airport and black dots show the daily air temperature measured at the hillslope site.

2.4.2 Hillslope saturation and thaw conditions

Distinct hillslope saturation patterns were observed as the snow free period progressed. At the hillslope scale, higher saturation conditions were observed on July 23 (the day after the major rainfall event) when across the site nearly the entire active layer was saturated; WLRGS values ranging from -1 cm to 5 cm (Figure 3a). In contrast, 13 days later during a rain-free period WLRGS values measured across the hillslope ranged from -9.5 cm to -1 cm. Locally, the highest WLRGS values were measured in the hillslope centre between August 12 and 19, where water varied between 7 cm and 8 cm above ground surface and while only the central and upper portions of the instrumented area were saturated to surface. The evolution of WLAFT values reflect the deepening of the frost table through the summer as well as the important variations in active layer depth (Figure 3b). The interpolated pattern of WLAFT values indicates that there was a negative downslope gradient in the volume of water within the active layer, with a downslope progression of elevated WLAFT values following the August 10 rainfall event.

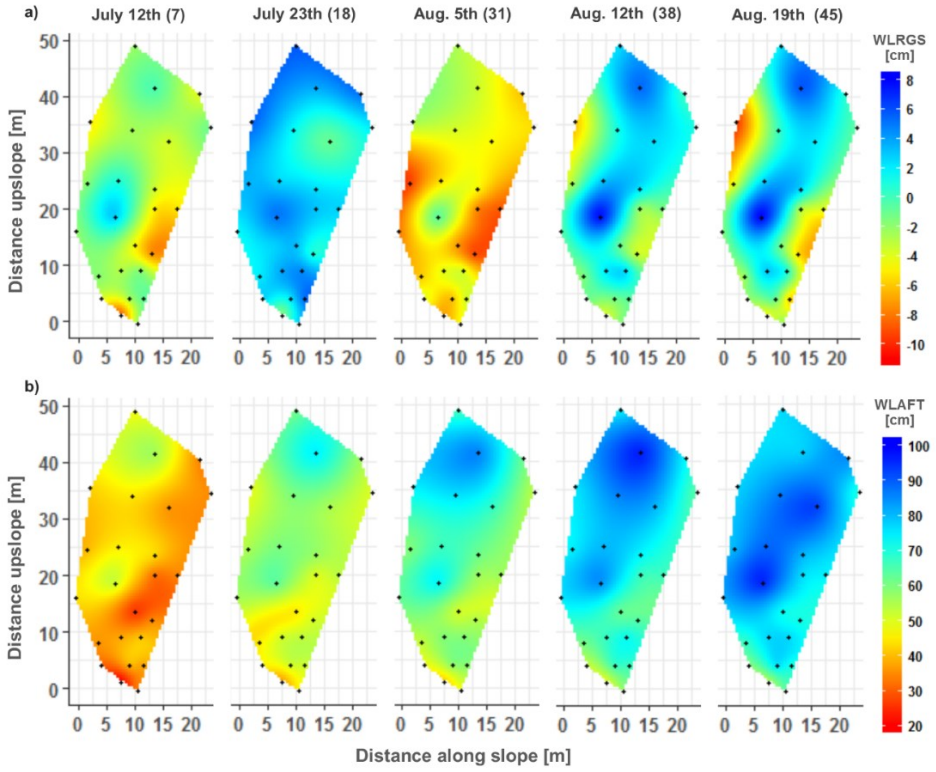

Figure 3.Maps of interpolated a) piezometer water level relative to ground surface (WLRGS) and b) piezometer water level above frost table (WLAFT), showing the evolution of the hillslope saturation conditions between July 12th and August 19th. Days since beginning of study are provided in parentheses to allow an easier reference for chemical analysis. Black dots are the piezometer location.

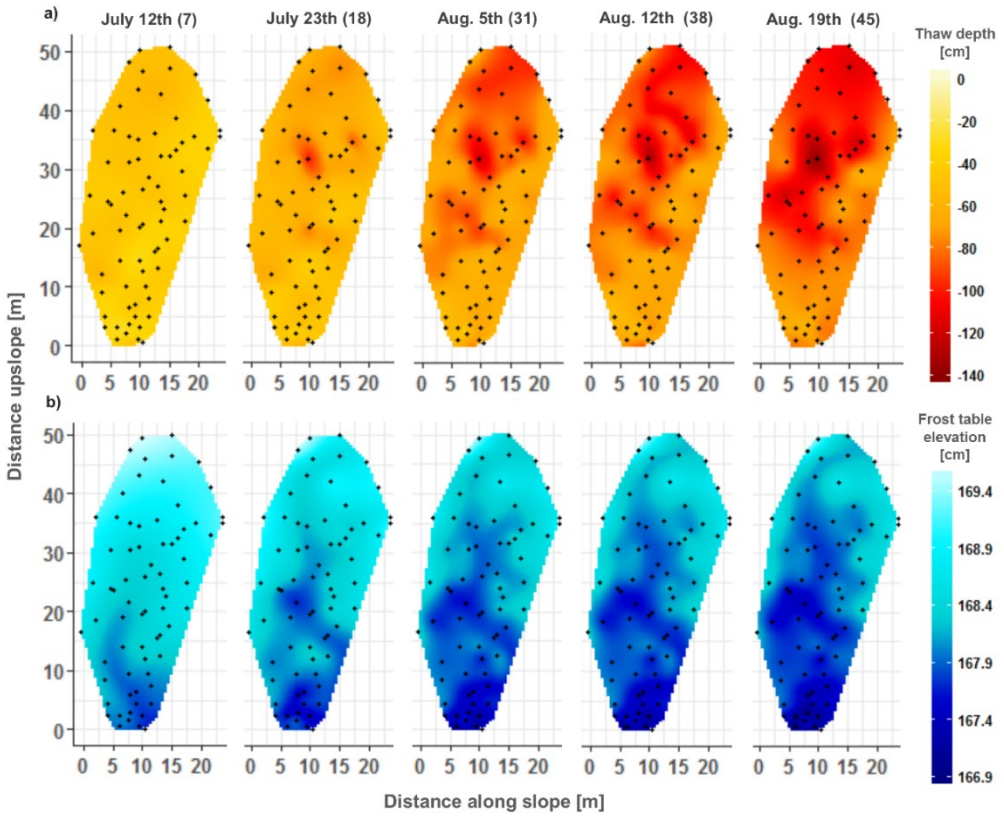

Figure 4. Maps of interpolated a) frost table depth relative to ground surface (GS) and b) frost table topography relative to local datum, showing the evolution of the hillslope thaw conditions between July 12th and August 19th. Black dots show frost table measurements locations.

During our study period, thaw depths evolved from shallow and spatially uniform to deeper and spatially variable (Figure 4a). On July 12, the depth of thaw across the hillslope was relatively uniform (mean depth: -41 cm; SD: 6.9). By August 19, thaw depths across the hillslope were in comparison to July 12: (i) on average 45 cm deeper; and (ii) much less uniform (mean depth: -85 cm; SD: 16). The increased rate of thaw and development of heterogeneity in frost table topography were especially marked during the July 23 to August 5 period (thaw: 1.2 cm/day); this corresponds to the period immediately following the major rainfall event that entirely saturated the hillslope and when mean daily air temperatures were consistently above 10 ^{O}C (Figure 2). Rates of thaw were slower during the following periods: 0.78 cm/day between August 5 and 12; and 0.95 cm/day between August 12 and August 19. As thaw progressed, there was an upslope propagation of a depression in the frost table surface (Figure 4b) with the development of a branching

pattern reminiscent of a tributary/gully network. Local thaw patterns also caused the formation of a ridge in the frost table situated approximately 10-15 m from the bottom of the slope. This ridge formed after July 23 and persisted until the end of the monitoring period (Figure 5a). The position of the frost table depression, immediately upslope of the aforementioned ridge, coincides with the higher WLRGS and WLAFT values measured here on August 12 and 19.

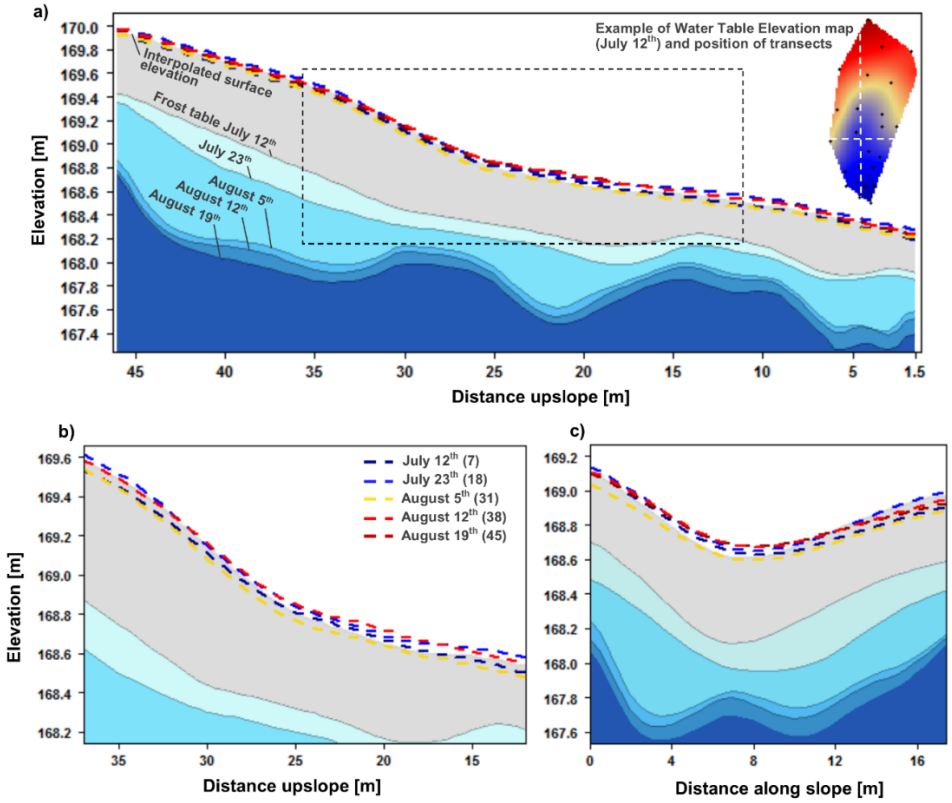

Figure 5. Transects of the interpolated water table and frost table elevation maps showing the changes in the elevation of both surfaces during our study. On the top-right corner of a) the positions of the longitudinal and cross-sectional transects are illustrated on the water table elevation map of July 12th, while the inset box emphasis the area illustrated on b). For clarity the August 19th water table is not shown on b) but was nearly identical to that of August 12th. Illustrated on c) is the cross-sectional transect extracted from the water elevation maps. Top of the grey layer corresponds to the interpolation of the ground surface elevation surveyed at each piezometer location (i.e., surface of the mineral layer).

Throughout the monitoring period water levels in the piezometers remained in close proximity to the ground surface both along and across the instrumented area (Figure 5). It is worth emphasizing that piezometers were installed in the troughs between turf hummocks where organic cover was either absent or had scant thickness (i.e. < 10 cm), thus

the hillslope profile shown here better reflects the form of the mineral layer rather than the undulating topography of the overlaying organic cover and turf hummocks. The interpolated water table surface follows the longitudinal profile of this mineral layer with important breaks in slope at distances of ~34 m, ~26 m, and ~9 m upslope creating a convex – concave – slightly convex longitudinal hillslope profile (Figure 5a). Here the local hillslope gradients immediately upslope from each of the aforementioned slope breaks change from 0.046, to 0.065 and to 0.019, respectively. Over the upper (convex) portion of the hillslope (> 30 m upslope) the water table resided above the interpolated hillslope surface only after the important rainfall event that occurred on July 21-22, otherwise water tables at this area of the hillslope resided within the mineral layer. Over the central (concave) portion of the hillslope (15-30 m upslope), the water table remained locally above the surface of the mineral layer for all measured dates expect August 5, with the greatest water elevations observed on August 12 and August 20. The water table dropped below the surface of the mineral layer across the lower (slightly convex) portion of the hillslope (< 15 m upslope) for all dates with the exception of July 23. Across the central portion of the instrumented area the hillslope gradient was relatively steeper on the left side (facing upslope) than on the right side (i.e., left side: 0.075; right side: 0.04 at cross-section shown on Figure 5c at 15m upslope). With the exception of August 5, water levels across the steepest left side of the instrumented hillslope were at or above the surface of the mineral layer, whereas water levels remained at or within the mineral layer over most of the right side of the hillslope. The mineral layer remained saturated only over the concave central portion of the instrumented area (18-22 m upslope; 3-10 m cross-slope; Figures 3a & 5bc), a location where we also observed the development of an important depression in the frost table (15-25m upslope Figures 4a & 5a).

2.4.3 Evolution of lake, stream and groundwater chemistry

Broadly similar trends were observed between water chemistry for samples collected from the stream adjacent to the hillslope, and from the lake discharge ~200 m upstream (Figure 6). There was a general increase in the values of all measured variables, with both lake and stream showing a progressive enrichment of δD (-143 to -106 0/00) and $\delta^{18}O$ (-18 to -13 0/00) isotopes through the sampling period. EC values also progressively

increased (Stream: 37.4 to 53.5; Lake 32.9 to 53.4 uS/cm), but for an abrupt punctual drop in EC values (Stream: -8.9 µS/cm; Lake: -9.3 µS/cm) during the rainfall event of July 21-22. Both stream and lake DOC concentrations slowly increased prior to an abrupt rise (Stream: +0.86 mg L-1, Lake: +0.7 mg L-1) associated with the same rainfall event, after which DOC values for the lake and stream showed no obvious trend, with more inconsistent differences and with generally higher values for the lake (mean: 3.23 $\pm$ 0.25) than for the stream (mean: 2.82 $\pm$ 0.23). We also observed that for EC, δD and $\delta^{18}O$ measured values, the maximum (EC: 6.5 uS/cm; δD: 5.1 0/00 and $\delta^{18}O$: 0.95 0/00) difference between stream and lake water samples occurred either during the D-35 or D-37 sampling dates. The latter two sampling dates correspond to the 15 mm mid-August rainfall event that reactivated overland flow on the hillslope. Sampling of this overland flow, and surficial water pounded, between August 11 and 25 indicate that this water had very similar DOC, δD and $\delta^{18}O$ values relative to the stream and lake. However, EC values for this surficial hillslope water were much lower (~15 µs/cm).

The chemistry of the shallow groundwater was distinct between piezometers, and these shallow groundwater chemical signatures were distinct from the surface water sampled on the hillslope, in the adjacent tributary, and in the upstream lake (Figure 6). Mean EC values of hillslope groundwater ranged from 62.6µS/cm (GW4) to 96.6 µS/cm (GW3) with EC values trending lower as the summer progressed. By the end of the monitoring period EC values in GW4 approached those measured in the stream and the lake samples (~ 50 µS/cm). However, over the course of the entire monitoring period mean EC values for groundwater were 1.4 to 2.2 times greater than the mean EC value for the lake and stream (44.9 and 44.4 µS/cm), and 2.1 to 3.2 times greater than of the surface water sampled on the hillslope (mean: 30.5µS/cm). DOC concentrations in hillslope groundwater rose slightly at the beginning of the monitoring period before also following a downward trend. By the end of the monitoring period only GW4 had DOC values (GW4 on Day 40: 9.6 mg L-1) that were notably distinct from that of the surface water samples (Stream: 2.5 mg L-1; Lake: 2.9 mg L-1). Relative to EC and DOC we observed more uniform values of δ D and $\delta^{18}O$ between shallow groundwater sampling sites, except for slightly greater values for GW4. Also relative to EC and DOC, we observed that groundwater average δD (GW1: -118.2; GW2: -118.0; GW3: -116.4; GW4: -113.7) and $\delta^{18}O$ (GW1: -15.3; GW2: -15.4; GW3: -

15.5; GW4: -14.8) isotopes values were much closer to the average values measured in the adjacent stream (-117.8 and -15.2) and the lake (-117.9 and -15.0).

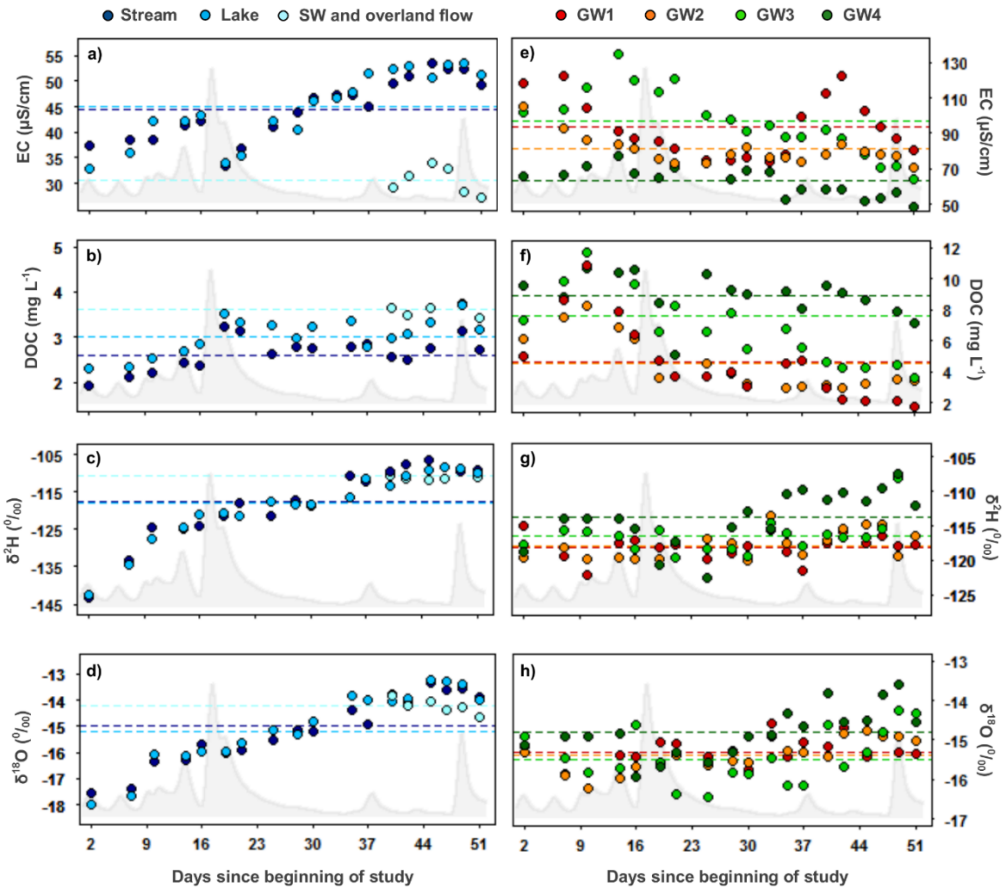

Figure 6. Evolution of: (a) water electrical conductivity (EC);(b) dissolve organic carbon (DOC); (c) deuterium (δD); and (d) oxygen ($\delta^{18}O$) isotopes for the stream and lake sampling locations, and for the hillslope surficial pounded water and overland flow. Plots e), f), g) and h) illustrate the evolution of water chemistry for the four-groundwater sampling piezometers, for sampling piezometers location refer to figure 1c and to black cross on figure 5b. The dashed line represents the means of each time series and the background grey hue represents the discharge of the adjacent hillslope tributary, for reference see Figure 2.

2.4.4 Ruptures and similarities in lake, stream and groundwater chemistry

Statistical analysis using PCA and Ward's methods highlighted several unique features of the stream and lake water chemistry time series. For the PCA, the first two principal components explained 96% of the variation in chemistry among the 18 sampling dates (Figure 7a). The correlation biplot shows that the correlation between stable water isotopes and EC was high, and that the variables EC and DOC were independent. The first PCA axis, associated with water isotopes and EC, reflects the progressive increase in the

value of each of these chemical variables during the monitoring period; from low EC, δD and $\delta^{18}O$ in early summer (D-2 to 16, lower left quadrant) to relatively high EC, δD and $\delta^{18}O$ by late summer (D-40 to 51, lower right quadrant). Along the second axis associated with DOC, lake samples were consistently higher than stream samples with exception of samples collected on Day 10 and Day 37, reflecting the generally lower DOC concentrations measured in the stream. Uniquely, the stream and lake samples collected on Day 19 and 21, corresponding to the major July 21-22 rainfall event, stand apart and reflect the spike in DOC values and drop in EC values observed for these sampling dates.

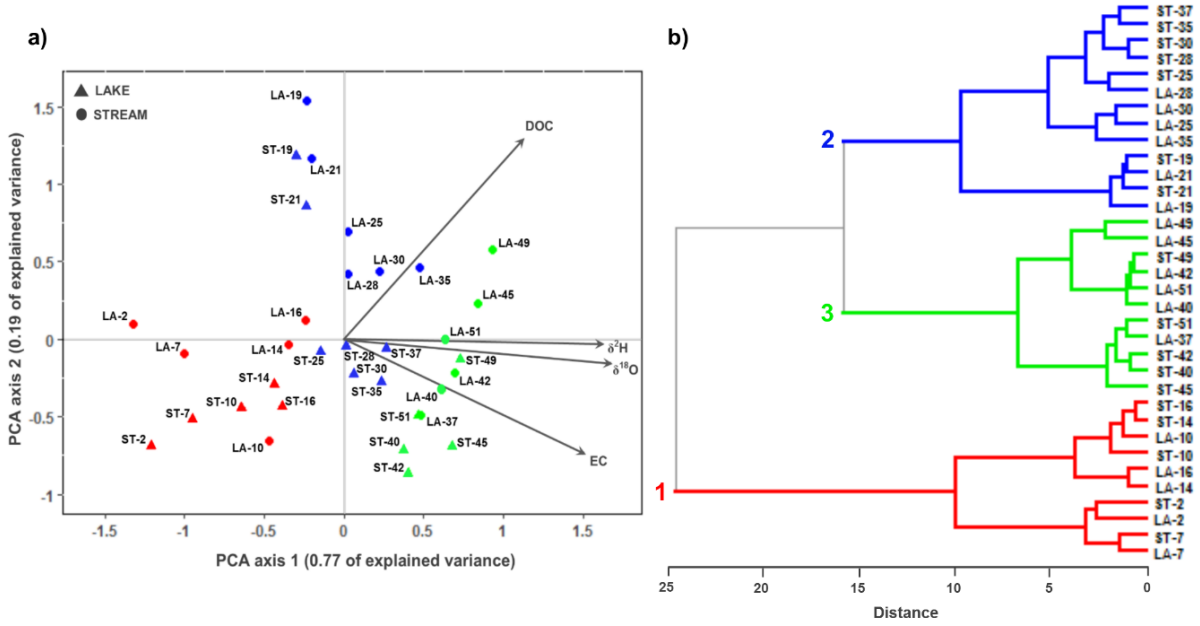

Figure 7. a) Principal component analysis and b) ward minimum variance clustering of the 17 stream (ST) and lake (LA) sampling dates. Descriptor axes (i.e., response variables; EC, DOC, δD, $\delta^{18}O$) are also illustrated in the correlation biplot a). Note that all stream and lake common sampling dates are clustered together and in the appropriate chronological order except for LA-37 and ST-37 corresponding to August 11th. Point colours in the PCA correlation biplot correspond to the colour of the three main groups of the Ward classification tree.

Analysis of the dataset using Ward's method shown that, with one exception, conjoint stream and lake sampling dates were clustered together (e.g., ST-2 with LA-2) in chronological order and were partitioned into three distinct period groups (group 1: D-2 to D-16; group 2: D-19 to D-35; group 3: D-40 to D-51). The notable exception being that of ST-37 and LA-37, which were respectively partitioned into groups 2 and 3 (Figure 7b). These latter samples correspond to the third day (August 11) of a 3-day 15 mm rainfall event, when water flowing was overland flow from approximately 35 m upslope and connected to

the stream downslope was punctually reactivated. The three main periods identified by the Ward clustering correspond respectively to: (i) early summer, characterized by multiple low magnitude rainfall events, (ii) mid-summer, associated with the peak streamflow event and the subsequent recession period; and (iii) late summer, corresponding to baseflow conditions punctuated by the aforementioned low magnitude rainfall event.

Regarding shallow groundwater chemistry, a PCA revealed that the water chemistry at GW4 was distinct from the other three sampling locations (Figure 8a). For the PCA, the first two principal components explained 79% of the variation in chemical variables (EC, δD, $\delta^{18}O$, and DOC) in the time series dataset. The first PCA axis is associated with EC, δD and $\delta^{18}O$ with negative correlation between the EC and both stable water isotopes. The second PCA axis is associated with DOC concentration. As with the surface water PCA, DOC is distinguished along the second PCA axis with weak to no correlation with the other water chemistry variables. For GW4 almost all sampling dates cluster into the upper-left quadrant. Sites GW1 and GW2 are clustered together whereas GW3 sampling dates are distributed across the reduced space. Though not as obvious as the temporal trend in surface water chemistry along the first PCA axis, the groundwater chemistry showed a slight trend along the first PCA axis from the upper-right quadrants (early snow-free period; green) to the lower-left quadrants (late snow-free period; brown). This trend is particularly evident for GW4.

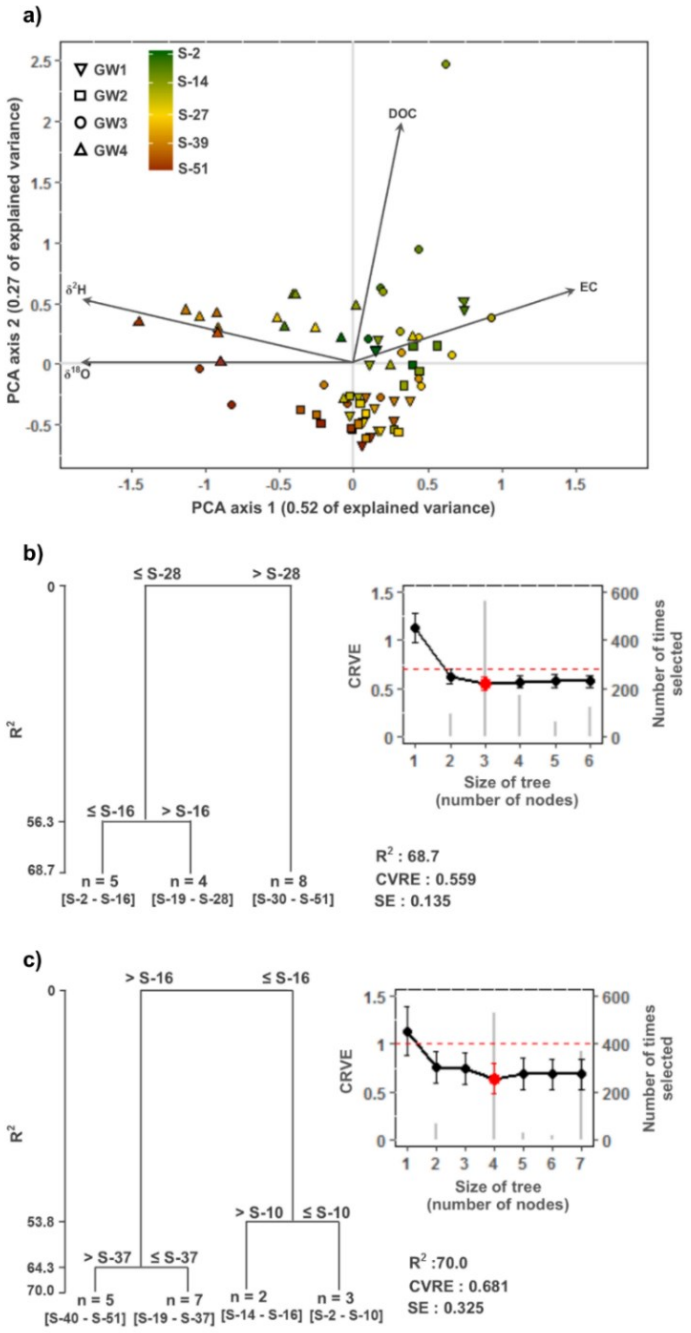

Figure 8. a) Principal component analysis of the 17 sampling dates of each groundwater sampling piezometer (GW1, GW2, GW3, GW4). Descriptor axes (i.e., response variables; EC, DOC, δD, $\delta^{18}O$) are also illustrated in the correlation biplot. Colour of point corresponds to the days of sampling. b) Time clustering by multivariate regression trees for the GW4 sampling piezometer site according to the four responses variables, and c) for the four piezometer sites according to their DOC time series. Groups delineated by the regression trees are identified as sample (S-) and the sampling day (e.g., S-2) and the vertical depth of each split on the classification tree is directly proportional to the variation (R2) explained by each split. For b) and c) Cross-validation relative error (CRVE) plots are illustrated to show the optimal size of tree (i.e., lower CRVE or red circle). The grey bars indicate the number of times the group models were selected as the lower CRVE during the 1000 cross-validation iterations.

Since unconstrained Ward minimum variance clustering not produced chronological clusters from the groundwater chemical time series, we performed time clustering by multivariate regression tree analysis (MRT) to identify distinct periods from the groundwater chemistry that could be (1) compared to surface waters chemistry and (2) associated with different drainage processes. As PCA results revealed the seasonal pattern was strongest at GW4, and because DOC was the response variable that individually explained the greatest portion of variance among sites, we performed MRT analysis on: (1) the GW4 sampling site with EC, δD, $\delta^{18}O$, and DOC as response variables (figure 8b), and (2) for the four piezometer sites according to their DOC time series (figure 8c). Cross-validation results show that the optimal tree size (group model with lower CRVE) for the time-clustering of GW4 and for the four piezometers, correspond respectively to three and four groups models. The first MRT explained a total variance of 68.7% with a CVRE of 0.559 and with the three defined period groups corresponding to sampling dates: D-2 to D-16; D-19 to D-28; and D-30 to D-51. The second time-clustering of the DOC time series of the four sampling sites explained a total variance 70.0 % with a CVRE of 0.681 and with four defined period groups corresponding to sampling dates: D-2 to D-10; D-14 to D-16; D-19 to D-37; and D-40 to D-51. The period-groups defined by MRT analysis of the groundwater chemistry data shows slight distinctions in the exact partitioning of the period-groups, but they show a general partitioning of the groundwater chemical time-series into early, mid and late summer periods; a division similarly identified in the surface water time-series data described above.

Analysis of variance (ANOVA) of the sampling periods defined by the first MRT time clustering revealed that at the beginning of the monitoring period (D-2 to D-16) there was little variance in the four response variables (EC, DOC, δD, $\delta^{18}O$) between the 4 shallow groundwater sampling sites, with the exception of EC at GW4. However, by late summer (D-30 to D-51) only GW1 and GW2 showed similar water chemistry. GW4 was distinct from GW1 and GW2 for all four water chemistry variables; and from GW3 for DOC and EC. GW3 was distinct from GW1 and GW2 for DOC. The post-hoc analysis of the periods defined through the second MRT time clustering indicated that during the mid-summer (D-19 to D-37) and late summer (D-40 to D-51) only GW1 and GW2 had broadly similar water chemistry. The difference in water chemistry between the remaining sites suggests that the

shallow groundwater sampled reported here either originated from different water sources or was subject to different flow processes.

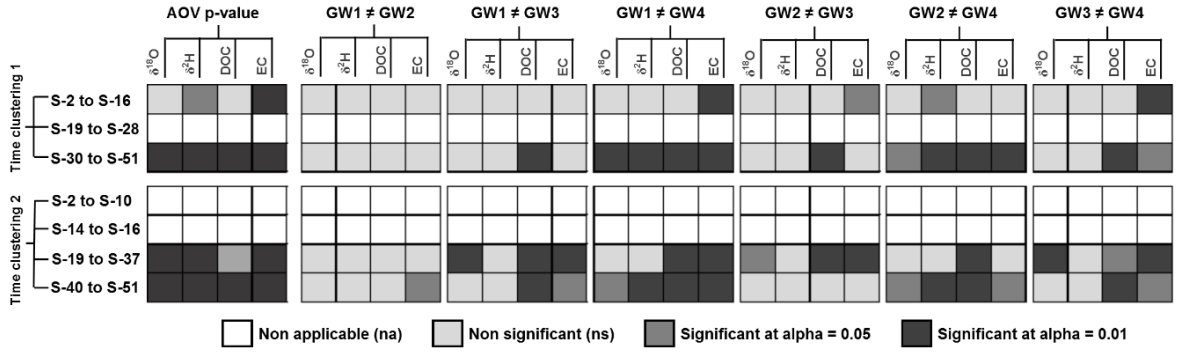

Figure 9. Results of Anova (AOV) and post-hoc analysis of the sampling periods computed through the MRT time clustering 1 (i.e., the GW4 sampling piezometer site according to the four responses variables) and 2 (i.e., for the four piezometer sites according to their DOC time series). Analysis of variance was not applicable for the periods S-19 to S-28, S-2 to S-10 and S-14 to S-16, since the number of observations within the periods were smaller or equal to the number (4) of groundwater sampling sites.

2.5 Discussion

2.5.1 Ground saturation and thaw patterns

Water level measurements presented in this study revealed that the active layer saturation remained close to the surface throughout the monitored period. Yet, larger spatial variability in WLRGS emerged latter during snow-free period, with locally higher/positive WLRGS in the central portion of the instrumented hillslope. Thaw depths during our monitoring period evolved from shallow and spatially uniform to deeper and spatially irregular. The resulting frost table topography was then characterized by a smooth microtopography and a concave profile early during the snow-free period, while a levelling of the frost table elevation over the monitored period was observed, as well as the emergence of localized depressions, especially marked on the hillslope centre, corresponding the area of high WLRGS. Thawing patterns observed over the summer led to a levelling of the frost table elevation over the summer, as well as the emergence of depressions, especially marked on the hillslope centre where high positive WLRGS were observed.

Observations of uneven thaw and development of an irregular frost table are supported by the study of Guan et al., 2010, conducted in three different environment types of the discontinuous permafrost region. Even if the observed snow-free and thaw periods started earlier during the year for the aforementioned than the present study, frost and water table depths remained relatively close below the ground surface (< 2 m) and site characteristics (i.e., organic cover thickness or deposit type) were, especially at the valley, similar to the present study. (Guan et al., 2010) clearly linked soil moisture conditions, subsurface flows and patterns of thaw depths and observed in areas of greater soil water content due to the enhancing transfer of thermal energy via heat advection. In less recent studies, but conducted on Arctic tundra hillslope underlain by continuous permafrost environments, Woo and Steer (1983) and Young et al. (1997) observed that deeper thaw was located in area prone to collect subsurface drainage. Hinkel and Nelson (2003) also highlighted the interannual variability in wetness conditions to explain the problematic of predicting circumpolar active layer thaw depths. Thought, regardless the landscape type or similarities with the present studied hillslope, wetness conditions seem to be one the key element for the understanding of thaw patterns.

In most of the studies investigating the evolution of active layer saturation conditions through the thawing period (Quinton and Marsh, 1999; Wright et al., 2009; Young et al., 1997) a lowering of the water table along with the deepening of the frost table and/or more variable degrees of active layer saturation were observed depending on water inputs. In comparison the present study showed that active layer saturation was always close or above ground surface. This is mainly attributable to the fact that we concentrated our measurements within the footslope portion of a bowl-shaped hillslope and that all hillslope drainage was directed toward our instrumented area. In this context, our site dynamics approach the lower hillslope or riparian hydrological zones described by van Meerveld et al. (2015) or Jensco et al. (2009), which can act as a buffering zones or transmit more quickly water from the hillslope to stream following wetness conditions and its storage capacity. This resolution allowed to confirm the field observations and simulation of Wright et al. (2009), that subsurface drainage directions can change as the thaw progress, to be directed toward depression formed in the frost table. Even if conducted in the discontinuous permafrost zone, links between Wright et al. (2009) conclusions and the

dynamics observed here can be made, since thick peat cover at their studied site allowed consistent permafrost cover compared to surrounding permafrost-free terrains. Water and frost table depths observed in that study were also greatly similar with depths measured in the present study and comparison are even more interesting that very few studies involving water and frost table depth measurements have been conducted at this resolution. The important thaw observed between July 23rd and August 5 fit well with the increase of air temperature, which was twice warmer than the previous 2 weeks and increasing of saturation conditions, with a hillslope entirely saturated on July 24th and high saturation conditions probably maintained the following days due to upslope drainage. Once again, observations highlighted the great importance of subsurface flow at the interface with the frost table on active layer thaw patterns.

Maps of hillslope saturation conditions (Figure 3) along with the transects showing the evolution of water table slope profiles (Figure 5) suggests for their part that (i) water drainage on the hillslope is directed toward the major depression that formed mid-slope following the major rainfall event of July 21-22, but also (ii) that the important ridge formed in the frost table downslope seem to impede subsurface flownet/flowpaths linking upslope to downslope areas (Conveyance of water downslope / to the stream) and enhanced the accumulation of water, resulting in above ground surface water level midslope. Three key patterns in our results corroborate these conclusions; (1) saturation increased mid-slope while a decrease in saturation was observed elsewhere across the hillslope, (2) water volume within the active layer was consistently higher on the upper than the lower portion of the hillslope, (3) water table was measured above ground surface just upslope of the frost table ridge, but remained below ground surface downslope.

2.5.2 Water chemistry as an indicator of water sources and potential hydrological connections between the hillslope and the adjacent stream

The stream and lake water chemistry evolved similarly throughout the monitored period, which was predictable, since the stream is mainly fed by the lake discharge and there is no other permanent surficial water contribution into the stream between lake discharge and the sampling location on the stream. All common stream/lake sampling dates were clustered together within three main periods; early (S-2 to S-16), mid (S-19 to S35) and late (S-40 to S-

51) summer, suggesting no significant differences between the lake and stream according to the trend present in the chemical time series, with the exception of the sampling date corresponding to the August 15 mm rainfall event (S-37), which will be discussed later in more details.

In early summer measured values of the geochemical and isotopic tracers analyzed were progressively increasing and suggest a contribution of water that has undergone greater exchange with soils than snowmelt water contributions which had most likely a greater importance during the preceding weeks (Koch et al., 2013). The major contributive areas of the lake are characterized by similar structure than the instrumented hillslope (i.e., organic surficial layer, underlying by a mineral layer) and thaw measurements showed that, at that time of the summer, frost table was already residing within the mineral layer, but remained shallow and smooth allowing the water table to easily reach the organic layer. Contribution to surface water of both subsurface flows originated from the mineral and that acquired more solute materiel or from organic soil layers that mobilized soil carbon could then explain respectively the increasing of the lake/stream water EC and DOC concentration then observed (Koch et al., 2014).

The midsummer period is punctuated by the major rainfall event of July 21-22nd and associated to a sudden drop of the water EC and rise of DOC, suggesting a greater contribution of water as overland or flow into the surficial organic layer (Carey and Quinton, 2005). The lake/stream δD and $\delta^{18}O$ water isotopes are not subject to significant changes during that period, but slightly increase which can be attributable to the slight differences of isotopic signature between summer rainfall and baseflow water that have been previously observed within the Niaqunguk watershed (Kjikjerkovska, 2016; Obradovic and Sklash, 1986). Throckmorton et al. (2016) observed similar isotopic signature of summer rainfall and water sampled from the active layer in late summer, they suggested that since the active layer remained frozen during snowmelt and that possible contributions from active layer ice melt are slight and occur slowly over multiple months, incoming summer precipitation essentially dominates the active layer water balance.

During the late summer period, the concentration of all geochemical tracers measured in both stream and lake stopped to increased, but stabilized to the higher measured EC values and isotopic concentration over the summer. Theses condition are similar to those observed

during the baseflow period of Arctic streams previously studied and are attributed to a smaller contribution proportion of water contributions from surficial flow paths and greater contribution from water flowing through the mineral soil layer (Koch et al., 2014; McNamara et al., 1997). Agreement between stream and lake chemistry throughout the monitored period suggests two dynamics; (1) the contribution of hillslope runoff to stream was too limited to significantly change the surface water chemistry between the lake and the stream sampling location or (2) that chemistry of runoff coming from the hillslope and lake water evolved similarly, and therefore runoff contributions didn't lead to significant change in water chemistry. Here we argue that both dynamics are applicable, but depend on hillslope saturation conditions, thaw patterns and rainfall events. It has been shown that chemistry of shallow lakes in the subarctic region depends on their water sources contributions, which in turn rely on the landscape and climatic conditions of the region (Balasubramaniam et al., 2015). Thus, as mentioned before the lake drained area is greatly similar to the hillslope characteristic. Lakes can also maintain sustained contributions during dry periods or act as buffer for surficial runoff (Woo and Mielko, 2007), thus during specific conditions, such as intense rainfall events surficial runoff could be generated quickly from hillslopes adjacent to stream, but increasing in lake discharge might be delayed due to the filling of lake storage capacity.

Chemical analysis of groundwater revealed higher EC and generally higher DOC concentrations than stream and lake water, whereas their isotopic signature fitted with the range of late summer surface water isotopic values. Observations differed about the possible isotopic and geochemical mixing between water sampled within active layer depths of tundra hillslopes, while some observed minimal mixing between water residing within the surficial organic and underlying mineral layers (Throckmorton et al., 2016) and others highlighted uncertainty regarding the degree to which water sampled from the active layer saturated zone can be used to distinguish both layers contributions (Carey and Quinton, 2005).

Since our sampling piezometers were maintained at the frost table interface within the mineral layer throughout the monitored period, there is no objective of defining clear organic or mineral end-members, but rather distinguish the chemical signature of potential subsurface flows contributions from the lake or overland flow water. The suggestion of greater relative contributions of subsurface flows within the mineral to surface water in late summer is

supported by surface water chemical signature approaching range of values measured in groundwater sampling piezometers. Since no significant change are observed between the lake and the stream at that time, we, however, cannot confirm a contribution of the hillslope to stream, but rather suggest that chemistry of the hillslope runoff was similar to the water that contributed to the upstream lake, which didn't lead to significant change in water chemistry.

As for the generally lower DOC concentration in the stream compared to the lake water, it can be attributable to DOC loss through hyporheic exchanges or mineralization (Battin et al., 2003; Vonk et al., 2015) during the course of water between the lake and the stream location rather than a contribution from the hillslope, since DOC concentration measured from groundwater or either surficial pounding water/overland flow sampled at the end of the monitored period show equal or higher concentration than the lake water. However, statistically significant difference in the stream and lake water observed on S-37 suggest a punctual contribution of water from the hillslope to the stream, supplied by different water sources or exposed to different flow paths that the water supplied the lake at that time of the summer. On sampling date S-37, that correspond to the 15 mm rainfall events of August 11th, significantly lower EC and depleted $\delta^{18}O$ are observed for the stream water, suggesting a contribution of newer water that didn't undertake subsurface flow paths into the mineral layer (Vonk et al., 2015), between the lake and stream sampling location. Sampling of surficial pounding water on the hillslope few days after that event, showed for their part significantly lower EC values than the stream/lake, but no significant differences in Isotopic signature. Since our instrumentation of the foot of a bowl-shaped hillslope confirmed that high saturation conditions were maintained during dry periods, we suggest here that the rainfall event reactivated the hillslope contribution to stream via saturated overland and that lower saturation conditions within the lake contributive areas, due to less conducive topographic settings (see Figure 1b), didn't allowed overland flow contributions but rather water infiltration, which could then explain the differences in chemistry between the lake and stream water for this sampling date. Similar dynamic observed by Roulet and Woo (1988), who stated that due to the great infiltration capacities of organic soil, minimal runoff occurs until the soil saturates and the water table rises above the surface.

The important intra and inter variability in groundwater chemistry sampled in the upslope to downslope piezometers appears to support the dynamics highlighted by (Carey and Quinton, 2005), whereby as water drains down the hillslope through the saturated layer, it encounters a wide variation of depth positions and possibly different soil layers, and even if all our sampling piezometers were located within the mineral layer groundwater geochemical and isotopic signature might vary seasonally and one from the others. Time clustering allowed to divided groundwater chemical time series in non-arbitrary periods, which are relatively close to period identified surficial water chemistry and suggest that ruptures in groundwater chemistry were partly influenced by similar meteorological, hydrological and geomorphological conditions of those influencing the stream/lake water chemistry. AOV conducted on identified groundwater periods also revealed that on early summer no significant chemical differences were present among groundwater sampling sites contrasting with the marked differences between piezometers groundwater chemistry that emerged in midsummer and increased in late summer. Differences in groundwater chemistry was especially marked between piezometer sampling site GW4, located downslope of the ridge that formed in the frost table and GW1-GW2 located on the upper portion of the instrumented area. This pattern fit well with the evolution of the frost table topography and since groundwater was sampled in piezometers maintained at the frost table, suggest either a rupture of hydrological connection in water draining at the frost table interface or a divergence of subsurface flow paths between upslope and downslope of our instrumented area. Finally, progressive decreasing in measured DOC concentration and δD and $\delta^{18}O$ isotopes enrichment observed for all groundwater sampling piezometers can be associated with the deepening of the frost table and flow paths with limited contact with the organic-rich layer important source of carbon (Mu et al., 2017), and longer flow paths or storage enhanced isotopes enrichment (Lamhonwah et al., 2017).

2.5.3 Inferring hillslope drainage dynamics from saturation, thaw and chemistry patterns

This study does not aim to present direct measurements of the surface and subsurface flows on tundra hillslope, thus by combining frost table depths and active layer saturation measurements with geochemical isotopic tracer's analysis, this work suggests that thawing patterns and wetness conditions observed during our study period were influencing the

transfer of water from hillslope to the adjacent stream. We can first identify distinct periods based on hydrometeorology conditions, maps of active layer saturation and thaw patterns, as well as water chemistry analysis;

- Period 1 (July 6 to 20 or days 1 to 15): multiple small rainfall events led to medium saturation conditions. The hillslope was drained through both mineral and organic flows allowed by the frost table that shallow and smooth and the water table that was maintained close to ground surface.
- Period 2 (July 21 to August 4 or days 16 to 30) a major rainfall event occurred above ground surface water level were observed on almost the entire hillslope. The frost table residing relatively shallow and smooth.
- Period 3 (August 5 to 9 or days 31 to 35) correspond to the tributary baseflow and a rain-free period during which the hillslope drained and saturation conditions significantly decreased except in the hillslope center. Thaw increased unevenly across hillslope and were especially marked mid-slope. Emergence of statistically significant differences in groundwater chemistry sampled from piezometers upslope (GW1, GW2) and downslope (GW4).
- Period 4 (August 10 to 14 or days 36 to 40) punctual rise of streamflow on a little rainfall event, rise of the saturation conditions were especially marked on the centre and upper portion of the hillslope. Thaw depths and frost table heterogeneity continued to increase. Temporary rupture between stream and lake water chemistry.
- Period 5 (August 15 to 25 or days 37 to 51) end of summer marked by baseflow conditions at beginning and a relatively important rainfall event on the second portion of the period. The saturation conditions continued to increased on the hillslope centre, but were also generally higher on the upper than lower portion of the hillslope. The frost table depth continued to increase.

The first key concept on which the aforementioned dynamics relies is the two layers flow system is clearly described by Quinton and Marsh (1999) or Carey and Woo (2001). Here we recall that piezometers were installed in area of thin organic cover (0 - 10 cm) and thus, based on this concept, water level measurements when piezometers screen reside within the mineral layer would not capture faster drainage through the surficial organic layer, but the

saturation relative to the surface of the mineral layer. However, if positive or above ground surface water levels are measured in the piezometer, they should be associated to surficial pounding water that allowed the piezometer hydraulic head measured at the frost table interface to stabilize with the surface saturation.

Woo (2012, Figure 6.38) well described the potential influence of hillslope profile on the drainage of shallow subsurface flow and their interactions with surficial runoff. In the presence of surficial runoff convex slope segments should enhance the infiltration of water, while when the water table resides close to the surface, concave segments will enhance the exfiltration or seepage of subsurface flows. Based on that conceptualization of slope profile controls on drainage, the convex - concave - slightly convex slope profile of the interpolated mineral layer surface should then favour mid-slope seepage (exfiltration) and then seeping out (infiltrating) further downslope at the lower slightly convex portion of the profile. Moreover, except during period 2 when the water table was significantly above the mineral layer surface across the entire hillslope, the water table position relative the mineral layer surface is in agreement with the process suggested by the mineral layer surface profile, since positive water levels are observed consistently observed midslope and water table residing below the surface of the mineral layer downslope.

During the monitored period, surficial runoff contributions from the hillslope to stream were suggested from either water level significantly above ground surface across all hillslope (period 2) or from rupture between lake and stream chemical time series (period 4). Even if constant water levels above ground surface were observed in the hillslope centre during the last portion of the monitored period no significant change were observe between lake and stream chemistry and water table resided below ground surface on the downslope portion of the hillslope. That highlighted the potential control of the surface microtopography on the hillslope drainage and water levels above minerals layer surface should not be associated automatically to saturated Hortonian flow due to surface microtopography or roughness that offer resistance to horizontal flow downslope. Besides, Carey and Woo (2001) showed on permafrost slopes for the subarctic region but with similar soil layers (i.e., mineral layer with an organic cover layer) than the present study, that when the water table reached the surficial organic layer the delivery of water downslope was controlled by the preferential flow paths and the interconnection between depressions in the surface organic layer. Thus, here we also

argue that the infiltration capacity needs to be completely filled, such as during the rainfall event of July 21-22nd (period 4) to a allow the delivery of water downslope through the preferential flow paths and the interconnection between depressions in the surface organic layer. On the contrary, if the infiltration capacity of a particular slope segment is not reached, such as we observed for the downslope convex section during dryer periods, that will favour the seeping out of water and prevent the delivery of water downslope through surficial flow paths. We also suggest that the influence of surficial microtopographic on hillslope drainage is similar to the fill-and-spill drainage over frozen soil describe by Cole and McDonnell (2018), but here faster surficial flows are allowed by the filled soil infiltration capacity instead of the low infiltration capacity of frozen soil.

The last dynamic to point out in relation with the aforementioned controls on the hillslope drainage is the effect of an uneven thaw and the emergence of important depressions and ridges in the frost table topography. Early during the snow-free period the frost table topography as the profile of the water table remained relatively smooth. It's clear that slope profile and depression in the surficial organic could have enhanced the accumulation of water midslope, which in turn led to localized thaw and the formation of a depression in the frost table. Young et al. (1997) had already identified that depression formed in the frost table enhanced higher saturation due to the drainage of subsurface flows toward the depression, Wright et al. (2009) observed similar dynamic but added that emergence of depression within the frost table led to a disconnection of subsurface flows and referred to the fill-and-spill to explain the reactivation of connections between depression when a certain saturation degree is reached. Here we add that uneven thaw can also lead to the formation of ridges in the frost table, which can have an impeding effect on subsurface flownet/flowpaths linking upslope to downslope. On the studied hillslope that process enhanced the accumulation of surficial pounding water that only connected downslope when a certain saturation threshold was reached.

Water movement has substantial implications for the dynamics of permafrost landscapes. Here, our high spatio-temporal resolution mapping of thaw depths and wetness conditions across a hillslope, linked with chemistry analysis showed that position of the water table, the surface and frost table microtopography, should be considered as a whole and not separately to understand both hillslope thaw and drainage dynamics. With the exemption of

the dynamic state of the frost table depth in environment undergoing seasonal thaw, our results also have a great implication at broader scale to help the understanding of hillslope drainage and hillslope-stream connections in all environment where an impeding layer (i.e., bedrock, fine-grained low-conductivity layers or seasonal frost) control the infiltration and movement of subsurface flows. If the fill-and-spill mechanism has been used to explain the drainage over frost table depressions (Wright et al. 2009) or frozen surficial soils (Coles and McDonnell, 2018), the connection between wetlands system (Brannen et al., 2015), for hillslope underlain by bedrock (Spence and Woo, 2003, Tromp-van Meerveld and McDonnell, 2006), or low conductivity layer (Ali et al., 2011), here we add that if sufficient soil saturation conditions are reached that could lead to fill and spill mechanism over surficial microtopography and the transmission of quick surficial flow downslope.

2.6 Conclusion

Hillslopes drainage dynamics in permafrost environments stand out from dynamics observed elsewhere due to the dynamics state of the active layer. By coupling measurements across a hillslope of thaw depths, water table elevation with chemistry analysis of different water sampled within the studied hillslope-stream system, our work highlighted the importance of integrating the thawing patterns and the evolution of the resulting frost table topography with wetness conditions and surficial microtopography to understand the drainage of permafrost affected hillslope. Feedback between the water distribution controlled by hillslope surface characteristics early on the snow-free period and the development of depressions and ridges in the frost table, which in turn will influence the distribution of water across the hillslope latter on summer was demonstrated as a key mechanism regarding the control of the hillslope drainage. Beyond improving our understanding of the key elements that need to be taken into account to understand the water delivery on permafrost hillslopes. We observed that delivery of water from upslope to downslope could be impeding mid-slope due to the filling of frost table depressions throughout dryer periods and that wetter conditions could thus reactive localized water contribution downslope via surficial drainage throughout the organic layer. The seasonal variation in the amount of water and the processes

controlling the delivery are also highlighted by the rupture of agreement between the stream and lake chemical time series. The stream and lake water chemistry suggested a transition from a system dominated by water contributions via organic flow paths during the early summer to a dominance of contributions via minerals flow path latter during summer. The antecedent saturation conditions associated with an unusually high July rainfall event could have led to much greater active layer saturation conditions that might normally occur during the later summer periods. A longer time window, covering several years would be required to better assess inter-annual variability in the hydrological processes discussed here, but we may advance that localized increasing in active layer thaw depth combine with dry summer will greatly limit the hydrological connection between slopes and stream. This research provides a unique resolution of frost table, water table and how they interact to influence the water delivery from landscapes to surficial water for a region where knowledge on hydrological dynamics remained limited. The generated knowledge will be essential in the development of models aspiring to predict the dynamics permafrost environment freshwater systems and the anticipated impacts of climate changes.

Chapitre 3 - Article 2

Titre : *Detailed geochemical and streamflow monitoring to understand the evolution of water sources and dominant hydrological processes during the early flow season of the Niaqunguk River, near Iqaluit, Nunavut.*

Auteurs : Gabriel Chiasson-Poirier, Jan Franssen, Mélissa Lafrenière

Ce deuxième article n'avait pas encore été soumis pour publication au moment du dépôt de ce mémoire. Il s'inscrit dans la continuité de l'article présenté au chapitre 2, en utilisant les connaissances acquises à l'échelle d'une pente, afin de mieux comprendre les dynamiques émergentes à l'échelle du bassin versant de la rivière Niaqunguk.

Le principal objectif de ce deuxième article est d'identifier quelles sont les principales sources en eaux pour la rivière Niaqunguk, ainsi que de caractériser l'évolution des processus contrôlant les écoulements de l'eau dans le bassin versant de la rivière au cours de la période de dégel. Pour ce faire, des mesures hydrologiques terrain et des analyses chimiques de l'eau ont été analysées en lien avec des index morphologiques et à travers différentes méthodes statistiques. Quatre périodes hydrologiques distinctes correspondant au début de la fonte des neiges, à la récession de la fonte, au débit de base et aux crues estivales ont été délimitées selon les caractéristiques physicochimiques de l'eau échantillonnée dans le bassin versant de la rivière Niaqunguk. Les principaux processus associés à ces périodes sont respectivement la contribution de la fonte des neiges, la distinction entre la contribution des neiges résiduelles et des lacs, les écoulements à travers la portion minérale de la couche active et les écoulements en surface à travers la microtopographie de la couche organique. Le rôle important joué par les lacs dans le bassin versant a aussi été mis en évidence.

Le design expérimental et les mesures hydrologiques ont été élaborés de façon conjointe entre Gabriel Chiasson-Poirier et Jan Franssen. Tandis que Mélissa Lafrenière a aussi contribué de manière significative par ses conseils prodigués en lien aux analyses chimiques et par le prêt de matériel.

Référence: Chiasson-Poirier, G., Fransen, J., Lafrenière Mélissa Detailed geochemical and streamflow monitoring to understand the evolution of water sources and dominant hydrological processes during the early flow season of the Niaqunguk River, near Iqaluit, Nunavut. En preparation.

Abstract

Despite recent advances in the hydrological knowledge of permafrost regions, precise predictions or modelling of climate-related changes remains difficult without fine scale characterization of landscape heterogeneity or calibration changing the true landscape structure. That highlight the deficient understanding of hydrological dynamics in these regions. This research aims to identify the importance of different water sources contributions to the Niaqunguk River, Iqaluit, Nu and the evolution of dominant hydrological processes through the thawing season and in different wetness conditions. Using Ward clustering analysis of the water chemistry measured across the 24 sampling sites we identified four distinct periods, based on chemistry changes, which corresponding to; early snowmelt; snowmelt recession; baseflow and summer rainfall runoff events. During the early melt period, slight differences between sites for all chemical parameters analyzed were observed, water was then mainly supplied by snowmelt, but different flow undertaken by the meltwater were suspected to explain the slight chemical variation among sites. Other water sources became important during the snowmelt recession as some river tributaries were mainly fed by late lying snowpack and another by lake contributions. Lakes and pools along the river had great hydrological impacts, though their influence was greatly related to their geomorphic settings. If they were generally acting as a buffer for the snowmelt or rainfall runoff, the degree of buffering changed among lakes, they also maintained either sustained discharge which increased their relative contribution during baseflow of enhanced the storage and connectivity ruptures along the rive network. Other water sources and runoff processes such as subsurface flows contributions within the hawed mineral layer and spilling of water stored in surficial depressions were suggested by respectively an increasing water conductivity across the river network during baseflow and by localized $\delta^{18}O$ enriched water contributions during rainfall events. Knowledge developed here is essential for the actual understanding of the hydrological dynamics of Tundra watershed, improving our knowledge of these dynamics is also the best way to improve our ability to predict the impacts of climate changes on the hydrology of Arctic rivers.

3.1 Introduction

The Arctic has experienced important climatic changes during the second half of the 20th century, which still ongoing and are anticipated to increase over the next century (AMAP, 2013; Walsh et al., 2011). The potential impact on the Arctic terrestrial freshwater system are numerous; localized increase of total precipitation (Anderson et al., 2018), along with the rainfall relative contribution (Bintanja, 2018), river baseflow and total streamflow (St. Jacques and Sauchyn, 2009), active layer thickness and contributions to river flow (Walvoord and Striegl, 2007) and magnitudes of nutrient cycling and export (Wrona et al., 2016). Despite recent advances in the hydrological knowledge of permafrost regions (Woo et al., 2008), prediction or modelling of these changes remains difficult at the small basin and nested scales (i.e., sub-basin, reach or hillslope) due to lack of understanding of interaction between processes controlling the water movement across landscapes and their link with wetness conditions (Bring et al., 2016). This type of detailed knowledge is necessary to assess the spatiotemporal extend of the expected changes to the hydrology of Arctic rivers.

Three key principles have recently been suggested to guide our approach of watershed hydrological dynamics characterization; (1) instead of focusing on the small-scale heterogeneity of the landscape (i.e., high-calibrated models), we may explore the process interactions that underlie the heterogeneity and complexity of watershed scale hydrology (McDonnell et al., 2007), (2) identifying the patterns of seasonality in river discharge and water chemistry could provide important indication of the temporal variation of runoff generation processes and their link with seasonal patterns in wetness conditions (Ali et al., 2014) and finally (3) characterizing the processes nested at different scales (i.e., water track, creek, sub-catchment) using field based streamflow and isotopic measurements should allow to better understand the dynamics emerged at the catchment scale (McNamara et al., 1998, 1997).

Studies that used one or many of these principles in their approach of Arctic river systems have already detailed key controls on the water delivery from landscapes to streams. Using isotopic tracers, some studies assessed the relative contributions to streamflow of melt water (event water), but also from water stored within the watershed (old water) in the fall and released in the spring when the soil remains almost entirely frozen (Carey and Quinton, 2004; Obradovic and Sklash, 1986). The increase of subsurface flow contribution as the surficial

soil layer (active layer) thaw during the summer and the two-layer flow system controlling the drainage of hillslope comprised of a mineral layer (slow flow) covered by an organic layer (fast flow) characteristic of tundra environment as also been detailed (Carey and Woo, 2001; Quinton and Marsh, 1999). Many already used the fill-and-spill concept to explain the reactivation during rainfall events of the connectivity between hillslopes and streams or between lakes, due to the spilling of waters downslope or downstream, while during dry periods sinks in the landscape or lake storage capacity could enhance the rupture of hydrological connectivity (Coles and McDonnell, 2018; Spence and Woo, 2003; Woo and Mielko, 2007). The timing or distribution of the above described processes thus differs from catchments located from one region to another (Bring et al., 2016), and even if we argue that process characterization should prioritize over the micro-scale characterization of landscape heterogeneity, there is still a need for further studies on the hydrological processes in Arctic watersheds and so for diverse landscape stetting. This need is particularly true for the Niaqunguk watershed, since hydrological dynamics of eastern Canadian low-Arctic catchments have been investigated in a limited way compared to other high-Arctic or western Arctic locations (Déry, 2008).

This study investigates, for the Niaqunguk River, a small watershed near Iqaluit, Nunavut, the evolution, thought the thawing period, of the dominant water and processes controlling the delivery of water from landscape to surface waters. To that aim, we investigated the variation in water chemistry sampled at 24 location across the river network using computed landscape proxies and advanced statistical analysis, the emerging dynamics were also linked with discharge measurements at sampling sites. The specific research objectives are to: (i) identify distinct hydrological periods from streams water chemistry time series, (ii) for the delineated hydrological period, determine if landscape features of spatial patterns can explain the chemistry variation among sampling sites and (iii) from the emerged patterns, investigated further which processes control the water contribution among sites and how they are related to wetness conditions. This knowledge is essential to assess how and when the landscape is hydrologically connected with Arctic river systems, and to eventually help our ability to predict the impacts climate-related changes on permafrost hydrology.

3.2 Methods

3.2.1 Site description

The Niaqunguk River is a fourth-order stream located northeastof the City of Iqaluit (63° 45' N, 68° 33' W) and draining an area of 58 km^2. This is a region of continuous permafrost with active-layer thickness varying between 1 and 2 m under natural ground and maximum thaw depths are reached around the end of August (LeBlanc et al., 2015). Elevations range between sea level at the river outlet and 360 m at the headwaters. The topography of the watershed is characterized by longitudinal bedrock hills trending northwest that have been smoothed by glacial erosion (Squires, 1984). Two surficial geology maps exist for the area, a small-scale map (1:100 000) that identifies till blanket as the largely dominant surficial deposit type within the watershed (Hodgson, 2003) and a larger scale map (1 : 15 000) covering only the southwest portion of the Niaqunguk watershed(Allard et al., 2012) that identifies a wide variety of Quaternary deposits (e.g., till blanket and veneer, glaciofluvial deposits, undifferentiated organic deposit, alluvial floodplain sediment). An end moraine forms the eastern border of the watershed, and boulder fields are abundant (~30% by area) adjacent to the moraine. The valley bottoms are covered with alluvial and organic deposits, while till deposits (i.e., blanket or veneer) are predominantly found on hillslopes, and ridge tops are mainly bedrock outcrops (Chiasson-Poirier et al., 2016; Hodgson, 2005).

The hydrological network of Niaqunguk River comprises three main tributaries (i.e., East, Central, West) with a fourth-order segment downstream of their confluence (Figure 10). The west tributary flows mainly through a depression between two bedrock ridges and drains an area of 13.2 km^2. The central tributary drains an area of 21.3 km^2, while the Eastern tributary drains an area of 12 km^2. The two largest lakes are situated within the Eastern subwatershed. Streamflow in the Niaqunguk River usually begins in May and ends in October, with peak annual discharge (~ 9 m^3/s) typically observed in early June during the spring snowmelt (Kjikjerkovska, 2016; Water Office Canada, 2019). Our study was conducted during the months of June and July when mean rainfall precipitation is 24 and 54 mm respectively; mean annual precipitation is 404 mm with 57% as snow (1973-2010; Environment Canada, station #2402596).

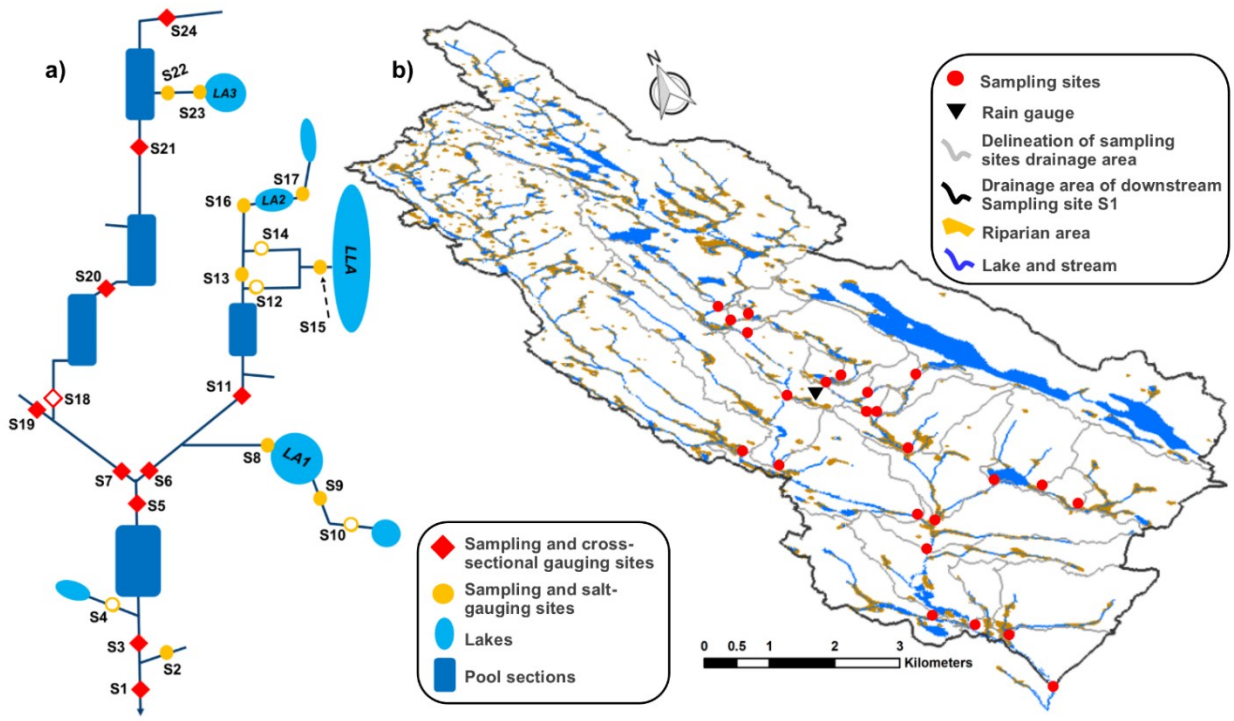

Figure 10. Schematic of hydrometric monitoring network (a) and oblique map (b) showing sampling site locations within the Niaqunguk River watershed, Iqaluit, Nunavut. Symbols on (a) indicate sites with (solid dot) and without (open circle) a continuous discharge record. Schematic is not to scale and shows only the important hydrological features along the network.

3.2.2 Sampling design

To the aim of using water chemistry analysis to identify ruptures along the Niaqunguk River network that could indicate different water contribution or change in water chemistry through time indicating different water flow paths, water samples were collected manually from 24 fixed locations distributed across the southern half of the river network (Figure 10a and b). Thirteen synoptic sampling events were completed between June 13 and July 30, 2017. All sites were sampled within a four hours period so that each sampling event provided a snap shot of streamflow chemistry across our monitoring network. Water was collected in 500 ml high-density polyethylene bottles, and was subsequently analyzed for stable water isotopes (δD, $\delta^{18}O$), dissolve organic carbon (DOC) and ions (Mg^{2+}) to provide insight into drainage processes along the Niaqunguk River network. Note that results for DOC concentrations are only available from June 26 to July 30 (also not available for the sampling of June 29) and that water isotopes results are not available for July 7.

Water samples for isotope and ion analysis were filtered through 0.22 µm PVDF filter membranes with a reusable polysulfone vacuum filtration unit and stored in 25-ml high-density polyethylene scintillation vials filled with no headspace. Water samples for DOC analysis were filtered through pre-combusted 0.7 µm glass fibre filters (GF/F, Whatman, Pittsburgh, United States) with a glass filtration apparatus and stored in 45 mL amber EPA vials fitted with Teflon-lined septa. All samples were kept refrigerated in the dark until analyzed at either at the FaBRECC laboratory at Queen's University or at the pedology laboratory at the Université de Montréal.

Water specific conductance (SpC) was measured in-situ at the time of sampling with a YSI PRO30 (YSI Inc., Yellow Springs, OH). Stable isotope composition (oxygen - $\delta^{18}O$ and hydrogen - δD) was analyzed with a liquid water isotope analyzer (Los Gatos Research, Mountain View, CA) and reported in parts per thousand (‰) relative to VSMOW (Vienna Standard Mean Ocean Water). The uncertainty ranges of this instrument are ±0.2 ‰ for $\delta^{18}O$ and ±0.8 ‰ for δD, respectively. DOC concentrations were determined using high-temperature combustion on a Shimadzu (TOC-V) organic carbon analyzer (Shimadzu TMN-1). DOC concentration was calculated as the average of three injections with standard deviation <0.1 % and coefficient of variance always <2%. Magnesium (Mg^{2+}) concentrations were measured byatomic absorption spectrometry (Lambda 1, Perkin Elmer, OakBrook, Illinois, USA).

3.2.3 Hydrometric measurement

Hydrometric data was collected at 19 of the 24 sampling sites (Figure 10a). Stream stages were monitored at 15 min intervals using either absolute (Onset U20water-level logger, ±0.05 cm accuracy, Bourne, MA; Solinst Levelogger 3001, water-level logger, ±0.03 cm accuracy, Georgetown, Ontario; self-manufactured pressure/logger sensors, see appendix A) or relative (WL16 Water Level Loggers, Global Water, Gold River, CA) pressure transducers. Absolute water levels obtained by subtracting atmospheric pressure measured at the closest air pressure measurements site (i.e., located either at the rain gauge station or a sampling site S9, see Figure 10) from total pressure recorded by the submerged pressure transducer. A rating curve was developed for each site by correlating site stage to site discharge. Depending on

stream morphology, measurements of discharge were made using either cross-sectional or salt-gauging methods (Figure 10a). Cross-sectional discharge measurements were made using an acoustic doppler velocimeter (FlowTracker2, SonTek, San Diego, CA), while salt dilution gauging measurements were made by measuring the stream water conductivity prior and after the slug injection of 100 mg of salt (NACL) in the stream. Following salt injections, measurements of the streamflow conductivity were made at 2s intervals using a YSI pro30 conductivity meter (YSI Inc., Yellow Springs, OH). To estimate the precision in our discharge measurements with cross-sectional gauging we repeated at two sites (i.e., S20, S21) three measurements per site each at near constant discharge (within less than 2 hours), the difference between these repeat measures was less than 1%. We also compared discharge estimates from salt and cross-sectional gauging at site S13; and the difference between measurements was less than 2%. Date of available discharge measurements, number of discharge measurements, rating curve relation type and significance of the relationship are presented in Table 3 for each site. Prior to the computation of the rating curves the measured water levels were smoothed using a loess smoothing span of 0.03 to remove the noise associated with sensor accuracy. The rating curves, measured and smoothed water levels for each site are provided in appendix B. Rainfall was measured with a tipping bucket rain gauge collector (TR-525I, Texas Electronic, 0.2 mm tip, ±1% accuracy) at a site centrally located within the Niaqunguk watershed (Figure 10b).

To compare among gauged sites both the discharge responses to rainfall events and streamflow during baseflow periods, we computed the event-based runoff (mm) for the drainage area (m^2) upstream of each gauging site. We computed the runoff at gauging sites for 4 specific event/periods: (i) the rainfall-runoff event of July 17-18; (ii) the rainfall-runoff event of July 27-28; (iii) the baseflow period between July 12 and July 17; and (iv) the baseflow period between July 21 and July 27. The rainfall-runoff events were delineated separately for each site, from the discharge observed at the beginning of the rise in flow to the return to this discharge post-storm (i.e., constant discharge method); this delineation all served to demark the baseflow periods between runoff events. To differentiate the relative water contribution among sites during the runoff period we calculated runoff volume to peak discharge for each event. We chose to use the discharge during the rising limb of the hydrograph so that we could include the July 27-28 event in our analysis for which we did not have discharge record to

baseflow recession at all gauging sites. Baseflow contributions were calculated from the discharge that marked the end of the previous runoff event (e.g., July 17-18 runoff event) to the discharged observed at the beginning of the following runoff event (e.g., July 27-28 runoff event). Here the aim was not to distinguish the runoff and baseflow contributions for a single stormflow event, but to related the discharges observed at network sites with: (i) discharge at adjacent sites; (ii) streamflow chemistry at these sites; and (iii) landscape characteristics within the contributing areas.

Table II. Computed landscape indices and suggested processes and/or implications for Niagunguk River hydrological dynamics.

Landscape indices	Suggested processes / implications	References
Drainage area (DA)	Scale related hydrological processes. Indication of uniform hydrological processes for the stations with smaller drainage area located further upstream along the hydrological network, and progressive change in dominant processes for stations with greater drainage area located in downstream direction.	Burgers et al., 2014; Galster et al., 2006; Hendriks et al., 2012; McNamara et al., 1998; Shaman et al., 2004)
Drainage density (DD)	Either (1) a faster response in stream chemistry at sites with great drainage density value due to shorter transit time for water to reach the streams, or (2) greater water concentrations from specific chemical variables enhanced for by high drainage densities.	Berger and Entekhabi, 2001; Carlston, 1963; Dingman, 1978; Horton, 1945; Preston et al., 2011
Lake proportion (LAKE)	Distinct water chemistry signature of lake fed streams due to lake filling and decreasing on water contribution relative to other sources, or inversely, maintained water contributions during dry period while other source contributions decrease.	Fergus et al., 2017; Martin and Soranno, 2006; Orlova and Branfireun, 2014; Pistocchi and Pennington, 2006; St Amour et al., 2005
Depth-to-Water proportion (DTW)	Computed from a threshold elevation-difference relation from landscape cells to the nearest water cell, the depth-to-water proportion within station drainage area can help to identify a greater storage potential or a postponement of water and solute contributions from hillslopes to stream.	Blume and Tromp-van Meerveld, 2015; Jencso et al., 2009; Murphy et al., 2009; Tiwari et al., 2017
Mean upslope contributive area (UCA) within delineated DTW area	Higher mean UCA values suggest riparian areas prone to greater saturation conditions and enhanced hillslope contribution to stream, while lower mean UCA values, suggest greater buffering against hillslope throughflow, but can also indicate a more persistent contribution of riparian groundwater to the stream.	Jencso et al., 2010; McDonnell and Beven, 2014
South exposed Drift area (DRIFT-SE)	A higher proportion of south-exposed drift areas within station drainage areas will suggest greater source of water during snowmelt which could lead to specific water chemistry signatures.	Pomeroy et al., 2003; Smith, 2018

3.2.4 Digital terrain analysis and landscape indices

We computed 6 landscape indices to investigate the relationship between landscape structure and streamflow chemistry. Pre-processing of a 1-m resolution digital elevation model (DEM) derived from WorldView-1 stereo-optical data collected in August 2008 (planimetric accuracy <40 cm, and vertical accuracy <50 cm, Budkewitsch et al., 2009) of the study area using ARC GIS (10.5, ESRI) proceeded as follows. First, the lake or pond areas were delineated using the Aspect tool which identifies the compass direction of the face of a downhill slope for each cell, perfectly flat areas (cells = 180^{O}) greater than 10 m^2 were assumed to reflect surface water (10 m^2 threshold area was conservative to discriminated flat ground area from surficial water). Secondly, the DEM was corrected to create a flow path compatible model, using filling depression algorithm, then flow direction and flow accumulation models were generated using the D8 algorithm (Jenson and Domingue, 1988). Subsequently, the Niaqunguk River channel network was topographically defined from the flow accumulation model using a flow initiation threshold of 0.2 km^2. Field validation showed that this procedure was accurate at defining permanent streams, without including water tracks or ephemeral streams. Visual inspections also allowed the correction of errors in the stream channel delineation that were associated with boulder field areas (Chiasson-Poirier et al., 2016). Landscape indices derived from the DEM are detailed below and summarized in table II.

Drainage area. In an idealized watershed where topography, landscape characteristic and hydrological processes are uniform we would expect a positive relation between discharge and drainage area (Burgers et al., 2014). However, in complex landscapes heterogeneous structure can lead to different residence times and flow trajectories and so variable streamflow geochemistry and biochemistry. Additionally, dominant hydrological processes are often related to a specific scale and for specific conditions the processes controlling the streamflow response can vary from headwater streams to downstream catchment (Shaman et al., 2004). For instance, chemical signature inherited of processes occurring in a large valley, important pool sections along the river network or in large lakes could not be associated to headwater sites even if water sampled at these sites present a similar chemical signature. Here, the statistical relevance of the drainage area to explain the variability in chemistry among the sampling stations will strictly emphasize that hydrological processes related to larger or smaller scale should be investigated further, in relation with other significant indices, to

explain the streamflow chemistry patterns. Drainage area for each sampling sites were derived from the filled 1 m DEM.

Drainage Density. The drainage density is a metric used to describe degree of landscape dissection by the hydrological network (Horton, 1945). Drainage densities are computed from the ratio between the total stream's length (km) and the drainage area of each sampling site (km^2). Studies have confirmed that drainage density is a key indicator of the hydrologic response, given the difference in velocity and residence time of water between the hillslopes and streams (Berger and Entekhabi, 2001). A positive correlation between drainage density and spatial extent of riparian areas has also suggested (Berger and Entekhabi, 2001). Preston et al. (2011), used drainage density in statistical models to identify areas of high delivery of total nitrogen and phosphorus to streams and explained that enhanced export of specific nutriment by soil wetness conditions that were likely to be higher in riparian along the channel network than on steep slopes or ridges.

Proportion of lakes. The lake index is derived from the proportion of sampling site drainage areas occupied by lakes of surficial water cells. The affect of lakes on watershed hydrological regimes is influenced by lake position within the network (e.g., upland, low land) and interaction (e.g., isolated, connected with streams of with lakes upstream) landscape with elements (Fergus et al., 2017; Martin and Soranno, 2006). Lakes storage potential is an important issue for hydrological modelling and estimation of river discharge, since advanced lake morphological knowledge are required to evaluate the lake volume and predict the lake storage or contribution to streamflow downstream (Pistocchi and Pennington, 2006). Lakes or ponds water chemistry is also influenced by hydrological processes (e.g., evapotranspiration, dilution) that can result in lake discharges with distinct chemical signatures (Mazurek et al., 2012; Morison et al., 2017). Lake affects on hydrological regimes may also evolve in response to changing climatic and wetness conditions. St Amour et al. (2005) and Orlova and Branfireun (2014) found that lakes and wetlands were a significant water source to streamflow of northern rivers during the summer baseflow period. From the dynamics identified above, the significance of the lake proportion index to streamflow discharge and chemistry could indicate a relative throughput from the lake in relation to other sources, due to either a filling of lake storage during rainfall events or a sustained spilling of lake stored water during dry period, explaining therefore the distinct streamflow chemistry for drainage are dominated by lakes.

Depth-to-water (DTW) index or proportion of riparian areas. The DTW index is used to represent the proportion of riparian areas within the catchment of each sampling site. A common method to delineate the extend of riparian areas is to use a threshold elevation-difference relation from landscape cells to the nearest water area (Jencso et al., 2009; Murphy et al., 2009; Tiwari et al., 2017). Here, we derived the extent of riparian areas or the DTW index, from a 1 m DEM and a threshold elevation distance value to the nearest water pixel (or DTW) smaller or equal to 1 m. The following equation was used to compute the DTW value of each DEM cells;

$$DTW(m) = \left[\sum \frac{dz_i}{dx_i} a\right] x_c$$

where $\frac{d_z}{d_x}$ is the slope change along the least slope path from any landscape cell to the nearest surface water cell i represents the cell along the path, a is 1 when the path crosses the cell parallel to the cell boundaries and $\sqrt{2}$ when it crosses diagonally, and xc is the grid cell size (1 m).

Because of their position at the intersection of bottom slopes and streams, riparian areas can act as a buffer for water and solute transit from slope to stream (Jencso et al., 2009). Riparian areas are generally characterized by deeper soils relative to hillslopes and hilltops and depending on the saturation conditions of the riparian area, runoff from hillslopes can either connect directly to stream, via saturated overland flow, or to recharge of riparian soils where there is a saturation deficit (van Meerveld et al., 2015). Specific to continuous permafrost environments, it was been shown that the storage potential of riparian zones increases as the active layer thaws (Chiasson-Poirier et al. non-published). As the summer advances, sustained water contributions may therefore be required to maintain fully saturated conditions in large riparian areas, enhanced the storage of water to the detriment of surficial runoff and lead to a distinct chemical signature for stations having variable proportions of riparian area within their drainage area. Here the station drainage area proportions occupied by delineated DTW areas can help to identify the potential for greater riparian area water storage capacity (i.e., reduced rates of hydrological turnover) and thus distinct water and solute contributions from hillslopes to streams.

Mean upslope contributing area (UCA) within delineated DTW area. The UCA index is computed from the mean upslope contributing area value of the cells containing in the

delineated extend of the riparian of DTW areas for each sampling site. Combining analysis of upslope contributive areas with the delineation of riparian can help to identify areas of quicker turnover and more persistent water contribution for hillslope to stream (Jencso et al., 2010). Saturation conditions of areas at the interface between hillslopes and streams can also help to understand the importance of contributions from old (i.e., water that was subjected to longer flow paths, storage or longer residence time) and new (i.e., water from snowmelt or rainfall that wasn't subjected to terrestrial processes that could change its chemistry). Higher saturation conditions of the riparian area will enhance contributions from new water to stream following rainfall events and the swift or celerity between a disconnected to a hydrologically connected hillslope-stream sequence (McDonnell and Beven, 2014). During dryer periods, sustained contributions to riparian areas from upslope could help to maintain wetter conditions, without allowing the contributions of new water, contributions may then be stored and be connected to stream only by translatory flow (Hewlett and Hibbert, 1967), which will also lead to important celerity of the hillslope-stream sequence during rainfall events, but could also help to maintain localized subsurface flows or old water contributions. High UCA index values will then represent (1) riparian areas subject to be characterized by greater saturation conditions and thus enhance the connexions of hillslope to stream during rainfall events, or (2) during dryer periods, allow more persistent contributions of riparian stored groundwater to stream.

Proportion of south-exposed drift area. Identification of drift areas within the Niaqunguk watershed is derived from a classification decisions tree including slope, topographic openness and wind shelter models computed from the raw DEM (see Smith, 2018 or annexe C for more classification details), while an aspect model to identify south-exposed area. Pomeroy et al. (1997) suggested that the distribution of tundra snow can be broadly explained by: (i) areas exposed to wind that favour erosion and transportation of snow (i.e., source areas); and (ii) sheltered areas that act as sinks for snow deposition. From that hypothesis, Smith (2018), in a three-year study conducted within the Niaqunguk watershed, quantitatively assessed significant terrain variables to classify the catchment in three snow accumulation classes; scour, tundra and drift areas. The computed drift areas fitted well with field measurements of high snow accumulation and were associated to lee slopes of ridges and local depressions like gullies and stream channels. Scour areas closely match the distribution

of bare rock on ridges, hilltops and centres of large lakes; areas prone to snow erosion and transport. The Tundra class corresponds to other areas not assigned to Scour or Drift, and this class occupied the largest portion or the watershed and represent areas mildly exposed to the wind and that often act as source areas for snow. Pomeroy et al. (2003) also observed that south-facing slope received higher radiation during sunny days in spring, therefore increasing the rate of thaw. Here we used a similar delineation of drift areas as Smith (2016) and added the discrimination of south-exposed areas, as a proxy to investigate if uneven snow accumulations, distributions of late-lying snow and areas subject to enhanced thaw during spring sunny days within the catchment could partly explain the differences of streamflow chemistry among sampling sites.

3.2.5 Statistics

A specific sequence of statistical analysis was used to distinguish the following trends from the collected or computed data: (i) ruptures and similarities in chemical time series that could reflect distinct hydrological/chemical periods, (ii) the repartition of the sampling sites based on the computed landscape indices, (iii) potential controls on water contributions highlighted by the ability of specific landscape indices to explain the chemical variation among sites; and (iv) significant watershed scale spatial patterns of similarities or dissimilarities in chemistry among sites for the identified hydrological periods. Logic and objectives of the selected statistical methods to address these objectives are discussed below.

(i) Clustering methods, such as unconstrained ward minimum variance clustering, are useful to identify ruptures and similarities in multivariate time series (e.g., multiple sampling dates for multiple sites). The ultimate objective of ward clustering analysis here is to build groups of sampling dates that are as homogeneous as possible (Legendre and Legendre, 2012).By grouping separately for each chemical variable analyzed (i.e., SpC, DOC, $\delta^{18}O$ and Mg^{2+}) the similar sampling dates based on streamflow chemistry at the 24 sites, we created a more parsimonious dataset that delineated the periods (or sampling dates) of the sampling season for which a particular chemical pattern was observed among sites. Since each chemical variable can be used as a natural tracer to identify potential water sources or processes, the identified periods are subject to change from one chemical variable to another and therefore separate clustering analysis allows the investigation of specific hydrological processes.

(ii) We used a principal component analysis (PCA) to show how sites relate to each other based on the six computed landscape indices described above. The advantage of the PCA is to enable the visual representation of the similarities between sites in the reduced-spaced ordination (only the first two PC axes are retained in this paper) while the proportion of variance explained by landscape characteristic is also demonstrated. Clusters in the reduced space that may by distinct elements (i.e., main tributaries or headwater stream) of the Niaqunguk River network that are characterized by the similar landscape structure within their drainage area.

(iii) The ability of specific landscape indices to explain the variation among sites for each chemical variable and for each identified period from clustering analysis were determined in two steps, (1) a forward selection procedure was first to select only the significant landscape indices. The forward selection is based on the total explained variance (adjusted canonical R_a^2) and the statistical significance ($alpha$), tested using permutations (i.e., 999 permutations), of the model of explanatory variables after the stepwise addition of variables (Blanchet et al., 2008). Here, we used a cut-off level of $alpha = 0.05$, for the selection of the significant landscape indices. The proportion of variance among sites explained by the selected landscape indices was assessed using variation partitioning analysis. In this common method, one partitions the variation of a response variable (i.e., chemical values among sites for the delineated dates of a specific period) among two or more sets of explanatory variables (i.e., landscape indices) using a series of regressions (or redundancy-RDA analyses). Here we focused on the individual contribution (R_a^2) of each selected index, though total portions of explained variance were also shown to highlight the amplitude of potential join effect between two indices.

(iiii) Finally, to identify the patterns of similarities or dissimilarities in chemistry among sites for the identified hydrological periods (only periods that delineated more than 1 sampling date) we used Asymmetric Eigenvector Maps (AEM).This method computes spatial variables, called AEM eigenfunctions, that represent different patterns of positive or negative correlation among sites (Blanchet et al., 2008b).The produced AEM eigenfunctions can then be used as explanatory variables in redundancy analysis (RDA), to investigate which spatial structures better explain the chemical patterns among sites (Legendre et Legendre, 2012).The computation of AEM eigenfunctions first requires the creation of a network of possible

connexions between sites that represent the physical connections (i.e., links and nodes) of the Niaqunguk River network (Figure 10a).The specificity of AEM analysis is to represent a directional process (i.e., water flowing downstream) along a specific pattern (i.e., fluvial network) of spatial connexions between sites. The connexions between sites are subsequently represented in the form of a binary matrix, where rows represent the sites, the columns the edges or connexion between sites and the values 1 or 0 in the matrix the presence or absence of a connexion. The AEM eigenfunctions correspond to the principal components or position of sites along a new system of axis of a PCA analysis conducted on the binary matrix centre by columns. The principal component produced a total of 15 distinct vectors (i.e., eigenfunctions) with positive and negative values representing different spatial of similarities or dissimilarities among sites. The use of the computed eigenfunctions in RDA analysis to investigate the variation in chemistry among sites provide: (1) a visual representation of the similarities between sites for a specific period of multiple sampled dates, using the repartition of the sites along the axis of the RDA reduced space, and (2) the proportion of chemical variation among sites explained by the repartition of the sites along each axis. Here we used unadjusted coefficient of determination (R^2) to determine the proportion of explained variance by the AEM eigenfunctions, since the same number of explanatories variable was always used. The advantage of using AEM eigenfunctions in RDA analysis, rather than Moran' s spatial correlation or multiple regression models, is to investigate the variation among sites for multiple sampling dates (i.e., multivariate analysis) and then visually represent a significant spatial pattern for a specific period. Step-by-step example of an AEM analysis and simple algebra of the PCA, RDA and variation partitioning analysis are provided in appendix D or described in Legendre and Legendre (2012).

3.3 Results

3.3.1 Discontinuities in chemical time series and sampling sites characteristics

Discharge monitoring at the outlet of the Niaqunguk River (Site S1) began during the rising limb of the snowmelt freshet (4.1 m^3/s; June 13) with discharge reaching a maximum of 11.8 m^3/s for the monitoring period during the following day (Figure 11). Snowmelt recession

extended until the beginning of July, and was punctuated by a rainfall event (13.5 mm) on June 23-24. There were three other notable rainfall events during the monitoring period: July 5-9 (12.2 mm); July 17-19 (10.8 mm); and July 27-28 (30.1 mm). Very low magnitude runoff responses were associated with the first two events (discharge < 1.5 m^3/s), with the final recorded rainfall event producing a moderate response (peak discharge of 2.1 m^3/s).

We observed an increasing seasonal trend in mean SpC, $\delta^{18}O$ and Mg^{2+} values for the 24 sites that comprised our sampling network (Figure 11). There was no obvious seasonal trend in mean DOC values but for slightly lower values at lower streamflows. SpC showed no obvious response to rainfall events, while we observed an abrupt spike in mean $\delta^{18}O$ values and a corresponding drop in mean Mg^{2+} values following rainfall events that occurred later in the monitoring period (i.e., July 17-19; July 27-28). A punctual and a considerable increase in the standard deviation of $\delta^{18}O$ values are noted following these later two rainfall events (i.e., $\pm$ 0.8 $^0/_{00}$ vs $\pm$4.6 $^0/_{00}$ on July 17 and July 20; and $\pm$0.8 $^0/_{00}$ vs $\pm$2.6 $^0/_{00}$ on July 24 and July 27). With the exception of these two events there was relatively little variability in $\delta^{18}O$ values across the sampling network during the monitoring period. Lower means and standard deviations for SpC, $\delta^{18}O$ and Mg^{2+} were observed for the samples collected prior to peak snowmelt runoff relative to the values measured after the freshet. Measurements of DOC concentrations were only available from June 26 and patterns in mean concentration values are less clear due to more constant values and higher standard deviations.

Ward clustering analysis of SpC values measured across the 24 sampling sites partitioned the sampling events into four distinct periods corresponding to: early snowmelt, snowmelt recession, early baseflow and late baseflow periods. A similar partitioning of sampling events was identified for the $\delta^{18}O$ and Mg^{2+} data, with the exception that the analysis distinguished the dates immediately following the late July rainfall events (i.e., summer rainfall runoff period). Ward's method also distinguished DOC concentrations measured at sampling sites during lower flows (i.e., <1.5 m^3/s) from those measured at relatively higher flows (i.e., >1.5 m^3/s). Ward's method distinguished the $\delta^{18}O$ values on July 20 from those measured on July 27, for the purpose of subsequent analysis we considered both dates as a single group given that both dates follow a late period rainfall event with summary statistics (i.e., mean; standard deviation) clearly distinct from all other sampling dates. Based on a combination of the identified periods for the SpC, $\delta^{18}O$ and Mg^{2+} we referred to these specific periods : (Period

1 or P1) early snowmelt, (Period 2 or P2) snowmelt recession, (Period 3 or P3) early baseflow and (Period 4 or P4) late baseflow and late summer rainfall events, for the subsequent analysis.

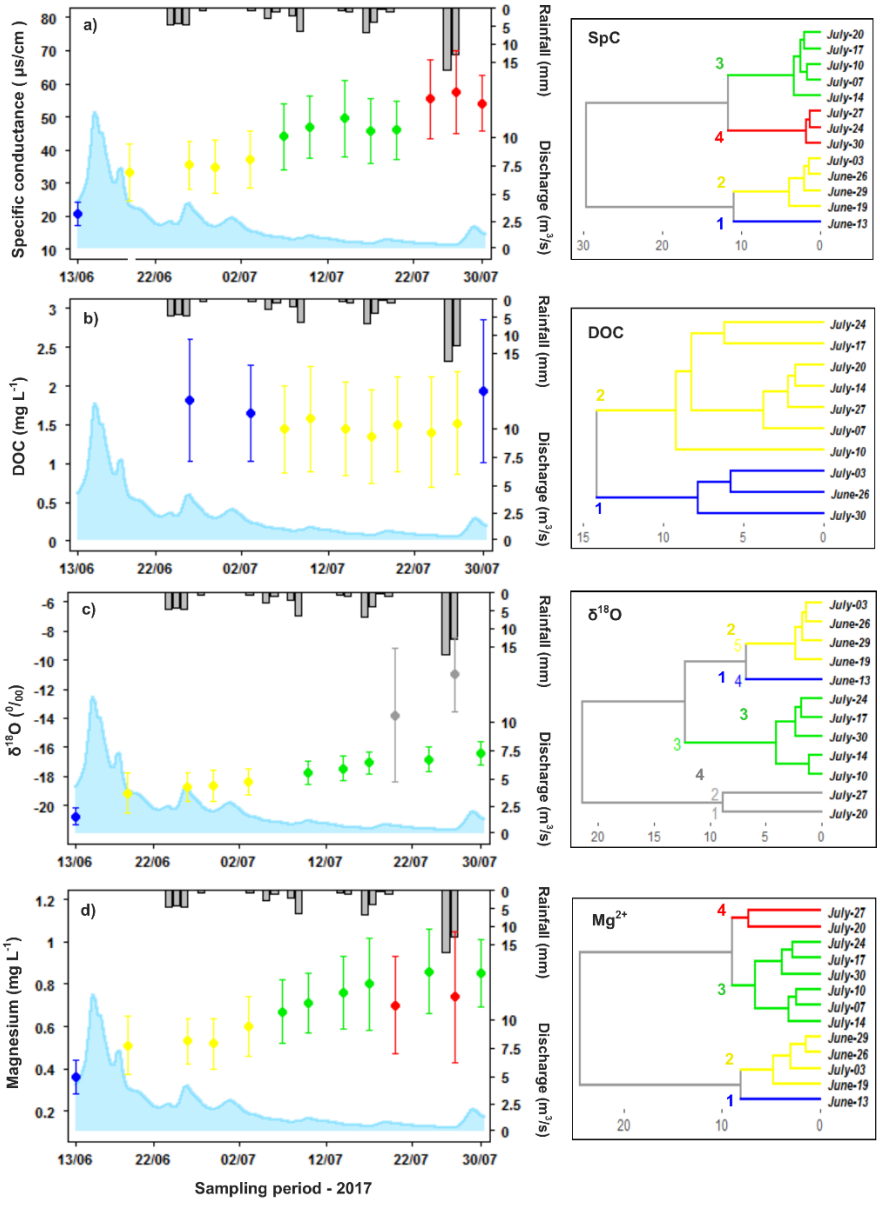

Figure 11. Seasonal trends in stream chemistry (mean, SD) measured across the 24 network sampling sites for (a) the 13 dates analyzed for specific conductance (SpC), (b) the 10 dates analyzed for dissolve organic carbon (DOC), (c) the 12 dates analyzed for oxygen isotopes ($\delta^{18}O$) and (d) for the 13 dates analyzed for magnesium concentration (Mg+). Colours (blue, yellow, green and red) reflect the degree of similarity in the values of the given chemical parameter across sampling dates according to Ward clustering analysis, for which clustering trees are shown adjacent to their corresponding chemical variable. Discharge is measured at basin outlet (station S1) and rainfall at rain-gauge site centrally located within the watershed.

Principal component analysis was used to determine which sampling sites were similar, based on the landscape characteristics within their drainage area, site repartition was greatly influenced by the size of drainage area, the proportion of lake coverage and by the combination of the proportion of depth-to-water areas, south-exposed drift areas and by the drainage density of sampling sites (Figure 12). The first two axes of a PCA explained 80% of the variance in landscape characteristics across site drainage areas. PCA axis 1 reflects the negative correlation between the proportion of lakes and either, the proportion of delineated riparian areas or south-facing drift areas within sampling sites catchment. Axis shows that high values for the drainage density and mean upslope contributing area indices are generally found for sites with the smaller drainage areas.

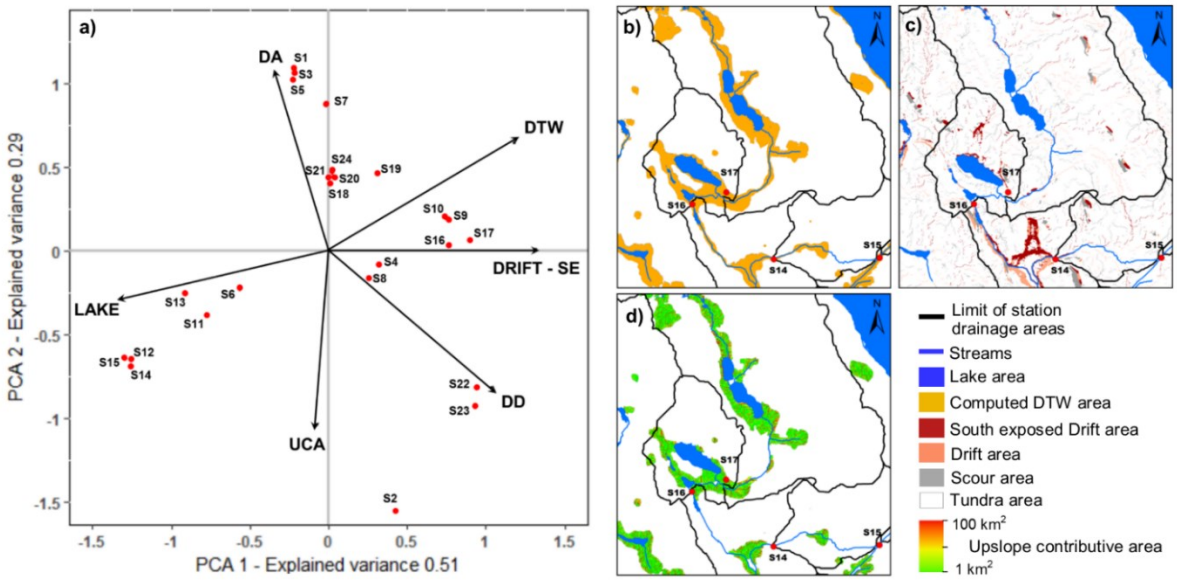

Figure 12. a) PCA biplot showing the distribution of the 24 sampling sites according to six landscape indices computed for each of their distinct drainage areas. Landscape indices correspond respectively to the drainage area (DA), drainage density (DD), lake proportion of the drainage area (LAKE), proportion of the drainage area occupied by the computed depth-to-water index (DTW), the mean upslope contributive area within the computed DTW areas (UCA) and the proportion of the station drainage area occupied by south-facing drift area (DRIFT-SE). Example maps of the area including sites S14-17 that show: b) DTW areas, c) DRIFT-SE (Drift, Scour and tundra or other non-classified area) areas and d) UCA areas.

Sites along the East tributary and located downstream of the watershed's largest lake (LLA; sites S6, S11-15) are distributed along the LAKE index arrow due to the important proportion of their drainage areas occupied by lakes (Table 3). Downstream sites with the largest drainage areas (i.e., sites S1, S3, S5) are clustered together on the upper-left quadrant

associated to the DA index arrow. Sites S18, S20-21 and S24 located along the central tributary are distinct from sites downstream based on their smaller drainage areas and greater drainage densities. Tributary sites along the downstream reach (i.e., S2, S4), the lake 1 area sites (i.e., S8, S9 and S10), the east tributary sites (i.e., S16, S17) and those along the central tributary (i.e., S22, S23) are distributed along the arrows corresponding to the DTW, Drift-SE, DD and UCA indices. Headwater sites are also distinguished from other sites in the network based on their higher drainage densities. Watershed scale maps show the computed landscape indices for the study area (see annexe E).

Table III. Summary of chemistry, landscape indices and hydrologic measurements for the 24 sampling/gauging sites.

	Streamflow chemistry (Mean / *SD*)				Landscape indices						Hydrologic measurements			
Site	SPC	DOC	$\delta^{18}O$	Mg^{2+}	DA	DD	LAKE	DTW	UCA	DRIFT-SE	Period	n	Rel.	RC (R^2)
1	42.8/9	1.1/0.2	-16.8/3	0.6/0.2	52.9	0.4	0.07	0.1	859	0.013	13/06 - 30/07	10	Log	0.99
2	39.7/13	2.3/0.4	-17.9/2	0.9/0.3	0.8	2.4	0.00	0.06	4650	0.020	01/07 - 30/07	4	Lin	0.95
3	40.4/10	1.2/0.2	-16.9/4	0.7/0.2	51.4	0.4	0.07	0.1	866	0.013	01/07 - 30/07	6	Log	0.99
4	54.3/14	2.4/0.4	-16.7/3	1.0/0.3	1.1	1.9	0.04	0.07	329	0.012	-	-	-	-
5	40.8/11	1.1/0.3	-17.8/3	0.7/0.3	49.2	0.4	0.08	0.1	865	0.012	03/07 - 30/07	6	Log	0.99
6	47.2/9	1.2/0.2	-15.6/5	0.7/0.2	12	0.6	0.14	0.06	1645	0.015	03/07 - 30/07	6	Lin	0.99
7	39.5/11	1.0/0.1	-18.2/2	0.6/0.2	36.2	0.5	0.06	0.12	634	0.011	10/07 - 30/07	5	Log	0.99
8	48.7/9	2.2/0.2	-17.3/3	0.6/0.2	2.1	1.3	0.05	0.07	885	0.008	30/06 - 30/07	4	Log	0.98
9	65.3/20	2.6/1.0	-17.5/2	0.9/0.3	1.2	1.8	0.02	0.1	553	0.008	30/06 - 30/07	6	Lin	0.99
10	65.6/20	2.8/0.4	-17.7/3	0.8/0.3	1	1.5	0.02	0.09	631	0.008	-	-	-	-
11	43.8/9	1.1/0.2	-16.4/3	0.7/0.1	9	0.6	0.17	0.05	1652	0.012	04/07 - 30/07	5	Lin	0.99
12	43.3/9	1.0/0.3	-16.6/1	0.6/0.1	6.4	0.8	0.23	0.03	1463	0.005	-	-	-	-
13	41.3/10	1.3/0.2	-17.0/3	0.6/0.1	7.8	0.7	0.19	0.04	927	0.009	04/07 - 30/07	5	Lin	0.98
14	43.5/10	1.0/0.2	-15.8/4	0.6/0.1	6.4	0.8	0.23	0.03	1439	0.005	-	-	-	-
15	42.8/9	1.2/0.2	-16.3/3	0.6/0.1	6.2	0.7	0.23	0.03	1456	0.005	04/07 - 30/07	6	Log	0.97
16	38.4/12	2.5/0.5	-17.5/3	0.7/0.3	1.2	2	0.04	0.11	347	0.012	06/07 - 30/07	4	Log	0.99
17	43/14	2.2/0.4	-17.9/2	0.7/0.3	1	2.1	0.03	0.1	394	0.009	05/07 - 30/07	4	Log	0.97
18	35.8/14	1.1/0.3	-17.8/1	0.5/0.1	21.3	0.8	0.07	0.11	784	0.010	-	-	-	-
19	37.3/12	1.1/0.2	-17.9/3	0.7/0.2	13.2	1	0.03	0.14	431	0.011	05/07 - 30/07	4	Log	0.99
20	36.7/9	1.1/0.2	-18.5/1	0.5/0.1	19.2	0.8	0.08	0.11	809	0.009	02/07 - 30/07	6	Lin	0.99
21	35.7/8	1.0/0.1	-18.0/3	0.5/0.1	18.3	0.7	0.08	0.11	694	0.008	02/07 - 30/07	6	Log	0.99
22	36.9/8	1.0/0.6	-16.0/5	0.5/0.2	0.4	2.8	0.04	0.07	1640	0.011	02/07 - 30/07	3	Lin	0.93
23	36.1/7	1.0/0.3	-16.4/5	0.5/0.1	0.4	3.2	0.04	0.07	1664	0.010	02/07 - 30/07	3	Lin	0.99
24	36.6/9	1.1/0.3	-17.8/3	0.5/0.1	16.8	0.7	0.08	0.12	551	0.007	02/07 - 30/07	6	Log	0.99

* Water sampled at the 24 sites analyzed for specific conductance (SpC: µs/cm), dissolve organic carbon (DOC: mg L^{-1}), oxygen isotopes ($\delta^{18}O$: $^{0}/_{00}$) and magnesium (Mg^{2+}: mg L^{-1}). Landscape indices computed for each site include: DA (station drainage area; km^2); DD (drainage density; km km^{-2}; LAKE (lake area as proportion of total site drainage area; %); DTW (proportion of the drainage area occupied by the computed depth-to-water or riparian area; %); UCA (mean upslope contributing area within the DTW area; m^2); Drift-SE (proportion of the station drainage area occupied by the south-facing drift area; %). Hydrologic measurement details include the date of the first and last gauging event (Period), the total number of gauging events (n), the form of the relationship (Rel.; Linear or Logarithmic) between discharge and depth, and the proportion of variance explained by this rating curve (RC R^2).

3.3.2 Partitioning of the chemical variation

No single landscape metric or group of metrics consistently explained the variation in streamflow chemistry among sites during the monitoring period. Instead, unique sets of indices were associated with the distinct sets of periods identified via Ward clustering analysis (results detailed above; Figure 11). For the snowmelt recession period (P2; SpC, $\delta^{18}O$ and Mg^{2+} time series), Drift-SE, LAKE and either UCA or DTW area were found as significant indices (Figure 13). Variation partitioning showed that for either SpC or Mg^{2+} the south-exposed drift area index explained the greater portion of the variation among sites; Ra2 values of 0.18 and 0.13 respectively. Though, the LAKE index explains the greater portion (R_a^2 = 0.53) of the variation in the oxygen isotope concentrations measured among sites during that period. During the following period delineated from the SpC, $\delta^{18}O$ and Mg^{2+} time series (P3; Baseflow period), the lake proportion remains the most significant (R_a^2 = 0.24) index to explain the variation in of $\delta^{18}O$ among sites, but also explained the greater portion of Mg^{2+} variance (R_a^2 = 0.18). During that period (P3) only slight portion (Ra2 = 0.08) of the variation in SpC values measured among sites is explained by the UCA index. For the fourth period delineated from the SpC time series, which correspond to the last three sampling dates, the upslope contributing area is still the only significant landscape indices to explain the variation in water conductivity measured among sites, but it explains more than twice (R_a^2 = 0.2) the variance relative to the previous period (i.e., R_a^2 = 0.08). For the sampling dates corresponding to the fourth period delineated from the $\delta^{18}O$ and Mg^{2+} time series (P4; summer rainfall runoff period), variation partitioning showed that for either $\delta^{18}O$ or Mg^{2+} the upslope contributing area was again the only significant index, explaining slightly less of the $\delta^{18}O$ or Mg^{2+} variation (respectively; R_a^2 = 0.12 and R_a^2 = 0.15) than for the SpC values measured among sites for the same period.

For the two periods delineated from the DOC time series (P1: higher flow conditions; P2: lower flow conditions), the dominant index to explain the variation in DOC concentration measured among sites is drainage density (DD), which explained a significant portion of variance (R_a^2 = 0.38) for both periods. A significant portion (R_a^2 = 0.17) of the variation of DOC concentrations measured across sites is also explained by the Drift-SE index, during P1 (i.e., higher flow conditions). The illustrated total portion of variance explained (i.e., dashed lines on Figure 13) by the explanatory models, including all selected indices for the specific periods

delineated from each parameter time series, are either equal or slightly above the sum of the variance explained by each the landscape indices individually, which shows that any additional variance explained by the intersection between indices is negligible.

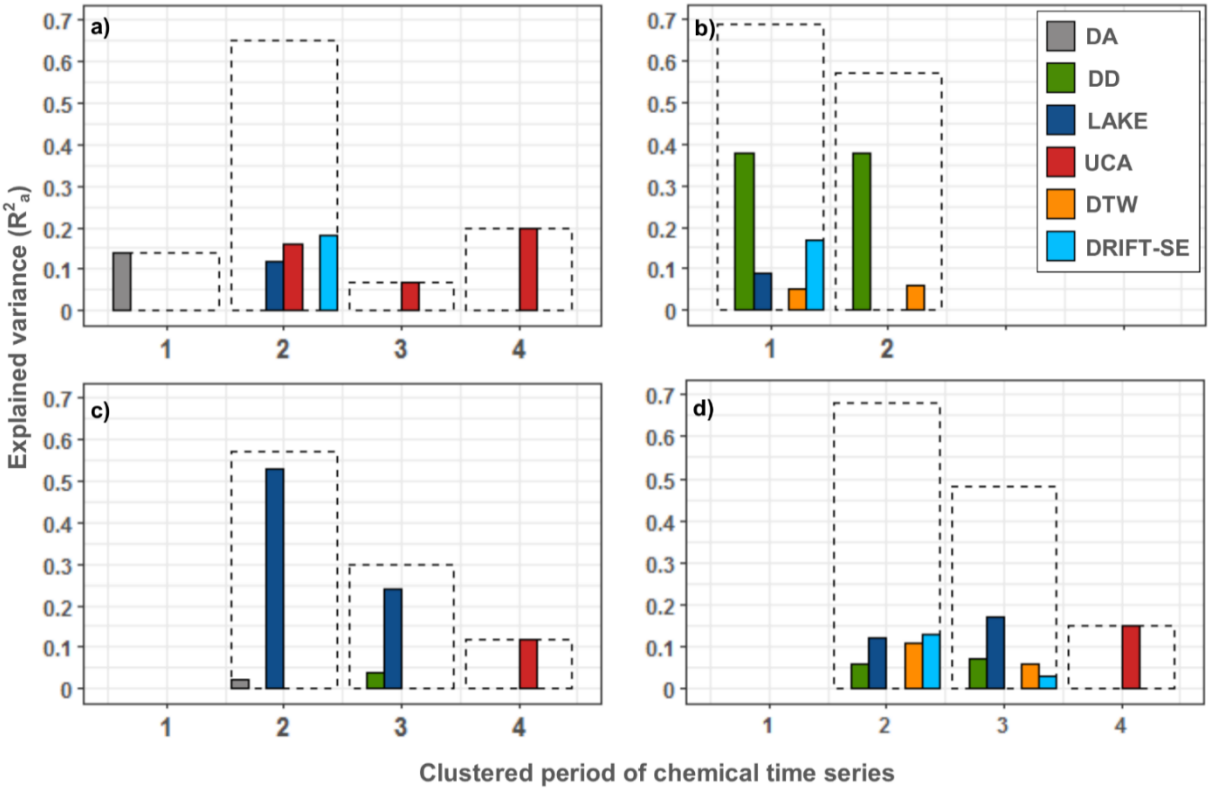

Figure 13. Fractions of chemistry variation between sampling sites explained by the selected significant landscape indices for the periods delineated by the Ward clustering of a) specific conductance, b) dissolve organic carbon, c) oxygen isotopes and d) magnesium values measured at the 24 sampling sites. No significant indexes were selected for the first periods of the oxygen isotope and magnesium time series. Since only one date was delineated for the period 1 of the SpC time series and that only one landscape index was found significant through forward selection, the portion of explained variance correspond to simple correlation analysis. Cumulative (dashed line) and individual proportions of explained variance were determined by variation partitioning analysis except for the first SpC period, which correspond to correlation coefficient of a simple regression analysis since only one sampling date is delineated.

3.3.3 Chemical patterns among sites

Redundancy analysis involving the AEM eigenfunctions explained great portions of the chemical variation among sites and demonstrate that (1) watershed scale differences in the spatial patterns explaining the variance among sites, are particularly marked between the early snowmelt period (P1; SpC and $\delta^{18}O$) and the subsequent periods, while, (2) localized or reach

scale differences in the significant spatial patterns are observed between periods 2 to 4, and between the analyzed chemical parameter (Figure 14). The SpC values measured for period 1 (only one sampling date) ranged from 13 to 28 µs/cm, with a clear distinction between the sites along the east tributary (mean: 17.5; SD: 0.9 µs/cm) from the downstream sites (S1 to S7, with the exception of S2; mean: 25.3; SD: 2.7 µs/cm) and from the sites situated in the lake 1 area (S8 to S10; mean: 22.4; SD: 1.3 µs/cm). For the SpC values measured on periods 2, 3, and 4, the repartition of sites along RDA axis-1 explain respectively 0.52, 0.77 and 0.79 of the variations among sites. Sites along the central, west tributaries and the downstream reach are consistently characterized by lower SpC values (mean: 39.8; SD: 8.9 µs/cm) than SpC values measured at sites along the east tributary (mean: 44.4; SD: 7.8 µs/cm). Water from headwater site S4 and from the lake 1 area (sites S8-10) showed the highest measured SpC values throughout the monitored period (mean: 61.4; SD: 15.0 µs/cm). Site S11 located downstream of a large pool section along the hydrological network of the east tributary showed a similar SpC signature to its upstream sites (i.e., S12-13) for periods 2 and 4, but different during period 3 (i.e., baseflow conditions). Differences in SpC values between sites located on lake inflows (i.e., sites 9 and 17) and lake outflows (i.e., sites S8 and S16) are also observed for periods 3 and 4.

Headwater sites (i.e., S2, S4, S8-10, S16-17, S22-23) are clearly characterized by higher DOC concentrations (mean: 2.4; SD: 0.9 mg L^{-1}) relative to sites located along the main stem of the river and from sites located downstream of lake LLA (mean: 1.3; SD: 0.3 mg L^{-1}). This spatial pattern characterizing the variation of DOC concentration measured among sites is very similar between periods 1 and 2 with RDA's axis-1 explaining 0.65 and 0.63 of the variances in measured DOC concentrations respectively.

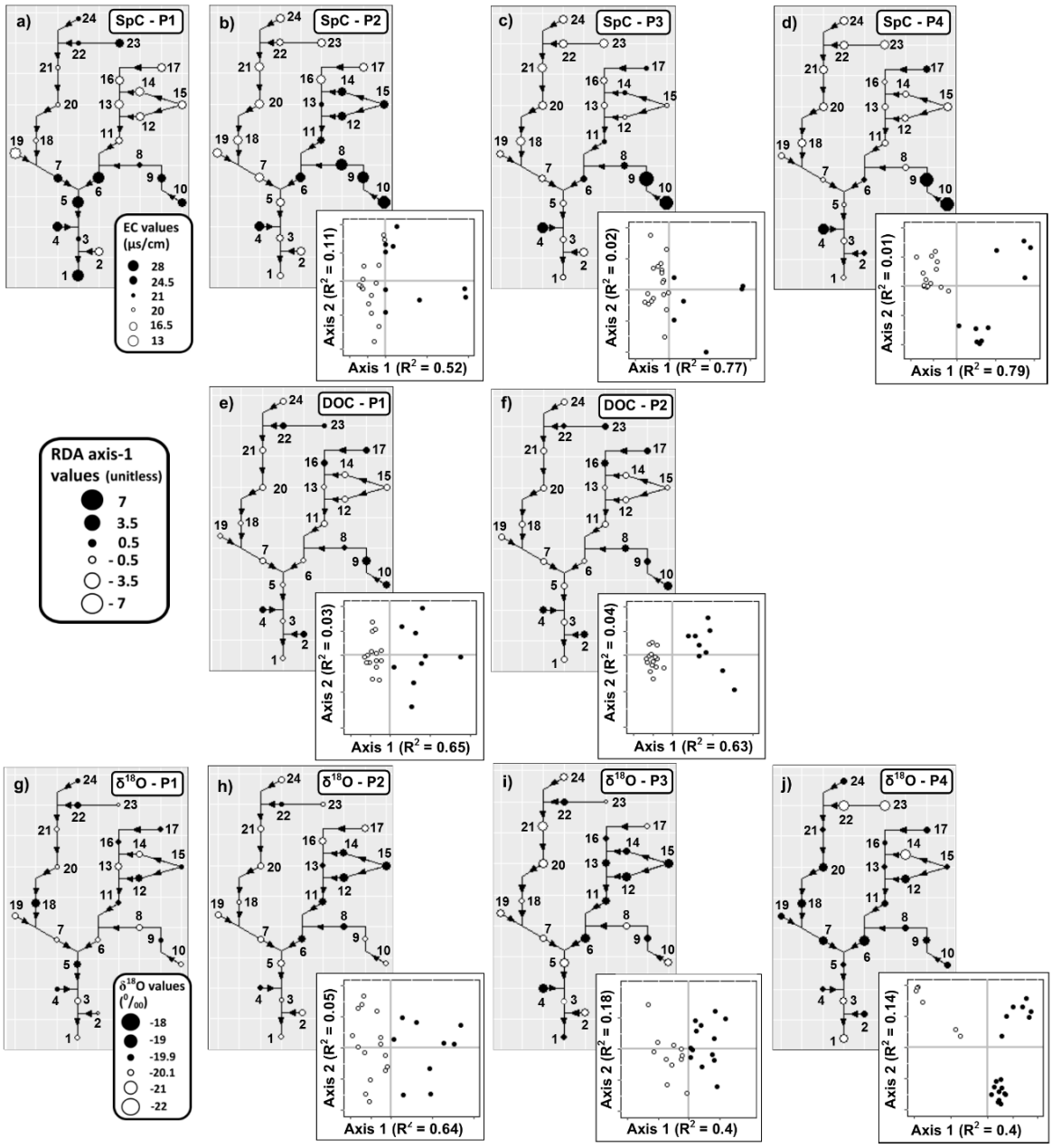

Figure 14. Bubble maps of the axis 1 RDA fitted scores for the hydrological periods delineated by the Ward clustering from the SpC (a, b, c, d), DOC (e, f) and $\delta^{18}O$ (g, h, i, j) chemical time series. Square inserts at the bottom-rigth of the bubble maps illustrate the redundancy analysis that involved the 15 produced AEM eigenfunctions used to explain the variation between site chemistry for the dates of a specific period. Black and white points represent the positive or negative values of a site relative to RDA-axis 1, while points size is proportional to the absolute site value along axis 1. Since only one date is delineated for period 1 of SpC, and $\delta^{18}O$ time series, the measured values are directly shown on the bubble maps.

Site $\delta^{18}O$ values for Period 1 (i.e., early snowmelt) exhibit a high degree of reach scale variability across the sampling network (i.e., individual sites are $\delta^{18}O$ depleted or enrich

relative to those immediately up/downstream). For the measured $\delta^{18}O$ concentrations during periods 2, 3 and 4, the reparation of the sites along the RDA axis-1 explain respectively 0.64, 0.40 and 0.40 of the variation of $\delta^{18}O$ values measured among sites. Slightly less variance in the $\delta^{18}O$ measured values comparatively to the first two parameters is explained on period 3 and 4, greatly because RDA axis-2 also explained important portions of variances (i.e., 0.18, 0.14) among sites. Though point sizes, proportional to the absolute value along the RDA axis-1, show which sites (i.e., smaller point), distributed either on the positive or negative side of the RDA biplot relative to axis-1 (i.e., black or white coloured point), are characterized by more similar chemistry.

During the snowmelt recession (P2), east tributary sites (i.e., S6, S11-15), except sites S16 and S17 situated upstream of the LLA discharge, were $\delta^{18}O$ enriched (mean: -17.3; SD: 0.7 $^{0}/_{00}$) relative to the rest of the network (mean: -19.2; SD: 0.8 $^{0}/_{00}$). A similar pattern of $\delta^{18}O$ concentrations is observed during the baseflow period (P3) relative to previous period pattern, with all sites are characterized by a $\delta^{18}O$ enrichment, though increasing in $\delta^{18}O$ values were more important for sites along the central tributary and the downstream reach (i.e., Sites S1, S3, S5, S7, S18-21, S24; mean: -17.5; SD: 0.9 $^{0}/_{00}$) diminishing the discrepancies with sites along the east tributary (mean: -16.5; SD: 0.5 $^{0}/_{00}$). Patterns in $\delta^{18}O$ concentrations were even more similar between east tributary sites (mean: -15.4; SD: 3.9 $^{0}/_{00}$) and sites located on the central and west tributaries (mean: -16.0; SD: 3.3 $^{0}/_{00}$) during the sampling dates corresponding to the summer rainfall events (P4). During P3, sites that are distributed near zero along the RDA axis-1 are respectively sites S1, S9, S17, S23 (i.e., negative or blacks' sites) showing slightly lower $\delta^{18}O$ values (mean: -16.8; SD: 0.8 $^{0}/_{00}$) and sites S3, S8, S16, S18, S22 (i.e., positive or white sites) (mean: -17.2; SD: 0.6 $^{0}/_{00}$). The distribution pattern of site along RDA axis is slightly different during P4, while axis-1 (R^2 = 0.40) clearly distinguished sites with higher $\delta^{18}O$ values which correspond to headwater sites 22 (mean: -6.6 $^{0}/_{00}$) and 23 (mean: -6.5 $^{0}/_{00}$), or downstream sites 1 (mean: -9.7 $^{0}/_{00}$) and 3 (mean: -13.2 $^{0}/_{00}$) located just upstream of site 1, but downstream of an important river pool section. Localized differences in $\delta^{18}O$ values observed between neighbour's headwaters sites (i.e., Sites 8 vs 9 vs 10, 16 vs 17 and 22 vs 23) during period 2 or 3, theses differences between neighbours' site are no longer observed on period 4. Distinction between sites highlighted by axis-2 (R^2 = 0.14) show that $\delta^{18}O$ values measured at sites S7, S-10, S12, S17-18, S20 (mean: -15.5; SD: 1.3 $^{0}/_{00}$) are generally slightly

higher than for sites S2, S4-5, S8, S13, S15-16, S19, S22, S25 (mean: -13.0; SD: 3.5 $^{0}/_{00}$), thus this pattern doesn't reflect a specific variation in chemistry among sites, but a greater variation in isotopic signature of water along the network. Results of RDA conducted from the Mg^{2+} concentration measured among sites explained fewer variances than RDA conducted for the other three parameters and so for any of the periods delineated from the Mg^{2}+ time series (i.e., period 2: 0.26; period 3: 0.35; period 4: 0.33), though visually, the spatial patterns that explained the Mg^{2+} variation among site were similar to those that emerged from the δ^{18}Ovalues.

3.3.4 Streamflow dynamics and relative contributions

Discharge measurements across our monitoring network allowed us to observe distinct hydrological responses and changes in relative flow contributions between sites (Figure 15). Daily oscillation patterns were observed in the streamflow of particular stations till the beginning of July, while negative net discharges were observed between downstream and upstream locations along single reaches during dry periods. These shows are associated to different processes controlling the water delivery to stream or the water flows along the river network. Hydrographs show that discharge response to rainfall events were considerable at some sites (i.e., S1, S3, S5, S7, S11, S16-17, S20-21, S24) and damped at others (i.e., S6, S8, S15). Even with limited rainfall, discharge remained high for most sites at the beginning of July, a period associated with the delineated snowmelt recession period from the chemical time series data. For sites from the downstream reach (i.e., S1, S3, S5) and from the headwater sites of the east tributary (i.e., S13, S16, S17), stormflow peak following the end of July rainfall event (~ 28th) surpassed the discharge measured in early July (~ 03rd). Important runoff following the end of July rainfall event, but similar or lower to discharge measured on the early July was characterising other gauged locations (i.e., S11, S20, S21, S24). Headwater sites situated upstream of lakes (i.e., S9, S17) showed smaller time lag between the end of July rainfall event and the following peak flow than sites at the lake outlet (i.e., S9, S13, S16). Diurnal cycles (varying between 0.01 and 0.05 m^3/s) in the measured discharge are also evident for some sites located further upstream of main tributaries (i.e., S6, S11, S20-21, S24) or located on headwaters tributaries (i.e., S13, S16-17), though the amplitude of these diurnal cycles tended

to decrease (i.e., S6, S11, S20-21, S24) or disappear altogether (i.e., S13, S16-17) as the summer advanced.

Contribution of west and central tributaries (S7) to downstream flow (S5) was more important than the east tributary (S6) contribution throughout the monitored period. However, their relative contributions changed according to the hydrometeorological conditions, so that discharge at S7 is 2-3 times, 3-4 times and fewer than 2 times more important than S6 with respect to these following hydrological periods; snowmelt recession, stormflow and baseflow. Differences in relative contributions are also observed for station S11 and site immediately upstream. The relative contribution from site S13, located downstream of the east tributary headwater, tends to decrease with discharge, whereas discharge at lake LLA outlet (S15) is more constant, though its relative contribution to downstream site S11 increases as flow decrease. Relative contribution from S13 only surpassed the S15 contribution during the stormflow event of the end of July. The discharge observed at site S13 was 2-3 time more important than at site S16 during the snowmelt recession, this difference in discharge tends to diminish toward baseflow, than flow measured at S16 surpassed S13 during the late July stormflow event.

Negative discharge between downstream and upstream neighbour sites along single reaches were observed between S3 (July 17-18: ~0.6 m^3/s; July 27-28: ~1.5 m^3/s) and S5 (July 17-18: ~0.74 m^3/s; July 27-28: ~1.8 m^3/s). The observed negative flow only lasted during upper portion of the stormflow events and revert to similar or positive discharge between site during the recession. During low flow conditions (between July 24-27) higher discharge was measured at site upstream S15 (~0.65 m^3/s) than downstream site S11 (~0.5 m^3/s), this pattern shifts as flow rise quickly at site S11 following the late July rainfall event, while discharge rise at site S15 was slight and delayed. Between July 14 and 18, higher discharge was also observed at upstream sites S21 (~ 0.26 m^3/s) and S24 (~ 0.26 m^3/s) compared to discharge observed at site S20 (~ 0.24 m^3/s) situated downstream of the same reach. This pattern was even clearer at lower flow conditions (July 24-27), while discharge at site S20 decreased as low as ~0.1 m^3/s and discharge at sites S21 and S24 remained more constant (~0.2 m^3/s). Discharge amplitude at site S21 (~0.7 m^3/s) exceeded S21 (~0.65 m^3/s) and S24 (~0.5 m^3/s) during the stormflow events at the end of July. Negative discharge between downstream sites S3 and its upstream neighbours' site S5 reflects the dissimilarities observed in the $\delta^{18}O$ concentrations measured

at these two sites and highlighted by the spatial pattern corresponding to baseflow and late summer rainfall events (Figure 14).

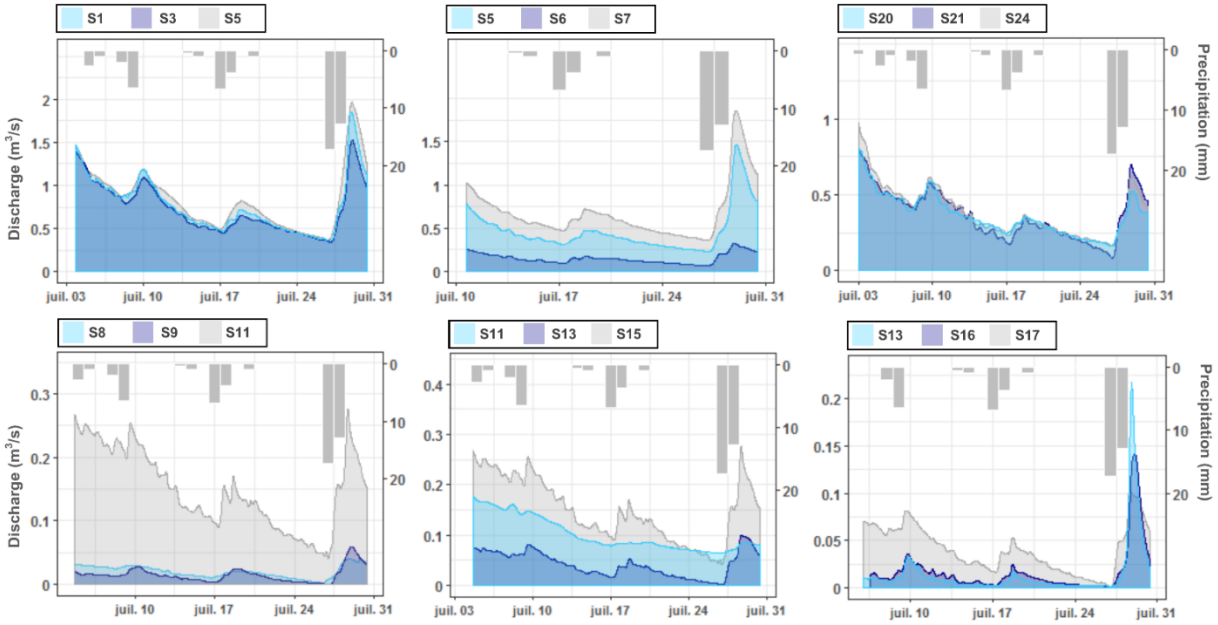

Figure 15. Hydrographs of the instrumented stations, flow period length varies upon the available minimum and maximum available discharge measurement at the stations used to establish stage/discharge relationship. Stations discharge measurements are compared to the discharge measured at their upstream or downstream neighbour hydrometric stations along the fluvial network.

3.3.5 Isotopic dynamics

Isotope values (δD and $\delta^{18}O$) in water sampled at the 24 sampling sites increased throughout the 2017 sampling season (Figure 16) due to evaporation or mixing with evaporated waters. Isotope values of rain sampled between June 29 and August 04 (n=7), in the Niaqunguk River area ranged from -54.9 and 129.8 ‰ δD or -5.3 and -16.2 ‰ $\delta^{18}O$, from these data a LMWL was calculated ($\delta D = 6.87*\delta^{18}O - 13.6$, r = .98. n = 7) with a similar slope and intercept to the global meteoric water line ($\delta D = 8*\delta^{18}O + 10$; Craig, 1961). Isotopic composition was more depleted (more negative values of δD and $\delta^{18}O$) for the first clustered period from the $\delta^{18}O$ time series corresponding to early snowmelt, with an average composition of −155.8‰ δD, −20.7‰ $\delta^{18}O$ and became progressively enriched on the following periods; period 2 or snowmelt recession (−141.8 ‰ δD, −18.7 ‰ $\delta^{18}O$), period 3 or baseflow conditions (−132.2‰ δD, −17.1 ‰ $\delta^{18}O$) and period 4 corresponding to sampling

following rainfall events (−126.7 ‰ δD, −12.4 ‰ $\delta^{18}O$). Period 2 points show the greatest scatter along the LMWL. Period 3 exhibits greater scatter perpendicular to the LMWL relative to P1 and P2, with points predominantly located below the LMWL (higher $\delta^{18}O$ values). For the first three periods the sites with isotope values deviating from the LMWL were mainly headwater streams of from the western tributary, while during period 4 all sites of the Niaqunguk stream network showedδ18O enriched water. The isotope values for period 4 show a substantial deviation from the LMWL, including a cluster of points > -10 ‰ $\delta^{18}O$. This aforementioned cluster of points are for some sites located along the downstream reaches (S1 -5) and either for some of the sites located within the east tributary drained area (S6, S11, S13-16) or from the central-west tributaries drained area (S19, S21-24).

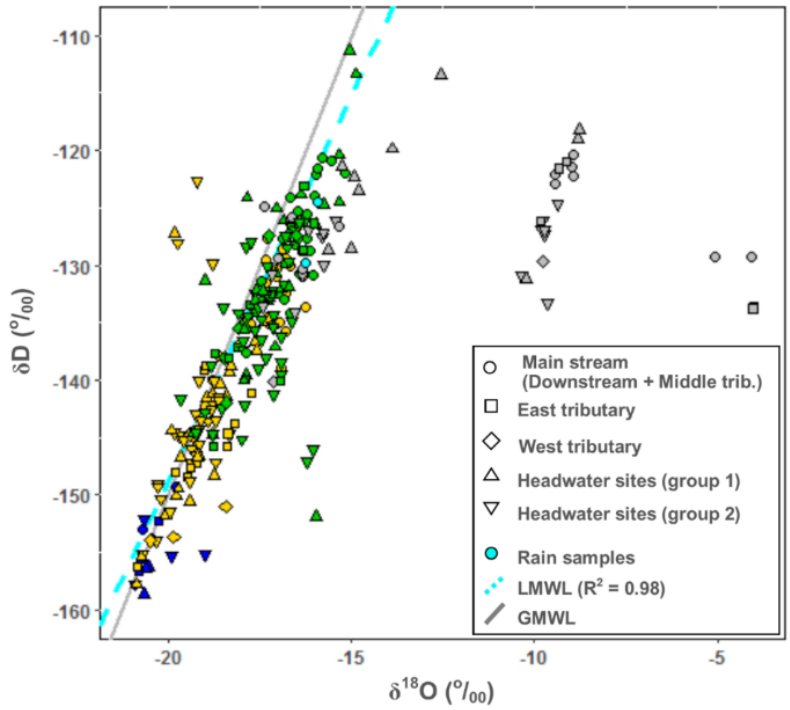

Figure 16. Isotopic composition of water sampled within the Niagunguk River watershed during the summer 2017, classified according to the periods identified by the ward clustering of the oxygen isotope time series (i.e., blue: period 1 or beginning of snowmelt; yellow: period 2 or snowmelt recession; green: period 3 or baseflow and grey: period 4 or rainfall runoff events) and from the sites position among the fluvial network of the Niagunguk River. The following sites classification (Mainstream: sites S1, S3, S5, S7, S18, S20-21, S24; East tributary: sites S6, S11-15; West tributary: site 19; Headwater sites group 1: sites S2, S22-23 and Headwater sites group 2: sites S4, S8-10, S16-17) reflect the PCA sites classification according to the landscape indexes. Only two rain samples are shown on the plot but local meteoric water line is traced from a total of 7 rain samples (other rain samples plot outside the plot range).

3.3.6 Geochemical and runoff dynamics

At each of the gauged sites the total runoff to peak flow values varied from 0.55 to 3.8 mm for the July 19-17 rainfall event, and from 0.94 to 6.4 mm for the July 27-28 rainfall event. The period range for the time when the flow begun to rise and to moment where the peak flow was reached for the first peakflow event was July 17 to July 20, while the second peak flow was shorter ranging from July 27 to July 29. The lag between of the runoff response and the peak flow also varied between sites and between each event (lag time range peak 1: 30 to 77 hours; peak 2: 41 to 66 hours). The two delineated baseflow periods ranged respectively between July 11 to 17 (baseflow runoff range: 1.6 to 9.9 mm) and from July 20 to 27 (baseflow runoff range: 0.05 to 6.2 mm). Figure 17a), b) and c) show that computed runoff to peak flow were generally higher following the rainfall event of July 27 (peakflow event 2) than 20 (peakflow event 2), either roughly linear relation (i.e., SpC) or nonlinear relation (i.e., DOC, $\delta^{18}O$) were observed between runoff to peak flow amplitude and streamflow chemistry is observed. Linear relation between streams chemistry and baseflow amplitude is inversed and less clear than for runoff to peak flow, though steep changes in means of some chemical parameter (i.e., DOC) and baseflow amplitude is observed (Figure d, e and f).

No clear relations were observed between the computed runoff to peak flow and any of the DA, DD and LAKE indices. The comparison between runoff to peak flow and SpC values measured during stormflow events showed that one increasing with the other (Figure 17a). During runoff event the amplitude of DOC or $\delta^{18}O$ concentrations measured at sampling sites were not related to the amplitude of the runoff computed for the same sites, but allowed to identify two clusters of sites with higher (DOC: ~ 2 mg L^{-1}; $\delta^{18}O$: ~ -10 $^{0}/_{00}$) and lower (DOC: ~ 1 mg L^{-1}; $\delta^{18}O$: ~ -16 $^{0}/_{00}$) DOC and $\delta^{18}O$ concentrations. Sites showing higher DOC concentration are clearly associated with the higher drainage density value computed among sites, while a clear relation is observed between SpC or $\delta^{18}O$ values and the DA or LAKE indices.

Sites where lower baseflow amplitude were measured are also generally associated to lower drainage area and drainage density values, while there is no clear trend between the proportion of lake areas within sites drained area and the baseflow contributions. During the baseflow periods, higher SpC values or DOC concentrations were generally observed for sites with smaller baseflow contributions, while once again no trends are present in the scattering of $\delta^{18}O$ concentrations along the computed baseflow. During baseflow conditions, higher $\delta^{18}O$

enriched waters were thus observed for sites with larger proportion of lake areas within their drainage area.

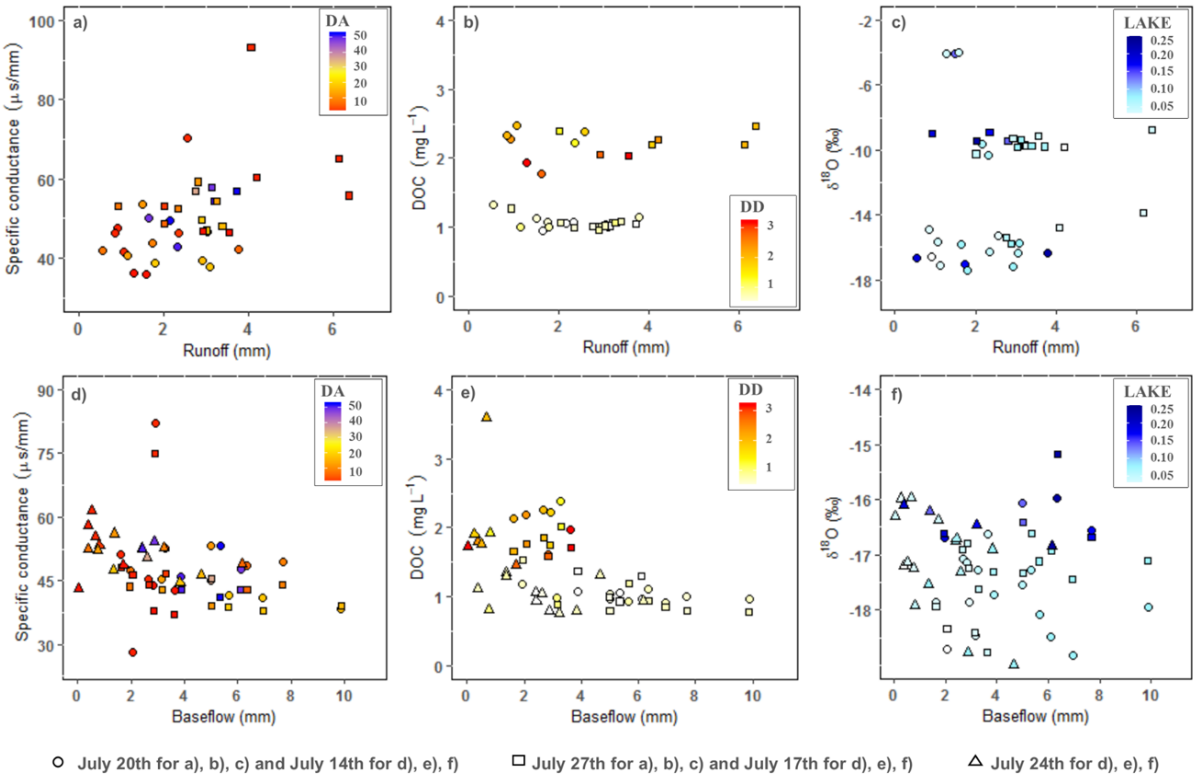

Figure 17. Relations between streamflow chemistry and total runoff measured at gauged sites for a), b) and c) total runoff to peak flow following the rainfall events of July 17-19 and July 27-28, for d), e) and f) baseflow periods preceding the stormflow events associated to the rainfall event aforementioned. July 20 and 27th are the of sampling conducted during the stormflow events, while July 14, 17 and 24 correspond to sampled dates during baseflow conditions. Color of points show the value of some specific landscape indices.

3.4 Discussion

By combining statistical analysis and field measurements investigating: (1) the evolution and ruptures in streamflow chemistry times series; (2) the influence of landscape features on the water chemistry sampled at 24 locations along the fluvial network of the Niaqunguk River; and (3) the significant watershed scale patterns explained the variability and similarity among sampling sites throughout different hydrological conditions, this work allowed us to identify four distinct hydrological period based on water chemistry and that

dominant landscape controls or spatial patterns of similarities or dissimilarities among sites evolved between periods. These observations pointed out specific hydrological processes that could explain the chemical variation and the evolution in relative water contributions observed among sites.

3.4.1 Watershed scale – temporal patterns

Statistical analyses of chemical-time series data from across our watershed sampling network led to the general delineation of 4 distinct hydrological periods corresponding to: early snowmelt, snowmelt recession, baseflow conditions and periods of late summer rainfall runoff (objective 1). Lower water SpC, water depleted in $\delta^{18}O$ and low Mg^{2+} concentrations were observed at the early snowmelt freshet, positive trend in the values of these chemical parameters was then observed as the flow decreased to low flow conditions and an increase in $\delta^{18}O$ and Mg^{2+} value ranges were observed during the flow rises that followed late summer rainfall event. We lacked DOC measurements prior to and immediately after the spring freshet but measurements made thereafter showed relatively higher values during higher flow conditions (i.e., end of snowmelt recession, peakflow following the rainfall event of July end) and slightly lower values during at lower streamflows. That relation between discharge and measured DOC concentration in streams differ from the observation of Moore (2003) made in a different environment type, but accord with relations observed by Carey (2003) or Finlay et al. (2006) made respectively in discontinuous and continuous permafrost watershed, characterized by variable extended of organic surficial cover. Standard deviation from mean DOC concentration measured among sites during higher flow conditions is, however, important and highlight the importance of better detailed the role played by landscape features (i.e., density of vegetation or organic deposits cover, degree of streams incision) in the control of DOC exports to streams. The temporal range of the delineated periods for the Niaqunguk River watershed fallow those of previous studies conducted on Arctic rivers systems of similar size (Battin et al., 2003; Lamhonwah et al., 2017a; McNamara et al., 1997), that respectively observed similar SpC/DOC, $\delta^{18}O$, $\delta^{18}O$/SpC variation dynamics through the snowmelt to the baseflow period or during important summer rainfall events. Our results suggest that water flows paths or major water sources to streamflow evolved during the arctic summer and that the four delineated periods can be used as specific temporal windows to

investigate dominant landscape controls and resulting hydrological processes within the Niaqunguk watershed.

3.4.2 Landscape controls on spatiotemporal patterns in streamflow chemistry

Landscape indices computed from characteristics of each sampling sites drainage area allowed a robust (R^2 = 0.8, Figure 12) repartition of the sampling sites based on their landscape similarities and dissimilarities. Variation partitioning analysis using the landscape indices thereafter explained significant portions (between 0.12 and 0.7) of the chemical variation in streamflow chemistry among sites. Here our objective was to identify potential landscape controls associated with temporal patterns in streamflow chemistry for the aforementioned hydrological periods (objective 2). For each of the four hydrological periods significant landscape indices were varying between chemical parameters (i.e., SpC, $\delta^{18}O$ or Mg^{2+}), providing insight on specific hydrological processes. Though Lake and Drift-SE were the dominant indices during the snowmelt recession period, Lake remained dominant during baseflow and UCA emerged during late summer rainfall runoff. The DD index was dominant for either the high or low periods delineated from the DOC time series. The obtained R2 were comparable with the results of other statistical models using landscape or other proxies (e.g., landscape entropy, soil moisture patterns, landscape composition) to investigate hydro-chemical dynamics and which did not have the aim of developing predictive models (Ali et al., 2010a; Tiwari et al., 2017; Williams et al., 2013). Instead of investigating the spatial patterns of the variation of water chemistry among sites for each of the sampling dates, the use of AEM eigenfunctions allowed to identify more parsimonious spatial patterns corresponding to the temporal scale of the delineated hydrological periods. Besides, these unique spatial patterns explained significant portion of chemical variations among sites (between 0.4 and 0.79) for the delineated hydrological periods. For either landscape indexes or models of AEM eigenfunctions, there was no unique explanatory variable that explained the variation of chemistry among sites and across periods, instead our results showed how controls on discharge and streamflow chemistry evolved across hydrological periods, the details of which are provided below.

3.4.2.1 Early snowmelt

In early snowmelt, water conductivity and oxygen isotope concentrations were significantly lower and with slight variability among sites compared to following periods. Only the DA index explained some of the SpC variation measured on June 13th, since slightly higher conductivity values were measured on the downstream section of the main river reach (Figure 14, SpC period 1). Spatial patterns of $\delta^{18}O$ measured among sites show that even if variation in concentration measured among sites was minor, the differences observed between neighbouring sites was more substantial relative to following periods when sites along the main reaches had more similar values. Studies investigating the relation between snowmelt dynamics and runoff showed that numerous processes, such as the drainage of meltwater over the snow surface or at the interface between snowpacks base and frozen ground (Lilbæk and Pomeroy, 2008), the variation in snow water equivalent or snow distribution within catchments (McCartney et al., 2006) and the differential rate of thaw (Quinton et al., 2009) need to be taking into account to understand hydrological dynamics during the snowmelt period. These studies also highlighted that variation in theses processes will affect the quantity and chemistry of water deliver to streams during snowmelt, but also have implication for the hydrological dynamic latter on the snow-free period. Woo and Throne (2006) showed that inter-annual variations in streamflow related to different snowmelt processes were particularly marked on headwater streams and even if the inter-annual variations were also observed along the main river system, the variability downstream was less marked. Streamflow chemistry observed at the catchment scale suggest that snowmelt was clearly the dominant water source during early snowmelt period, the slight variation in streamflow chemistry observed between neighbouring reaches may be related to different flow paths taken by this meltwater upgradient of the stream network, however the local effect of such variable meltwater trajectories would appear to be damped downstream by the convergence and mixing of water sources.

3.4.2.2 Snowmelt recession

Dominant landscape controls during the snowmelt recession period were the proportion of lakes and southern exposed drift areas, which explained respectively 0.53, 0.18 and 0.13 of the variation in $\delta^{18}O$, SpC andMg^{2+}values measured among sites. There was a clear

distinction between SpC and $\delta^{18}O$ values measured at sites along the east tributary, with the exception of sites S16 and S17 located upstream from the confluence with LAA discharge, from values measured at sites located either on the west, middle tributaries and the downstream reach. Higher SpC values and enriched $\delta^{18}O$ water were observed at lake dominated sites, while lower conductivity and isotopically depleted waters were observed at sites showing higher proportions of Drift-SE area. During snowmelt recession we suggest there was a change from a meltwater dominated system to one dominated by two distinct water sources: (i) meltwater from late lying snowpack along the middle tributary and at sites located downstream of the west tributary and (ii) contributions from lakes discharge at sites located downstream of lakes LA1 and LLA along the east tributary. Discharge measurements at sites S7 were not available until July 7th (i.e., baseflow period) which prevented us from establishing the exact streamflow discharge from these two portions of the river network. The similar water chemistry between downstream sites and upstream sites along the west and middle tributaries suggests that discharge was greater from the west/middle branches of the network relative to the eastern branch where our results suggest that lake discharge was dominant.

In arctic watersheds with undulating topography there is multiscale spatial variability in snow accumulation (Clark et al., 2011). Here the computed Drift-SE indices represent the variability in snow accumulation related scales between10-100 m, that is associated with both the preferential snow deposition in small hollows and in the lee of hillslopes or ridges, and the scouring of snow off exposed areas and its redistribution into more sheltered areas(Smith, 2018). Middle and west tributary stream valleys are often confined between ridges with surficial deposits dominated by till blanket. Till blanket areas are characterized by a higher density of stabilized gullies relative to areas of bedrock, till veneer or boulder fields that are dominant in other areas of the watershed.

The greater proportion of Drift-SE areas are found for sites located along the main reaches of the west and middle tributaries, which agrees with the landscape characteristic of these areas that favour snow accumulation and the formation of deep snow drifts. Important contributions from late lying snowpack and channels snow meltwater to stream during the snowmelt recession period has also been observed in other Arctic watersheds (Bolduc, 2015, Lamhonwah et al., 2017b) and highlighted the important role of residual snowpack and watershed geomorphology on the stream water geochemistry (Lisi et al., 2015).Since

landscape characteristic along the middle and west tributaries favour snow accumulation rather to landscape characteristics (i.e., in drainage areas of sites S6, S8 and S11-15 (i.e., east tributary sites downstream of LLA and LA1), greater and sustained snowmelt contributions are suggested in these areas and could then explain the depleted isotopic and lower SpC signature observed in streamflow of these sites.

Higher SpC values and enriched $\delta^{18}O$ water from lake dominated sites can be related to contributions of water stored in lakes from the previous year, which have been subject to $\delta^{18}O$ enrichment by evaporation and contributions from subsurface flow with higher conductivity (Dean et al., 2016; Gibson et al., 2002).The suggested smaller contribution from the east tributary to streamflow downstream can be first explained by its smaller drained area relative to the area drained by the combination of the middle and west tributaries. However, Woo et al. (1981) and Woo and Mielko (2007) showed the important role that arctic lakes play in modulating snowmelt discharge, as these lakes retain and more gradually release upgradient/upstream snowmelt contributions to the stream network; water that may also mix with the water stored in the lake from the previous year(s). Lag of the snowmelt runoff and mixing with previous year stored water could then also explain the relatively smaller and chemically different contribution from the east to streamflow downstream. Another process suggesting the limited contribution of lakes discharge relative to snowmelt earlier in the snowmelt recession is the persistence of snow sills at lake outlets that can result in important increases in lake storage capacity until flow from the lake can breach the snow dam (Woo, 1980). Field survey in mid June confirmed the presence of a snow or ice sills at the lake LLA discharge, that restricted its outflow. We subsequently observed ice debris flow downstream of LLA on June 20th that we suspect may have been associated with the breach of this ice/snow sill at the outlet of LLA.

3.4.2.3 Baseflow periods

Values measured for all chemical parameters (SpC, $\delta^{18}O$ and Mg^{2+}) increased during the baseflow period relative (Figure 11). If variability in SpC or Mg^{2+} values measured among sites remained similar or slightly increased during baseflow, the range of $\delta^{18}O$ values decreased compare to the previous hydrological period (P2). During the baseflow period the lake proportion remained the most significant (R_a^2 = 0.24) index to explain the variation in $\delta^{18}O$

among sites, but this index also became significant to explain the variation of Mg^{2+}measured among sites. Water chemistry observed during baseflow suggest that as basin snow was depleted, the Niaqunguk River system transited from snowmelt dominated to a system dominated by lake discharge contributions and by rainfall or snowmelt stored in the unfrozen portion of the active layer which contributed to streamflow via subsurface flow paths.

Increases in water conductivity as water flows within the mineral layer as the active layer thaws is a well-studied dynamic of watersheds underlain by continuous or discontinuous permafrost (Koch et al., 2014; Lamhonwah et al., 2017; Obradovic and Sklash, 1986). Increasing of water conductivity due to more important contributions of subsurface flows might also be enhanced by the decrease of contributions from other sources (i.e., meltwater from late lying snowpack, rainfall runoff via surficial paths) with lower conductivity, due to dryer conditions, increasing of the active layer storage capacity and the disappearance of snowpacks (Blaen et al., 2014).The reduced network scale variance in $\delta^{18}O$ between the snowmelt recession and baseflow periods can be explained by the distinct isotopic signature of lake outflows. The decreasing distinction between lake outflow and streamflow chemistry during the baseflow period was previously observed in the Niaqunguk watershed (Kjikjerkovska, 2016) and in other Arctic or Northern watersheds (Dean et al., 2016; Orlova and Branfireun, 2014). Other water contributions to streamflow suggested by the literature (Balasubramaniam et al., 2015; Obradovic and Sklash, 1986; Orlova and Branfireun, 2014; Walvoord et al., 2012; Woo and Mielko, 2007) during the baseflow period include: (i) water stored in ponds or surface depression that can connect to streams only during rainfall events; and (ii) contributions from slower water fluxes through the thawed portion of the active layer. These sources should then diminish the isotopic distinctions from lake contributions, since they have been to subject to evaporative enrichment and should both deliver relatively enriched $\delta^{18}O$ to stream (Tetzlaff et al., 2015; Throckmorton et al., 2016). The processes influencing the rates and timing of theses contributions is discussed in more details below.

Similar chemical signature among sites of the west and middle tributary and from the downstream reach was persistent during the baseflow period, though dissimilarities between water chemistry sampled at neighbouring sites along the east branch (i.e., 11 vs 12 and 13) or some headwater tributaries appeared (i.e., 10 vs 9 and 17 vs 16). This could suggest (1) a rupture of hydrological connectivity or rupture of flow; (2) a localized contribution of water

with a distinct chemical signature between sites; or (3) a decreasing in flow contribution from upstream that allowed a localized contribution of small amplitude to cause a distinction in water chemistry between sites, a chemical distinction that was not allowed when higher discharge was supplied from upstream. Katsuyama et al. (2009) showed that water contributions to streamflow that have taken slower flow paths or that have had longer residence times, are subject to various biogeochemical exchanges (e.g., enrichment, oxidation, reduction, cation exchange) and are more likely to have different geochemical signatures. Decreases in flow and enhanced storage in pool or lake area are some processes occurring at low flow that, combined with the contribution of water from hillslopes that have been subject to longer residence times, could enhance the chemical distinction in water sampled between neighbours' sites.

3.4.2.4 Late baseflow or summer rainfall runoff

The fourth period delineated from the $\delta^{18}O$ and Mg^{2+} time series is associated with both an abrupt rise in mean values of $\delta^{18}O$ and drop in mean values of Mg^{2+}, following rainfall events that occurred later in the monitoring period (i.e., July 17-19; July 27-28). The ranges of $\delta^{18}O$ and Mg^{2+} values measured across sites during these periods also increased considerably compared to previous periods. Water SpC showed no obvious response to rainfall events, instead a rise in water conductivity was observed for the last three sampling dates. Mean upslope contributing area computed in riparian area became the dominant index to explain the variation in chemistry (SpC, $\delta^{18}O$ and Mg^{2+}) among sites during that period. Spatial patterns showed that some water conductivity or isotopic differences that emerged between sites during baseflow (e.g.,S8 vs S9 orS11 vs S12 and S13 or S16 vs S17) were no longer prevalent late in the summer showing that sites S11-13 were back to similar SpC and $\delta^{18}O$ values and sites S8-9 or S16-17to similar $\delta^{18}O$ values.

If water conductivity generally increases as flow decreases in arctic streams, due to the rising importance of the subsurface contributions of water through the mineral layer relative to other sources such as surficial flows (Blaen et al., 2014), SpC values measured at sampling sites in this study do not show any significant drop during streamflow rise following rainfall events. That suggests either an increase of water contributions through mineral layers along within other sources or a greater contribution of lakes discharge with generally higher SpC

during stormflow events. In another landscape type, dominated by peat deposit and in much flatter areas, but where hydrological dynamics were closely related to permafrost, Connon et al. (2014) suggested that increasing in runoff was related to increasing thaw induced by land-cover change. Based on study conducted at the hillslope scale within the Niaqunguk watershed, Chiasson-Poirier et al. (see chapter 1) showed that increasing in active layer thaw can increase water storage and that higher saturation conditions could allow the overtaking of active layer sills or ridges and the connection of subsurface flows downslope. A similar dynamic was also suggested by Woo and Steer (1983) on a continuous permafrost hillslope near Resolute, NU. Thus, we suggest here that increasing of subsurface flows during the important rainfall event associated with an increasing thaw and thicker space for subsurface flows and allowed by the higher wetness conditions reached at the end July.

The relevance of UCA to explain the variation in chemistry among sites, reflects that areas subject to maintain higher saturation conditions during dry periods due to sustained water contributions could enhance localized rainfall-runoff contributions, but could also confirm our hypothesis of sustained subsurface flows due to higher wetness conditions. Jencso et al. (2010) showed that the combined analysis of upslope contributive areas with the delineation of riparian could be used to identify areas of enhanced contributions from new water to stream following rainfall events and riparian areas prone to maintain subsurface contributions to streamflow during dryer period. It was also shown that wetter areas could be associated to active layer deeper thaw due to greater heat transfer(Guan et al., 2010) These areas could after enhance the storage or the contributions of surface flow (Guan et al., 2010; Walvoord and Kurylyk, 2016).Higher saturation conditions should then (1) allow the new water (i.e.; water from snowmelt or rainfall that wasn't subjected to terrestrial processes that could change its chemistry) from hillslope to easily reach the stream via surface flow due to lower infiltration and rapid filling of riparian areas saturation deficit, and (2) favour thaw depth and more important contributions from old (i.e.; water that was subjected to longer flow paths, storage or longer residence time). Here we suggest that the increase in water conductivity without significant distinctions during rainfall events can be associated with an increase of subsurface flows along with active layer thaw depths and that importance of subsurface flows also increase along with active layer saturation increase during rainfall events.

Although, the aforementioned processes highlighted by the importance of the UCA index to explain the chemical variation among sites and suggesting localized water contribution to streams, slightly more similar chemistry was observed between the east, middle and west tributaries, while differences between neighbouring site chemistry disappeared during the late baseflow or summer rainfall runoff period. If water contributions that undertaken slower flow paths or that had longer residence time are more likely to have a greater variability in their geochemical signatures, event water, on the contrary, resulting from a stormflow wave will move rapidly throughout the catchment, have a shorter residence time and should have a more uniform chemical signature, similar to rainfall or snowmelt, thus a more similar chemical signature should be observed among water sources during stormflow event (Ali et al., 2010b). Woo and Mielko (2007) highlighted that the now well recognized processes of fill-and-spill of water over surficial or underground microtopography, could also be applied to lakes to explain the decreasing in discharge due to storage during dryer period and the abrupt increase in discharge when lake levels rise to a particular elevation. Even if the range of $\delta^{18}O$ values is greater during that period due to localized contributions associated to areas of higher UCA, the slightly more similar chemical signature between the three main tributaries could be explained be the mixing of old and new water contributions that led to more similar chemical signature to the one observed at the discharge of lake LLA. If lake discharge contributions increase due to spilling, but decreasing in chemistry differences between sites situated upstream and downstream is observed, that confirmed that the potential mixing between runoff sources contribution is more similar than lake water chemistry during that period. Localized surficial and subsurface runoff contributions, lake effects on runoff and water chemistry will be discussed in more details in the hydrological processes section.

3.4.2.5 Distinct dynamics in DOC concentrations

Throughout the period of available DOC concentration measurements, the drainage density index explained a large portion of the variation in concentration among sites, this index allows a clear distinction between headwater and sites located along the main streams, without regard for the progressive change in drained area for the latter sites, which fits well with the spatial patterns (headwater vs sites along main reaches) identified to explain DOC

variation. Here, the time clustering of the DOC time series didn't allow the distinction of sampling dates associated to stormflow events, due to the lack of increasing DOC relation along with stream discharge, DOC concentrations were only slightly higher and variable among sites during snowmelt recession and after the important rainfall event of July end, compared to low flow periods.

DOC concentration measured throughout summer were significantly lower than concentrations measured in other Arctic or Subarctic watersheds where peat or surficial organic cover layer are more important (Carey, 2003; Dean et al., 2016; Koch et al., 2014). However, they are comparable to those measured in catchments characterized by more sparse organic cover layer, bare mineral soil or dominated by bedrock outcrops (O' Donnell et al., 2016; Stewart and Lamoureux, 2011). Contrary to other basins underlain by permafrost and characterized by an important peat coverage, that shows sustained DOC contributions to streams, due to important flows through the surface organic layer (Carey, 2003), the delivery of DOC to stream in the Niaqunguk watershed seems to be more localized and enhanced during wetter periods.

In the Niaqunguk watershed there is an agreement between area of high upslope accumulation area (permanent or ephemeral headwater stream) and accumulation of organic deposits (Chiasson-Poirier et al., 2016), it also suggest that areas with abundant headwater stream (high drainage density) could explain the observed the higher DOC concentration in streams due more abundant surficial or shallow subsurface flows within these deposits. Increasing of surficial flow within the organic layer due to shallow active layer and high wetness conditions (i.e., snowmelt recession conditions) or related the saturation of the entire thawed mineral layer underlying the organic deposits (i.e., end of July higher wetness conditions) could explain the observed difference in localized higher and lower DOC concentrations associated respectively to higher and lower flow periods (Mu et al., 2017).As for the generally lower DOC concentrations observed in the main streams compared to headwaters, processes such DOC loss through hyporheic exchanges or mineralization (Battin et al., 2003; Vonk et al., 2015) during the course along the fluvial network can be considered.

3.4.3 Emerging hydrological processes

Evolution of spatial patterns in stream chemistry and significant landscape controls discussed above suggest that the following processes; snowmelt, lake storage and sustained contributions, subsurface flows, landscape storage and surficial runoff, controlled the delivery of water to stream. We observed that these processes were not only spatially nested, but also related to specific periods according to physicals or wetness conditions in the catchment.

3.4.3.1 Snowmelt contributions

Chemical results and landscape indices clearly suggested that snowmelt was the dominant water source during early snowmelt period, thus as melt progressed (i.e., snowmelt recession) other important water sources emerged and spatial patterns suggested the influence of landscape controls, such lakes, on the relative proportion of meltwater contributions to stream. Lack of discharge data early during the sampling period limits further discussions on the processes of drainage during the early snowmelt, though isotopic signature of most sites on the early snowmelt plotted along the LMWL in the range associated to snowmelt contributions observed elsewhere (Lamhonwah et al., 2017b; Throckmorton et al., 2016).Some headwater tributaries showed, however, already enriched δ^{18}Owater on June 13th. McNamara et al. (1997) also observed δ^{18}O enriched water flowing from a water than relatively to downstream water during snowmelt, rather to different water sources, they attributed these differences to differential isotopic fractionation of lighter or heavier δ^{18}O snowpacks, unevenly distributed between upland hillslope and stream valley. To this hypothesis, we can also add that some lakes can retain an isotopic signal closer to those of the previous year precipitations and then act as buffers for seasonal variation in isotopic signatures of water sources (e.g. snowmelt)(Jonsson et al., 2009).Early contributions from upland lakes located in scouring areas could also be considered to explain the enriched δ^{18}O signature observed at some sites.

The distinction between sites fed by snowmelt and by lake contributions was clear during the snowmelt recession period, because of the contribution of late lying snowpack in the drainage basin of sites with the greatest proportion of Drift-Se area that shows relatively depleted δ^{18}O values, comparatively to sites with greater proportion of lakes. The role of lakes in controlling discharge and streamflow chemistry during snowmelt recession is further

discussed below. The important contribution of meltwater to west, middle tributaries and to the river downstream is confirmed by the discharge observed at sites located along these streams (see Figure 15), which shows important diurnal cycles, indicating an increase of water delivery to stream during the day, due to higher solar radiation and warming air temperatures. Moreover, these diurnal cycles decreased or disappear following the snowmelt recession period. The long rain-free period that characterized the early snowmelt and the first portion of the snowmelt recession period could have enhanced the chemical distinction between sites dominated by snowmelt from those by lake water. Indeed rainfall event allows the connexion of surficial pounding water subject to evaporative $\delta^{18}O$ enrichment and displacement to the river of this water with chemical signature more similar to lake water, which could have been led to a rise in $\delta^{18}O$ values in streams then mainly fed by depleted snow melt (Ala-aho et al., 2018).

3.4.3.2 Lake storage and sustained contributions

Discharge measured at lake outlets sites and at sites along the east tributary greatly influenced by lake contributions highlighted three distinct dynamics; (1) the buffering effect of lakes on runoff during either the snowmelt recession or the summer rainfall periods, and (2) that some lakes maintained more constant discharge during dry periods which led to a rise of their relative contribution compared to other sources in the watershed, while inversely (3) lake could have led to flow cessation at downstream sites (see Figure 15). Here, discharge measured at the outlet of LA1 and LLA lakes (i.e., sites 8 and 15) show that outflow peaks were reduced in comparison with inflows (site 9) or from stormflow observed along other streams within the same area (sites 11 and 13), both lakes have retained the runoff water and releases it more gradually to outflows. The influence of these two lakes, however, changed during dry conditions, since LA1 outflow decreased along with inflows later on during baseflow period, while relatively constant discharge was observed at the LLA lake outflow. Woo (2012) detailed the relation between the lake storage capacity and the quantity of water released at the outflow, which relies on the lake level and the shape/elevation of the lake spillway. It has also been shown that lake size will be a significant factor in the determination of how lake will affect streamflow (Woo and Mielko, 2007), or water chemistry (Jonsson et al., 2009). If both LLA and LA1 lakes acted as buffers for snowmelt runoff, the greater storage capacity of the LLA lake

compared to LA1 due to its size, could than explain its sustained contribution during dry periods compared to LA1 that contributed significantly less to downstream flow during baseflow. During all sampling dates associated to baseflow conditions higher $\delta^{18}O$ values were observed for sites with the greatest proportion of lake areas or more precisely, sites along the east tributary and located downstream of the LLA, there is, however, no relations with the runoff amplitude computed at these stations (see Figure 17).As the LLA lake is subject to a more stable chemical signature, higher $\delta^{18}O$ concentrations were maintained at LLA discharge during baseflow compared to other lakes, moreover, its greater relative contributions during baseflow due to its constant discharge, can explain that water sampled at its downstream sites was also $\delta^{18}O$ enriched.

If the first two discussed lakes (i.e., LA1, LLA) were acting as buffers for runoff, resulting in significantly lower stormflow peak compared to upstream or other sites, the effect was not observed between sites S16 and S17 located along the east tributary headwater and separated by lake LA2. This highlights the importance of taking into account the lake position along the fluvial network and its geomorphological characteristics to assess its impact on the water flow and chemistry in different hydrological contexts (Martin and Soranno, 2006).If the three lakes discussed are located relatively upstream along the river network, they are characterized by different morphologies and position relative to landscape features, the first two are located more uplands and enclosed between bedrock ridges or moraine deposits and they both delayed the runoff, LLA due to is larger size also maintained consistent discharge during baseflow. The third (LA2) was located lower in a flat valley covered by glacial fluvial and organic deposits and did not change the dynamics between inflow and outflow. The lake position within the fluvial network, its storage capacity and its morphology are all key factors to consider how a specific lake will affect water flux in hydrological system, and studies previously conducted within the Niaqunguk watershed (Kjikjerkovska, 2016; Obradovic and Sklash, 1986), did not sufficiently consider lake affects, which, based on our observation of streamflow contributions from LLA, led to inadequate understanding of the hydrological dynamics within the watershed.

3.4.3.3 Subsurface and surficial runoff

Measured SpC values increased throughout the sampling period, although slightly lower values were observed on days following the rainfall events, the clustering of the SpC time series didn't allow to clearly distinguish the baseflow periods from the summer rainfall runoff periods. From that dynamic, we suggest an increase of subsurface flows along with active layer thaw depths, but also enhanced by higher subsurface wetness conditions following the important the rainfall event at the end of July. Here we observed that (1) slightly higher SpC values during baseflow were associated with smaller flow contributions and drained areas and (2) that water conductivity was increasing with runoff contributions during storm flow events, without relation with the drained area (Figure 17). This could suggest that, during baseflow, the proportion of mineral subsurface flows contributions were more important to the streamflow of headwater tributaries relative to their contributions to main streams. Decreasing of other source contributions than subsurface flows to sites with smaller drainage area will also enhance higher SpC values and explain that smaller baseflow runoff is also observed for these sites relative to site with larger drainage area, where other sources continue to contribute to streamflow. In contrast, we suggest that during stormflow events, the contribution from subsurface flows are more proportionally distributed among sites. Since there is no relation between the drainage area and either, the amplitude of computed runoff or the measured water conductivity, but that SpC increased along with runoff amplitude computed at sampling sites, it is more likely that the dynamic observed here is a mixing of the more conductive waters (i.e., mineral flows) distributed in the basin with important contributions more dilute water (i.e., lake outflow) further downstream, which corroborates dynamics observed in other arctic watershed (Blaen et al., 2014; Dugan et al., 2009).This dynamic would also confirm our hypothesis that higher saturation conditions lead to increasing of subsurface flows contributions when active layer thaw depths are important.

Instead of a direct contribution of new or rainfall water to stream due to saturation of the riparian area, high $\delta^{18}O$ values observed during stormflow event suggest that an important portion of water that connected to stream has prior been subject to previous isotopic evaporative enrichment. From that pattern, we propose that contributions to riparian areas from upslope could help to maintain wetter conditions and surficial ponding water, increasing of water contributions from upslope during rainfall event may then lead to displacement of

stored water and their reconnection to stream. In a study conducted within the Niaqunguk watershed by Obradovic and Sklash (1986) suggested that a great portion of stormflow event during the snowmelt was composed of old water stored during the previous summer and displaced downstream by infiltrating meltwater, explanation that has been used since in other studies (Blaen et al., 2014; Kjikjerkovska, 2016). Since the signature of pre-event water used to estimate their contribution to discharge was based on the isotopic signature of water sampled at the river outlet during baseflow, we argue that their estimation rather reflects the important and $\delta^{18}O$ enriched contributions from lakes during baseflow and the contribution from the spilling of water stored on the landscape to stream is overestimated. This process is, however, valuable to explain important surficial water contributions to stream during stormflow events. On a hillslope centrally located within the Niqunguk watershed and composed from fine-sand deposit covered with organic material, Chiasson-Poirier et al. (see chapter 1) showed that micro depressions on the surficial organic cover layer were enhanced the accumulation of water during snowmelt, which in turn enhanced the thaw, creating local depression in the frost table and contributed to sustain higher localized saturation conditions and surficial pounding water. Surficial pounding waters are subject to evaporative $\delta^{18}O$ enrichment (Tetzlaff et al., 2018)and as they spill downslope to reach the stream, they are also subject, if they flow over organic material, to become also enriched in dissolve organic carbon (Tetzlaff et al., 2015).

These processes will then explain the observed clusters of sites with higher DOC or $\delta^{18}O$ values during sampling dates corresponding to stormflow events (see Figure 17b and c).Sites with higher DOC concentrations mainly correspond to headwater sites (see higher drainage density) and the absence of relation with runoff amplitude suggests either a dilution of DOC in water by other sources with lower concentrations or as mentioned before, could be attributable to DOC loss through hyporheic exchanges or mineralization in larger streams (Battin et al., 2003; Vonk et al., 2015).While for the cluster of high $\delta^{18}O$ values observed during stormflow flow, the sites with large proportion of lakes are only displayed significantly higher $\delta^{18}O$ values during the rainfall event of July 27th higher in amplitude and intensity than the preceding event, which suggests that for the same runoff the relative contribution from the surface runoff of $\delta^{18}O$ enriched pounding water was more important due to the buffering effect at lake outflows.

3.5 Conclusion

This research provides insights into the contributions of different water sources and the evolution of dominant hydrological processes through different wetness conditions within the Niaqunguk River watershed. Four periods, corresponding to early snowmelt, snowmelt recession, baseflow and summer rainfall events, were delineated from the streamflow chemistry sampled along the river network. Water isotopic signature showed that at the end of the snowmelt recession the system transited from snowmelt to rainfall dominated. Lakes and pools along the river had important hydrological impacts by buffering snowmelt or rainfall runoff and by either sustained discharge or enhanced storage during baseflow, thus their influence was greatly related to their geomorphic settings. Relative contribution from subsurface flows increased during baseflow and we suggested that their absolute contribution increased during stormflow, spilling of surficial pounded water was, however, a more important water delivery source following rainfall events. Uncertainties with the determination of end member chemistry is an issue for the Niaqunguk watershed due to the overlap in chemistry of lake water and water store in the active layer or at its surface. More knowledge on the evolution the undersurface structure of boulder fields on its influence on water pathways or storage is still essential for further understanding of hydrological processes in this landscape.

Chapitre 4 - Discussion générale et conclusion

Plusieurs recherches récentes ont clairement démontré que la région Boréal-Arctique connait actuellement un réchauffement des températures de l'air (ACIA, 2013) qui impact de manière significative sur toutes les grandes sphères environnementales (atmosphère, biosphère, hydrosphère, cryosphère). Le cycle terrestre de l'eau en Arctique est intrinsèquement lié à la présence de pergélisol et aux profondeurs de dégel de sa couche superficielle (ou couche active) sujette au gel/dégel saisonnier, par ailleurs, plusieurs études ont aussi démontré que la prédiction des dynamiques de cette partie de la cryosphère, n'était possible qu'avec une meilleure compréhension de la répartition de l'eau et des échanges thermiques dans le paysage (de Grandpré et al., 2012; Hayashi et al., 2007; Hinkel and Nelson, 2003; Park et al., 2013).Une augmentation de la capacité de stockage de l'eau dans le sol, une modification de la connectivité entre les nappes d'eau souterraine supra-pergélisol avec les eaux de surface sont des processus susceptible de subir d'importants changements dans le contexte du réchauffement climatique (Bring et al., 2016). Ceux-ci impacteront certainement la manière dont l'augmentation prévue des précipitations en Arctique influencera la dynamique hydrologique des rivières. À l'échelle du paysage, nombreux autres processus reliés aux particularités locales du biome de la toundra arctique peuvent influencer les écoulements et les sources en eau pour les rivières de cette région. Ceux-ci devront être mieux compris pour confirmer que l'augmentation du débit observé pour quelques rivières arctiques (Smith et al., 2007; Walvoord and Striegl, 2007) est généralisable et amplifiera dans le futur. Cette recherche combine une caractérisation de l'évolution (1) des écoulements à l'échelle d'une pente durant la période de dégel de la couche active et (2) des processus et contrôles physiques dominants à l'échelle d'un petit bassin versant en fonctions de différentes périodes hydrologiques, afin d'améliorer notre compréhension des dynamiques hydrologique en milieux de pergélisol et des possibles impacts liés aux changements climatiques.

4.1 Liens entre dynamiques de drainage et de dégel de la couche active

Les dynamiques de drainage d'une pente, peu importe la présence ou non, de pergélisol, sont d'abord et avant toutes liées à la composition de celle-ci. Toutefois, le pergélisol limite la capacité de stockage de l'eau et les écoulements souterrains de sous-

surface à partie dégelée de la couche active (Woo, 2012). La présence de roche-mère, de dépôts meubles de différentes granulométries, d'un couvert organique ou encore d'une couche de faible conductivité hydraulique influencent la quantité d'eau de pluie ou de fonte des neiges qui sera stockée dans les dépressions de surface ou dans le sol après s'être infiltrée, de même que la quantité qui ruissèlera jusqu'au bas de la pente en surface ou à travers les dépôts. La pente instrumentée dans le premier article de ce mémoire est composée d'une couche de dépôts meubles et d'un couvert de matière organique d'épaisseur très variable. Ce type de structure est d'ailleurs typique de paysage de la toundra (Quinton and Marsh, 1999) et du bassin versant de la rivière Niaqunguk. Cette structure est aussi souvent associée aux zones d'importante accumulation topographique (Chiasson-Poirier et al., 2016).

Les connaissances acquises dans le premier chapitre de ce mémoire sont donc très importantes pour comprendre les mécanismes de circulation de l'eau du haut des pentes jusqu'aux cours d'eau dans ce type d'environnement. Les résultats apportent de nouvelles preuves de la grande influence de la microtopographie de surface sur les patrons d'écoulements et renforcent le concept de « *Fill-and-spill* » ou de remplissage-déversement pour expliquer la connectivité hydrologique entre le haut et le bas de la pente. Les dynamiques observées de dégel de la couche active sont irrégulières dans l'espace et dans le temps, tandis que l'influence de la microtopographie de surface s'opère aussi sur les patrons de dégel. Au début de la période étudiée, les profondeurs de dégel de la couche active étaient faibles et homogènes, à la suite de fortes précipitations, le dégel a augmenté de manière drastique et a été beaucoup plus important aux endroits où l'eau s'accumulait en surface selon les dépressions dans la microtopographie, créant du même coup des dépressions dans le plafond de gel. Contrairement aux dynamiques modélisées par Wright et al. (2009), les crêtes formées dans le plafond de gel de la pente étudiée n'ont pas engendré une rupture des écoulements souterrains, toutefois, elles ont semblé favoriser le maintien localisé de conditions de saturation plus importante de la couche active. Selon nos données sur la pente étudiée, il semble que la contribution des écoulements à travers la couche minérale de dépôts au ruisseau adjacent était trop faible pour entrainer des modifications de sa signature chimique, contrairement à la contribution des eaux stockées dans les dépressions de surface et qui ont ruisselé à travers les dépôts organiques jusqu'au ruisseau en période de précipitation. Les résultats de cette étude sont novateurs, car il présente une résolution spatiotemporelle de

mesure des conditions de dégel et de saturation de la couche active, qui, à notre connaissance, n'a pas encore été réalisée en Arctique. En liens avec plusieurs dynamiques décrites dans différentes recherches (Coles and McDonnell, 2018; Guan et al., 2010; Wright et al., 2009), notre étude permet d'améliorer notre compréhension du flux d'eau dans la couche active, pour lequel il y a actuellement un manque de connaissance important (Walvoord and Kurylyk, 2016).

4.2 Liens entre les échelles et dynamiques émergentes dans le bassin versant de la rivière Niaqunguk

La compréhension des dynamiques de drainage et de dégel de la couche active acquise à l'échelle d'une pente du bassin versant de la rivière Niaqunguk a grandement aidé l'interprétation des dynamiques observées dans le deuxième article de ce mémoire, qui a été réalisé à l'échelle du bassin versant de la rivière. Cette deuxième étude a permis d'identifier des caractéristiques physiques et les processus associés pouvant expliquer la variabilité des composantes chimiques et des volumes d'eau observée à travers le réseau hydrographique de la rivière Niaqunguk. De plus, elle démontre que les processus n'étaient pas statiques, mais évoluaient selon quatre grandes périodes hydrologiques qui correspondent au début de la fonte des neiges, à la récession de la fonte des neiges, à l'étiage estival et aux périodes de crues associées à certains évènements de précipitation estivale. En période de fonte des neiges, les données sur la proportion du territoire occupée par des lacs et sur les caractéristiques physiques propices à l'accumulation de neige nous permettent d'expliquer les différences chimiques entre les principaux cours d'eau de la rivière Niaqunguk et donc d'identifier les sources potentielles d'eau qui contribuent au débit de la rivière. Les lacs du bassin versant jouent un rôle très important, car ils constituent une source d'eau très importante en période d'étiage, ils peuvent aussi, selon leurs conditions morphologiques et leur emplacement sur le réseau hydrographique de la rivière, tamponner le ruissèlement de l'eau lors d'évènements de précipitation. Par ailleurs, nous constatons un autre processus important à l'échelle du bassin versant en période de précipitation. Il s'agit du ruissèlement de l'eau, stockée en surface soit dans les étangs ou dans de petites dépressions ~~et~~ qui est sujette à un enrichissement isotopique par évaporation, jusqu'aux cours d'eau, processus qui avaient d'ailleurs été observés à l'échelle de la pente,

L'étude nous a aussi permis de questionner l'hypothèse d'Obradovic et Sklash (1986) qui propose que l'importante proportion de la crue printanière associée à de vieilles eaux soit associée à une remise en circulation de l'eau stocker dans la couche active à l'automne précédent. Nous proposons plutôt, que cette importante proportion de vieilles eaux soit en fait associée à la contribution de l'eau stockée dans les lacs ayant généralement une signature chimique plus près des écoulements souterrains ou des eaux stockées en surface que des eaux de fonte. Notre étude à l'échelle de la pente démontre que la profondeur de dégel demeurait très faible au début du mois de juillet, période généralement associée à la récession de la crue de fonte des neiges. À cette période, même si la portion dégelée de la couche active était saturée, les contributions de la pente au cours d'eau adjacent ne permettaient pas de distinguer sa signature chimique de celle du lac en amont, sa principale source d'eau. Nous questionnons ici les travaux de Obradovic et Sklash (1986), principalement dans leur utilisation de la signature chimique de la rivière durant la période d'étiage comme traceur représentant la contribution de vieilles eaux ou de l'eau stockée dans la couche active, qui pourrait avoir menée à une confusion entre la signature isotopique de l'eau stoker dans la couche active et de l'eau des lacs. Ces résultats mettent en lumière l'importance de bien différentier la signature chimique des sources d'eau entre elles, lors de futures études biogéochimiques dans le bassin versant de la rivière Niaqunguk.

4.3 Changements potentiels des dynamiques hydrologiques dans un contexte de changement climatique

Les recherches récentes permettent d'affirmer que le pergélisol se réchauffe, conséquemment ce réchauffement devrait mener à une dégradation du pergélisol de surface généralisée à l'ensemble de l'Arctique (Pastick et al., 2015; Romanovsky et al., 2010; Slater and Lawrence, 2013). De nombreux facteurs peuvent influencer le régime thermique du pergélisol et mener à une dégradation non homogène de celui-ci (Jorgenson et al., 2010), toutefois le mode de dégradation le plus probable et le plus rependu du pergélisol s'opère par un approfondissement de la couche active. Selon les dynamiques observées dans notre premier article, il est aussi possible de suggérer que la dégradation du pergélisol sera plus importante aux endroits hydrologiquement actifs. Il a d'ailleurs été démontré que les écoulements et l'accumulation d'eau favorisent le transfert thermique et la dégradation du pergélisol de

surface par l'approfondissement de la couche active (de Grandpré et al., 2012). Dans une étude transarctique, Park et al. (2013) soulèvent l'importance de considérer des variables hydrologiques, comme les conditions d'humidité du sol et l'épaisseur du couvert de neige, dans les modèles de prévision de l'évolution du pergélisol, car celles-ci peuvent amplifier l'approfondissement de la couche active lié au réchauffement atmosphérique.

Les projections actuelles suggèrent une augmentation générale des précipitations en Arctique. Cette augmentation des précipitations totales devrait toutefois s'opérer par une augmentation de la fraction des précipitations sous forme de pluie et une diminution de celle sous forme de neige (AMAP, 2017). Cette diminution des précipitations sous forme de neige, accompagnée d'une diminution potentielle de l'épaisseur du couvert neige offrant une isolation au sol et une propagation du gel durant l'hiver (Quinton et al., 2005), pourrait suggérer une atténuation de la dégradation du pergélisol. Toutefois, en ce qui a trait au bassin de la rivière Niaqunguk, il a été démontré que les accumulations de neige sont grandement influencées par la topographie et qu'elles remplissent souvent les vallées des cours d'eau (Smith, 2018). Si un couvert neigeux prolongé peut retarder le dégel de la couche active au printemps (Quinton et al., 2009), il offre aussi une source d'eau importante pour combler la capacité de stockage de la couche active tôt durant la période de dégel. Nos données nous amènent à suggérer que les dynamiques de dégradation du pergélisol ne s'opèreront pas de manière uniforme et que plusieurs facteurs doivent être pris en compte pour prédire l'ampleur du dégel localement, toutefois une augmentation des conditions d'humidité durant l'été devrait favoriser de manière générale le dégel de la couche active lié au réchauffement des températures de l'air.

Un des principaux impacts hydrologiques que pourrait engendrer une dégradation du pergélisol de surface est l'augmentation des flux verticaux et latéraux des eaux souterraines suprapergélisol, qui sont limités par le caractère imperméable de celui-ci. Même si très peu d'études ont été réalisées, il est actuellement proposé, que le drainage des sols et la connectivité des écoulements dans la couche active augmenteront avec un approfondissement accentué de la couche active (Walvoord and Kurylyk, 2016). Connon et al. (2014), dans une des rares recherches sur le sujet, suggère que la dégradation du pergélisol peut autant limiter la connectivité de sous-surface en favorisant le stockage de l'eau que l'augmenter en créant de nouvelles trajectoires d'écoulements, mais que peu importe est sujet

à influencer les amplitudes de ruissèlement. Cette étude de Connon et al. (ibid) ayant toutefois été réalisée en milieu de pergélisol discontinu-sporadique n'est pas uniquement liée à l'approfondissement de la couche active. Les dynamiques étant toutefois sujettes à changer selon le contexte des sites d'études; la rivière Niqunguk étant située en zone de pergélisol continu, il est plausible que les changements de dynamiques hydrologiques risquent dans un avenir rapproché d'être reliés à l'augmentation de profondeur de la couche active dans ce bassin versant. Selon les dynamiques observées dans nos travaux, il est suggéré qu'un approfondissement de la couche active augmenterait les possibles connexions entre les nappes d'eau suprapergélisol. Toutefois, pour que ces connexions soient possibles, les conditions de saturation de la couche active devront être maintenues très élevées afin de permettre de surpasser les dépressions qui se forment dans le plafond de gel.

Considérant que l'approfondissement de la couche active augmente son volume de stockage, les apports en eau devront être de plus en plus important pour maintenir la saturation de celle-ci et permette une augmentation de la connectivité en période de sècheresse ou de déficit hydrique. Lors d'années particulièrement sèches, c'est plutôt une diminution de la connectivité des nappes suprapergélisol qui pourrait être observé. Enfin, l'augmentation des débits de base observée pour plusieurs rivières de l'Arctique (McClelland et al., 2006b) laisse suggérer qu'une augmentation de la contribution des écoulements de sous-surface aux rivières associée à une plus grande connectivité des écoulements souterrains soit actuellement le processus dominant. Toutefois, une bien meilleure compréhension de ces dynamiques est requise pour confirmer l'hypothèse de Walvoord and Kurylyk (2016) suggérant que nous assistons actuellement à une transition des systèmes hydrologiques de l'Arctique, voulant que les systèmes actuellement dominés par les écoulements de surface soit dans le futur dominés par les écoulements souterrains.

4.4 Limitations de l'étude

L'étude des dynamiques hydrologiques des environnements de pergélisol continu présente de nombreux défis en raison de leur éloignement géographique, du manque d'infrastructure ou de données cartographiques. S'ajoute aussi les aléas climatiques et les contraintes physiques avec lesquels nous devons composer sur nos terrains d'étude. Bien que la localisation de la rivière Niaqunguk à proximité de la ville d'Iqaluit, donnant accès aux

infrastructures les plus développées du Nunavut, soit facilitante, certains éléments comme les méthodes de suivi des écoulements dans la couche active, l'installation des instruments de mesure des débits au printemps et les données disponibles quant aux dépôts de surface dans le bassin versant ont limité les conclusions possiblement tirées dans ce travail.

L'installation de piézomètres pour le suivi des niveaux de la nappe d'eau souterraine et les mesures de gradient hydraulique est une méthodologie bien adaptée aux milieux tempérés. Toutefois, leur utilisation fut plus complexe en milieu de pergélisol en raison de l'aspect dynamique de la couche active, pour laquelle le plafond de gel s'approfondit durant l'été. Pour pallier à cette dynamique et s'assurer que les piézomètres ne se situaient pas au-dessus du niveau de la nappe, ceux-ci ont été renfoncés jusqu'au niveau du plafond de gel plusieurs fois durant la période d'étude. Cette procédure a engendré un décalage entre l'abaissement du niveau d'eau mesuré dans le piézomètre associé à l'abaissement de celui-ci au niveau du plafond de gel et le moment où le niveau d'eau se restabilisait à la hauteur réelle de la nappe, selon le gradient hydraulique. Cette dynamique a été expliquée par la faible conductivité hydraulique du matériel minéral de la pente et l'obstruction partielle des ouvertures du piézomètre. Les données de niveaux d'eau mesurées en continu n'ont donc pas pu être utilisées. Seules les mesures ponctuelles de niveau effectuées deux à trois jours après le repositionnement des piézomètres ont pu être utilisées. L'installation de puits d'observation perforés sur l'ensemble de la profondeur de la couche active serait mieux adaptée à l'étude des dynamiques d'écoulement dans la couche active. Elle nécessiterait toutefois l'installation des puits à l'automne lorsque l'amplitude maximale de dégel de la couche active est atteinte.

L'installation des enregistreurs de niveaux d'eau nécessaires au calcul de courbes de tarages utilisées pour estimer en continu le débit des cours d'eau à travers le bassin versant de la rivière Niaqunguk à l'été 2017, n'a été possible qu'au milieu du mois de juillet. Contrairement aux rivières similaires en zone tempérée, les écoulements sont stoppés durant l'hiver dans le bassin de la rivière Niaqunguk et le lit de la plupart des cours d'eau gel entièrement. Au printemps, les écoulements provenant de la fonte des neiges ne sont rarement canalisés dans le lit de la rivière qu'ils empruntent durant l'été. Ces écoulements s'effectuent à travers des canaux supra-neige, rendant impossible l'installation d'instrument de mesure permanente. Seules certaines sections de canyon s'incisant dans la roche sont dégelées assez tôt et condensent les écoulements printaniers permettant les mesures de débit

en continu. Ces sections sont toutefois toutes situées en aval du bassin versant. La mesure des flux hydrologiques durant la première partie de la crue de la fonte des neiges représente une limite importante pour l'étude des dynamiques hydrologiques dans le bassin de la rivière Niaqunguk. Il y a lieu de souligner que sans installations de grande envergure, la mesure de ces flux demeura limitée. Une densité d'échantillonnage plus importante et plus d'analyse chimique de l'eau à différents emplacements dans le bassin à cette période auraient toutefois pu permettre une meilleure compréhension des dynamiques d'écoulements.

Une étude réalisée dans le bassin versant de la rivière Niaqunguk (Chiasson-Poirier et al., 2016) a démontré que la délimitation du réseau hydrographique de la rivière pouvait être problématique en utilisant des modèles d'accumulation topographique basés sur des données d'élévation de surface, même de très haute résolution (< 1m). Les erreurs de délimitation étaient surtout localisées dans des zones où l'on retrouvait des champs de blocs. Ce type de dépôt, lorsque situé sur des pentes d'une certaine inclinaison (> 5º), sont souvent dépourvus de matrice fine et offre des chemins d'écoulement préférentiel pouvant ne pas correspondent aux élévations de surface. Dans le second article de ce mémoire, il a aussi été démontré que ces champs de blocs peuvent aussi favoriser le stockage de l'eau et la déconnexion entre certaines sources d'eau et la rivière en période plus sèche et lorsque le dégel de la couche active est avancé. Les données actuellement disponibles sur les dépôts de surface dans le bassin de la rivière Niaqunguk sont toutefois fragmentaires (Tremblay, Unpublished) ou de résolution grossière (Allard et al., 2012; Hodgson, 2003). Une meilleure cartographie des dépôts de surface dans le bassin versant de la rivière Niaqunguk, qui intègrerait une distinction entre les champs de blocs bien drainés (pente > 5º) et les champs de blocs en zone relativement plane qui présente des dynamiques hydrologiques différentes, souvent présents dans des milieux humides, aurait aider à pousser plus loin la compréhension des dynamiques hydrologiques dans ce bassin versant. Cette cartographie améliorée sera essentielle afin de réaliser une meilleure modélisation physique de ces dynamiques. Cette cartographie gagnerait aussi à être accompagnée d'une caractérisation de la structure physique souterraine des champs de bloc, ainsi que d'une étude plus poussée des dynamiques de gel/dégel et d'écoulement s'y opérant.

4.5 Implications pour la rivière Niaqunguk

Globalement, cette recherche propose des connaissances fondamentales essentielles à la compréhension des dynamiques hydrologiques en milieu de pergélisol. Ces connaissances favoriseront une meilleure compréhension des effets du réchauffement climatique et des changements qui en découlent dans les systèmes hydrologiques de l'Arctique. Ces connaissances sont d'autant plus importantes lorsque nous considérons que la rivière Niaqunguk a été ciblée comme source alternative d'eau potable par la ville d'Iqaluit, car la source actuelle deviendra, d'ici quelques années, insuffisante afin de répondre aux besoins d'une population qui s'accroit rapidement. Les lacs dans le bassin versant ont été identifiés comme une source d'eau majeure durant la période d'étiage. Donc, même si la majorité de l'eau durant la saison de débit provient des zones drainées par les tributaires Ouest et centraux, une exploitation de l'eau de la rivière en amont de la confluence avec le tributaire Est ne serait pas efficace en période d'étiage lorsque la demande d'eau est plus importante. La majeure partie de l'eau drainée par la rivière survient lors de la période de crue de la fonte des neiges. Un pompage de l'eau de la rivière ne sera fort probablement pas possible à cette période, car cette eau pompée devrait être stockée dans le lac Géraldine, qui sera alors à son niveau maximal. Il devient donc important d'évaluer si le débit estival de la rivière sera suffisant pour répondre au besoin accru d'eau de la ville. Localement, ces connaissances nous semblent essentielles afin de guider les décisions relatives à un emplacement durable pour une future exploitation de l'eau de la rivière. L'impact d'une diminution du débit de la rivière Niaqunguk et donc des éléments qu'elle transporte vers la Baie de Frobisher sur l'écosystème de la Baie devrait aussi faire l'objet d'un suivi avec la mise de l'avant du projet. Enfin, la rivière Niaqunguk, par sa taille, la diversité des processus hydrologiques qui s'y opèrent et sa proximité d'une ville arctique importante comme Iqaluit, s'avère être un site d'étude idéal. Cette étude, s'ajoutant aux études hydrologiques conduites dans le bassin versant de la rivière Niaqunguk (Chiasson-Poirier et al., 2016; Kjikjerkovska, 2016; Smith, 2018; Thiel, 2016) propose des connaissances et des questionnements essentiels à la compréhension de sa dynamique.

Bibliographie

ACIA, 2013. Impacts of a warming Arctic: Arctic Climate Impact Assessment (pp. 1-139). Cambridge University Press.

Akerman, H.J., Johansson, M., 2008. Thawing permafrost and thicker active layers in sub-arctic Sweden. Permafr. Periglac. Process. 19, 279–292. doi: 10.1002/ppp.626

Ala-aho, P., Soulsby, C., Pokrovsky, O.S., Kirpotin, S.N., Karlsson, J., Serikova, S., Manasypov, R., Lim, A., Krickov, I., Kolesnichenko, L.G., Laudon, H., Tetzlaff, D., 2018. Permafrost and lakes control river isotope composition across a boreal Arctic transect in the Western Siberian lowlands. Environ. Res. Lett. 13, 034028. doi: 10.1088/1748-9326/aaa4fe

Ali, G., Tetzlaff, D., Kruitbos, L., Soulsby, C., Carey, S., McDonnell, J., Buttle, J., Laudon, H., Seibert, J., McGuire, K., Shanley, J., 2014. Analysis of hydrological seasonality across northern catchments using monthly precipitation–runoff polygon metrics. Hydrol. Sci. J. 59, 56–72. doi: 10.1080/02626667.2013.822639

Ali, G.A., L'Heureux, C., Roy, A.G., Turmel, M.-C., Courchesne, F., 2011. Linking spatial patterns of perched groundwater storage and stormflow generation processes in a headwater forested catchment. Hydrol. Process. 25, 3843–3857. doi: 10.1002/hyp.8238

Ali, G.A., Roy, A.G., 2010. Shopping for hydrologically representative connectivity metrics in a humid temperate forested catchment: hydrologically representative connectivity. Water Resour. Res. 46. doi: 10.1029/2010WR009442

Ali, G.A., Roy, A.G., Legendre, P., 2010a. Spatial relationships between soil moisture patterns and topographic variables at multiple scales in a humid temperate forested catchment: soil moisture patterns and topography at multiple scale. Water Resour. Res. 46, n/a-n/a. doi: 10.1029/2009WR008804

Ali, G.A., Roy, A.G., Turmel, M.-C., Courchesne, F., 2010b. Multivariate analysis as a tool to infer hydrologic response types and controlling variables in a humid temperate catchment. Hydrol. Process. 24, 2912–2923. doi: 10.1002/hyp.7705

Ali, G.A., Roy, A.G., Turmel, M.-C., Courchesne, F., 2010c. Source-to-stream connectivity assessment through end-member mixing analysis. J. Hydrol. 392, 119–135. doi: 10.1016/j.jhydrol.2010.07.049

Allard, M., Doyon, J., LeBlanc, A.M., Mathon-Dufour, V., Oldenborger, G.A., Sladen, W.E., 2012. Surficial Geology, Iqaluit.

AMAP, 2017. Snow, Water, Ice and Permafrost in the Arctic (SWIPA). Arctic Monitoring and Assessment Programme, Oslo, Norway, 269pp.

AMAP, 2013. Arctic climate issues 2011: changes in Arctic snow, water, ice and permafrost. SWIPA 2011 Overview report. Arctic Monitoring and Assessment Programme, 97pp.

Anderson, A.E., Weiler, M., Alila, Y., Hudson, R.O., 2010. Piezometric response in zones of a watershed with lateral preferential flow as a first-order control on subsurface flow. Hydrol. Process. 24, 2237–2247. doi: 10.1002/hyp.7662

Anderson, B.T., Feldl, N., Lintner, B.R., 2018. Emergent Behavior of Arctic Precipitation in Response to Enhanced Arctic Warming: Enhanced Arctic Precipitation. J. Geophys. Res. Atmospheres 123, 2704–2717. doi: 10.1002/2017JD026799

ASTM D6913M-17, 2017. Standard Test Methods for Particle-Size Distribution (Gradation) of Soils Using Sieve Analysis. ASTM International, West Conshohocken, PA.

Battin, T.J., Kaplan, L.A., Newbold, J.D., Hendricks, S.P., 2003. A mixing model analysis of stream solute dynamics and the contribution of a hyporheic zone to ecosystem function*. Freshw. Biol. 48, 995–1014. doi: 10.1046/j.1365-2427.2003.01062.x

Berger, K.P., Entekhabi, D., 2001. Basin hydrologic response relations to distributed physiographic descriptors and climate. J. Hydrol. 247, 169–182. doi: 10.1016/S0022-1694(01)00383-3

Bintanja, R., 2018. The impact of Arctic warming on increased rainfall. Sci. Rep. 8. doi: 10.1038/s41598-018-34450-3

Blaen, P.J., Hannah, D.M., Brown, L.E., Milner, A.M., 2014. Water source dynamics of high Arctic river basins. Hydrol. Process. 28, 3521–3538. doi: 10.1002/hyp.9891

Blanchet, F.G., Legendre, P., Borcard, D., 2008a. Modelling directional spatial processes in ecological data. Ecol. Model. 215, 325–336. doi: 10.1016/j.ecolmodel.2008.04.001

Blanchet, F.G., Legendre, P., Borcard, D., 2008b. Forward selection of explanatory variables. Ecology 89, 2623–2632. doi: 10.1890/07-0986.1

Blume, Tromp-van Meerveld, 2015. From hillslope to stream: methods to investigate subsurface connectivity. Wiley Interdiscip. Rev. Water 2, 3415–3422. doi: 10.1002/wat2.1071

Bolduc, C., 2015. Thermal Evidence for Surface and Subsurface Water Contributions to Baseflow in a High Arctic River, Queen's University, Kingston, On.

Bolduc, C., Lamoureux, S.F., Franssen, J., 2018. Thermal and isotopic evidence for surface and subsurface water contributions to baseflow in a high Arctic river. Hydrol. Process. 32, 602–616. doi: 10.1002/hyp.11427

Borcard, D., Legendre, P., 2002. All-scale spatial analysis of ecological data by means of principal coordinates of neighbour matrices. Ecol. Model. 153, 51–68. http://dx.doi.org/10.1016/S0304-3800(01)00501-4

Brannen, R., Spence, C., Ireson, A., 2015. Influence of shallow groundwater-surface water interactions on the hydrological connectivity and water budget of a wetland complex: Shallow Groundwater-surface Water Interactions in a Wetland Complex. Hydrol. Process. 29, 3862–3877. doi: 10.1002/hyp.10563

Breiman, L., Friedman, J.H., Stone, C.G., 1984. Classification and Regression Trees. Wadsworth International Group, Belmont, CA.

Bring, A., Fedorova, I., Dibike, Y., Hinzman, L., Mård, J., Mernild, S.H., Prowse, T., Semenova, O., Stuefer, S.L., Woo, M.-K., 2016. Arctic terrestrial hydrology: A synthesis of processes, regional effects, and research challenges: Arctic Terrestrial Hydrology. J. Geophys. Res. Biogeosciences 121, 621–649. doi: 10.1002/2015JG003131

Brown, J., Ferrians, O.J., Heginbottom, J.A., Melnikov, E.S., 1997. Circum-Arctic map of permafrost and ground-ice conditions.

Burgers, H.E.R., Schipper, A.M., Jan Hendriks, A., 2014. Size relationships of water discharge in rivers: scaling of discharge with catchment area, main-stem length and precipitation. Hydrol. Process. 28, 5769–5775. doi: 10.1002/hyp.10087

Carey, S.K., 2003. Dissolved organic carbon fluxes in a discontinuous permafrost subarctic alpine catchment. Permafr. Periglac. Process. 14, 161–171. doi: 10.1002/ppp.444

Carey, S.K., Quinton, W.L., 2005. Evaluating runoff generation during summer using hydrometric, stable isotope and hydrochemical methods in a discontinuous permafrost alpine catchment. Hydrol. Process. 19, 95–114. doi: 10.1002/hyp.5764

Carey, S.K., Quinton, W.L., 2004. Evaluating snowmelt runoff generation in a discontinuous permafrost catchment using stable isotope, hydrochemical and hydrometric data. Hydrol. Res. 35, 309–324. doi: 10.2166/nh.2004.0023

Carey, S.K., Woo, M., 2005. Freezing of Subarctic Hillslopes, Wolf Creek Basin, Yukon, Canada. Arct. Antarct. Alp. Res. 37, 1–10. doi: 10.1657/1523-0430(2005)037[0001:FOSHWC]2.0.CO;2

Carey, S.K., Woo, M., 2001. Slope runoff processes and flow generation in a subarctic, subalpine catchment. J. Hydrol. 253, 110–129. http://dx.doi.org/10.1016%2FS0022-1694(01)00478-4

Carlston, C.W., 1963. Drainage Density and Streamflow. USGS 422–C, 8.

Chiasson-Poirier, G., Franssen, J., Fortier, D., Prince, A., Tremblay, T., Lafrenière, M., Shirley, J., Lamoureux, S., 2016. Methodological approach to characterize flow paths and water sources during the active-layer thaw period, Niaqunguk River watershed, Iqaluit, Baffin Island, Nunavut. Can. Nunavut Geosci. Off. - Summ. Act. 2016 105–119.

Clark, M.P., Hendrikx, J., Slater, A.G., Kavetski, D., Anderson, B., Cullen, N.J., Kerr, T., Örn Hreinsson, E., Woods, R.A., 2011. Representing spatial variability of snow water equivalent in hydrologic and land-surface models. Water Resour. Res. 47. doi: 10.1029/2011WR010745

Coles, A.E., McDonnell, J.J., 2018. Fill and spill drives runoff connectivity over frozen ground. J. Hydrol. 558, 115–128. doi: 10.1016/j.jhydrol.2018.01.016

Connon, R.F., Quinton, W.L., Craig, J.R., Hayashi, M., 2014. Changing hydrologic connectivity due to permafrost thaw in the lower Liard River valley, NWT, Canada. Hydrol. Process. 28, 4163–4178. doi: 10.1002/hyp.10206

Cooper, L.W., Solis, C., Kane, D.L., Hinzman, L.D., 1993. Application of Oxygen-18 Tracer Techniques to Arctic Hydrological Processes. Arct. Alp. Res. 25, 247. doi: 10.2307/1551821

de Grandpré, I., Fortier, D., Stephani, E., 2012. Degradation of permafrost beneath a road embankment enhanced by heat advected in groundwater [1] This article is one of a series of papers published in this CJES Special Issue on the theme of *Fundamental and applied research on permafrost in Canada* . Can. J. Earth Sci. 49, 953–962. doi: 10.1139/e2012-018

Dean, J.F., Billett, M.F., Baxter, R., Dinsmore, K.J., Lessels, J.S., Street, L.E., Subke, J.-A., Tetzlaff, D., Washbourne, I., Wookey, P.A., 2016. Biogeochemistry of “pristine” freshwater stream and lake systems in the western Canadian Arctic. Biogeochemistry 130, 191–213. doi: 10.1007/s10533-016-0252-2

Déry, S., 2008. Decreasing river discharge in northern Canada. Geophysical Research Letters 32. doi: 10.1029/2005GL022845

Dingman, S.L., 1978. Drainage density and streamflow: A closer look. Water Resour. Res. 14, 1183–1187. doi: 10.1029/WR014i006p01183

Dray, S., Legendre, P., Peres-Neto, P.R., 2006. Spatial modelling: a comprehensive framework for principal coordinate analysis of neighbour matrices (PCNM). Ecol. Model. 196, 483–493. doi: 10.1016/j.ecolmodel.2006.02.015

Dugan, H.A., Lamoureux, S.F., Lafrenière, M.J., Lewis, T., 2009. Hydrological and sediment yield response to summer rainfall in a small high Arctic watershed. Hydrol. Process. 23, 1514–1526. doi: 10.1002/hyp.7285

Fergus, C.E., Lapierre, J.-F., Oliver, S.K., Skaff, N.K., Cheruvelil, K.S., Webster, K., Scott, C., Soranno, P., 2017. The freshwater landscape: lake, wetland, and stream abundance and connectivity at macroscales. Ecosphere 8, e01911. doi: 10.1002/ecs2.1911

Fortier, D., Allard, M., Shur, Y., 2007. Observation of rapid drainage system development by thermal erosion of ice wedges on Bylot Island, Canadian Arctic Archipelago. Permafrost and Periglacial Processes 18, 229–243. doi: 10.1002/ppp.595

Galster, J.C., Pazzaglia, F.J., Hargreaves, B.R., Morris, D.P., Peters, S.C., Weisman, R.N., 2006. Effects of urbanization on watershed hydrology: The scaling of discharge with drainage area. Geology 34, 713. doi: 10.1130/G22633.1

Gao, T., Zhang, T., Wan, X., Kang, S., Sillanpää, M., Zheng, Y., Cao, L., 2016. Influence of microtopography on active layer thaw depths in Qilian Mountain, northeastern Tibetan Plateau. Environ. Earth Sci. 75. doi: 10.1007/s12665-015-5196-7

Gibson, J.J., Prepas, E.E., McEachern, P., 2002. Quantitative comparison of lake throughflow, residency, and catchment runoff using stable isotopes: modelling and results from a regional survey of Boreal lakes. J. Hydrol. 17. doi: 10.1016/S0022-1694(02)00022-7

Godin, E., Fortier, D., Coulombe, S., 2014. Effects of thermo-erosion gullying on hydrologic flow networks, discharge and soil loss. Environmental Research Letters 9, 105010. doi: 10.1088/1748-9326/9/10/105010

Godin, E., Fortier, D., Lévesque, E., 2016. Nonlinear thermal and moisture response of ice-wedge polygons to permafrost disturbance increases heterogeneity of high Arctic wetland. Biogeosciences 13, 1439–1452. doi: 10.5194/bg-13-1439-2016

Guan, X.J., Westbrook, C.J., Spence, C., 2010. Shallow soil moisture – ground thaw interactions and controls – Part 1: Spatiotemporal patterns and correlations over a subarctic landscape. Hydrol. Earth Syst. Sci. 14, 1375–1386. doi: 10.5194/hess-14-1375-2010

Haught, D.R.W., van Meerveld, H.J., 2011. Spatial variation in transient water table responses: differences between an upper and lower hillslope zone: spatial variation in transient water table response on a hillslope. Hydrol. Process. 25, 3866–3877. doi: 10.1002/hyp.8354

Hayashi, M., Goeller, N., Quinton, W.L., Wright, N., 2007. A simple heat-conduction method for simulating the frost-table depth in hydrological models. Hydrol. Process. 21, 2610–2622. doi: 10.1002/hyp.6792

Hendriks, A.J., Schipper, A.M., Caduff, M., Huijbregts, M.A.J., 2012. Size relationships of water inflow into lakes: Empirical regressions suggest geometric scaling. J. Hydrol. 414–415, 482–490. doi: 10.1016/j.jhydrol.2011.11.025

Hewlett, D.M., Hibbert, A.R., 1967. Factors affecting the response of small watersheds to precipitation in humid areas. Int. Symp. For. Hydrol. 275–290. doi: 10.1177/0309133309338118

Hinkel, K.M., Nelson, F.E., 2003. Spatial and temporal patterns of active layer thickness at Circumpolar Active Layer Monitoring (CALM) sites in northern Alaska, 1995–2000. J. Geophys. Res. 108. doi: 10.1029/2001JD000927

Hinzman, L.D., Deal, C.J., McGuire, A.D., Mernild, S.H., Polyakov, I.V., Walsh, J.E., 2013. Trajectory of the Arctic as an integrated system. Ecol. Appl. 23, 1837–1868. doi: 10.1890/11-1498.1

Hinzman, L.D., Kane, D.L., Gieck, R.E., Everett, K.R., 1991. Hydrologic and thermal properties of the active layer in the Alaskan Arctic. Cold Reg. Sci. Technol. 19, 95–110. http://dx.doi.org/10.1016/0165-232X(91)90001-W

Hodgson, D.A., 2005. Quaternary Geology of Western Meta Incognita Peninsula and Iqaluit Area, Baffin Island, Nunavut (No. 582). Geological Survey of Canada, Ottawa, Canada.

Hodgson, D.A., 2003. Surficial geology, Frobisher Bay, Baffin Island, Nunavut.

Horton, E.R., 1945. Erosional development of streeams and their drainage basins; Hydrophysical approach to quantitative morphology. Bull. Geol. Soc. Am. 56, 275–370. doi: 10.1130/0016-7606(1945)56[275:EDOSAT]2.0.CO;2

Iqaluit General Plan (No. By-law 703), 2010. Planning and Lands Department City of Iqaluit, Iqaluit.

Iqaluit Sustainable Community Plan, 2014. The Municipal Corporation of the City of Iqaluit, Iqaluit.

Jencso, K.G., McGlynn, B.L., Gooseff, M.N., Bencala, K.E., Wondzell, S.M., 2010. Hillslope hydrologic connectivity controls riparian groundwater turnover: Implications of catchment structure for riparian buffering and stream water sources. Water Resour. Res. 46, n/a-n/a. doi: 10.1029/2009WR008818

Jencso, K.G., McGlynn, B.L., Gooseff, M.N., Wondzell, S.M., Bencala, K.E., Marshall, L.A., 2009. Hydrologic connectivity between landscapes and streams: Transferring reach- and plot-scale understanding to the catchment scale. Water Resour. Res. 45, n/a-n/a. doi: 10.1029/2008WR007225

Jenson, S.K., Domingue, J.O., 1988. Extracting Topographic Structure from Digital Elevation Data for Geographic Information System Analysis. Photogramm. Eng. Remote Sens. 54, 1593–1600.

Jonsson, C.E., Leng, M.J., Rosqvist, G.C., Seibert, J., Arrowsmith, C., 2009. Stable oxygen and hydrogen isotopes in sub-Arctic lake waters from northern Sweden. J. Hydrol. 376, 143–151. doi: 10.1016/j.jhydrol.2009.07.021

Jorgenson, M.T., Romanovsky, V., Harden, J., Shur, Y., O'Donnell, J., Schuur, E.A.G., Kanevskiy, M., Marchenko, S., 2010. Resilience and vulnerability of permafrost to climate changeThis article is one of a selection of papers from The Dynamics of Change in Alaska's Boreal Forests: Resilience and Vulnerability in Response to Climate Warming. Can. J. For. Res. 40, 1219–1236. doi: 10.1139/X10-060

Kjikjerkovska, E., 2016. Long-term hydroclimatic change and interannual variability in water sources, Apex River (Iqaluit), Baffin Island, Nunavut. Queen's University, Kingston, Ontario.

Koch, J.C., Kikuchi, C.P., Wickland, K.P., Schuster, P., 2014. Runoff sources and flow paths in a partially burned, upland boreal catchment underlain by permafrost. Water Resour. Res. 50, 8141–8158. doi: 10.1002/2014WR015586

Koch, J.C., Runkel, R.L., Striegl, R., McKnight, D.M., 2013. Hydrologic controls on the transport and cycling of carbon and nitrogen in a boreal catchment underlain by continuous permafrost. J. Geophys. Res. Biogeosciences 118, 698–712. doi: 10.1002/jgrg.20058

Lamhonwah, D., Lafrenière, M.J., Lamoureux, S.F., Wolfe, B.B., 2017a. Evaluating the hydrological and hydrochemical responses of a High Arctic catchment during an exceptionally warm summer. Hydrol. Process. 31, 2296–2313. doi: 10.1002/hyp.11191

Lamhonwah, D., Lafrenière, M.J., Lamoureux, S.F., Wolfe, B.B., 2017b. Evaluating the hydrological and hydrochemical responses of a High Arctic catchment during an exceptionally warm summer. Hydrol. Process. 31, 2296–2313. doi: 10.1002/hyp.11191

Lamoureux, S.F., Lafrenière, M.J., Favaro, E.A., 2014. Erosion dynamics following localized permafrost slope disturbances. Geophys. Res. Lett. 41, 5499–5505. doi: 10.1002/2014GL060677

LeBlanc, A.-M., Oldenborger, G., Short, N., Allard, M., Mathon-Dufour, V., 2015. Ground temperatures and spatial permafrost conditions in Iqaluit, Baffin Island, Nunavut. Canada-Nunavut Geoscience Office, Iqaluit.

Legendre, P., Legendre, L., 2012. Numerical Ecology, 3nd ed. Elsevier Sci., Amsterdam, Netherlands.

Lilbæk, G., Pomeroy, J.W., 2008. Ion enrichment of snowmelt runoff water caused by basal ice formation. Hydrol. Process. 22, 2758–2766. doi: 10.1002/hyp.7028

Lisi, P.J., Schindler, D.E., Cline, T.J., Scheuerell, M.D., Walsh, P.B., 2015. Watershed geomorphology and snowmelt control stream thermal sensitivity to air temperature. Geophys. Res. Lett. 42, 3380–3388. doi: 10.1002/2015GL064083

Martin, S.L., Soranno, P.A., 2006. Lake landscape position: Relationships to hydrologic connectivity and landscape features. Limnol. Oceanogr. 51, 801–814. doi: 10.4319/lo.2006.51.2.0801

Mazurek, M., Paluszkiewicz, R., Rachlewicz, G., Zwoliński, Z., 2012. Variability of Water Chemistry in Tundra Lakes, Petuniabukta Coast, Central Spitsbergen, Svalbard. Sci. World J. 2012, 1–13. doi: 10.1100/2012/596516

McCartney, S.E., Carey, S.K., Pomeroy, J.W., 2006. Intra-basin variability of snowmelt water balance calculations in a subarctic catchment. Hydrol. Process. 20, 1001–1016. doi: 10.1002/hyp.6125

McClelland, J.W., Déry, S.J., Peterson, B.J., Holmes, R.M., Wood, E.F., 2006a. A pan-arctic evaluation of changes in river discharge during the latter half of the 20th century. Geophys. Res. Lett. 33. doi: 10.1029/2006GL025753

McClelland, J.W., Déry, S.J., Peterson, B.J., Holmes, R.M., Wood, E.F., 2006b. A pan-arctic evaluation of changes in river discharge during the latter half of the 20th century. Geophys. Res. Lett. 33. doi: 10.1029/2006GL025753

McDonnell, J.J., Beven, K., 2014. Debates-The future of hydrological sciences: A (common) path forward? A call to action aimed at understanding velocities, celerities and residence time distributions of the headwater hydrograph. Water Resour. Res. 50, 5342–5350. doi: 10.1002/2013WR015141

McDonnell, J.J., Sivapalan, M., Vaché, K., Dunn, S., Grant, G., Haggerty, R., Hinz, C., Hooper, R., Kirchner, J., Roderick, M.L., Selker, J., Weiler, M., 2007. Moving beyond heterogeneity and process complexity: A new vision for watershed hydrology. Water Resour. Res. 43. doi: 10.1029/2006WR005467

McNamara, J.P., Douglas, L., Hinzman, L.D., 1998. An analysis of streamflow hydrology in the Kuparuk River Basin, Arctic Alaska: a nested watershed approach. J. Hydrol. 206, 39–57. doi: 10.1016/S0022-1694(98)00083-3

McNamara, J.P., Douglas, L., Hinzman, L.D., 1997. Hydrograph separations in an Arctic watershed using mixing model and graphical techniques. Water Resour. Res. 33, 1707–1719. doi: 10.1029/97WR01033

Morison, M.Q., Macrae, M.L., Petrone, R.M., Fishback, L., 2017. Hydrology drives chemical synchronicity in subarctic tundra ponds. Biogeosciences Discuss. 1–28. doi: 10.5194/bg-2017-142

Mu, C.C., Abbott, B.W., Wu, X.D., Zhao, Q., Wang, H.J., Su, H., Wang, S.F., Gao, T.G., Guo, H., Peng, X.Q., Zhang, T.J., 2017. Thaw Depth Determines Dissolved Organic Carbon Concentration and Biodegradability on the Northern Qinghai-Tibetan Plateau: Thaw Depth Determines Dissolved C Export. Geophys. Res. Lett. 44, 9389–9399. doi: 10.1002/2017GL075067

Murphy, P.N.C., Ogilvie, J., Arp, P., 2009. Topographic modelling of soil moisture conditions: a comparison and verification of two models. Eur. J. Soil Sci. 60, 94–109. doi: 10.1111/j.1365-2389.2008.01094.x

Nelson, F.E., Hinkel, K.M., Shiklomanov, N.I., Mueller, G.R., Miller, L.L., Walker, D.A., 1998. Active-layer thickness in north central Alaska: Systematic sampling, scale, and spatial autocorrelation. J. Geophys. Res. Atmospheres 103, 28963–28973. doi: 10.1029/98JD00534

O. van Everdingen, R., 1998. Multi-language glossary of permafrost and related Ground-Ice terms. International Permafrost Association, Calgary.

Obradovic, M.M., Sklash, M.G., 1986. An isotopic and geochemical study of snowmelt runoff in a small arctic watershed. Hydrol. Process. 1, 15–30. doi: 10.1002/hyp.3360010104

O'Donnell, J.A., Aiken, G.R., Swanson, D.K., Panda, S., Butler, K.D., Baltensperger, A.P., 2016. Dissolved organic matter composition of Arctic rivers: Linking permafrost and parent material to riverine carbon: DOM Composition in Arctic Rivers. Glob. Biogeochem. Cycles 30, 1811–1826. doi: 10.1002/2016GB005482

Oksanen, J., Blanchet, G., Friendly, M., R, K., Legendre, P., McGlinn, D., Minchin, P.R., O'Hara, R.B., Simpson, G.L., 2018. vegan: Community Ecology Package. R package version 2.4-6.

Orlova, J., Branfireun, B.A., 2014. Surface Water and Groundwater Contributions to Streamflow in the James Bay Lowland, Canada. Arct. Antarct. Alp. Res. 46, 236–250. doi: 10.1657/1938-4246-46.1.236

Paquette, M., Fortier, D., Vincent, W.F., 2018. Hillslope water tracks in the High Arctic: Seasonal flow dynamics with changing water sources in preferential flow paths. Hydrological Processes 32, 1077–1089. doi: 10.1002/hyp.11483

Paquette, M., Fortier, D., Vincent, W.F., 2017. Water tracks in the High Arctic: a hydrological network dominated by rapid subsurface flow through patterned ground. Arctic Science 3, 334–353. doi: 10.1139/as-2016-0014

Park, H., Walsh, J., Fedorov, A.N., Sherstiukov, A.B., Iijima, Y., Ohata, T., 2013. The influence of climate and hydrological variables on opposite anomaly in active-layer thickness between Eurasian and North American watersheds. The Cryosphere 7, 631–645. doi: 10.5194/tc-7-631-2013

Pastick, N.J., Jorgenson, M.T., Wylie, B.K., Nield, S.J., Johnson, K.D., Finley, A.O., 2015. Distribution of near-surface permafrost in Alaska: Estimates of present and future conditions. Remote Sens. Environ. 168, 301–315. doi: 10.1016/j.rse.2015.07.019

Pistocchi, A., Pennington, D., 2006. European hydraulic geometries for continental SCALE environmental modelling. J. Hydrol. 329, 553–567. doi: 10.1016/j.jhydrol.2006.03.009

Pomeroy, J.W., Toth, B., Granger, R.J., Hedstrom, N.R., Essery, R.L.H., 2003. Variation in Surface Energetics during Snowmelt in a Subarctic Mountain Catchment. J. Hydrometeorol. 4, 702–719. doi: 10.1175/1525-7541(2003)004<0702:VISEDS>2.0.CO;2

Preston, S.D., Alexander, R.B., Schwarz, G.E., Crawford, C.G., 2011. Factors Affecting Stream Nutrient Loads: A Synthesis of Regional SPARROW Model Results for the Continental United States1: Factors Affecting Stream Nutrient Loads: A Synthesis of Regional SPARROW Model Results for the Continental United States. JAWRA J. Am. Water Resour. Assoc. 47, 891–915. doi: 10.1111/j.1752-1688.2011.00577.x

Quinton, W.L., Bemrose, R.K., Zhang, Y., Carey, S.K., 2009. The influence of spatial variability in snowmelt and active layer thaw on hillslope drainage for an alpine tundra hillslope. Hydrol. Process. 23, 2628–2639. doi: 10.1002/hyp.7327

Quinton, W.L., Marsh, P., 1999. A conceptual framework for runo€ generation in a permafrost environment. Hydrol. Process. 13, 2563–2581. doi: 10.1002/(SICI)1099-1085(199911)13:16%3C2563::AID-HYP942%3E3.0.CO;2-D

Quinton, W.L., Marsh, P., 1998. The influence of mineral earth hummocks on subsurface drainage in the continuous permafrost zone. Permafr. Periglac. Process. 9, 213–228. doi: 10.1002/(SICI)1099-1530(199807/09)9:3<213::AID-PPP285>3.0.CO;2-E

Quinton, W.L., Shirazi, T., Carey, S.K., Pomeroy, J.W., 2005. Soil water storage and active-layer development in a sub-alpine tundra hillslope, southern Yukon Territory, Canada. Permafr. Periglac. Process. 16, 369–382. doi: 10.1002/ppp.543

R Core Team, 2017. R: A language and environment for statistical computing.

Romanovsky, V.E., Smith, S.L., Christiansen, H.H., 2010. Permafrost thermal state in the polar Northern Hemisphere during the international polar year 2007-2009: a synthesis. Permafr. Periglac. Process. 21, 106–116. doi: 10.1002/ppp.689

Roulet, N.T., Woo, M.-K., 1988. Runoff generation in a low Arctic drainage basin. J Hydrol 213–226. http://dx.doi.org/10.1016/0022-1694(88)90036-4

Shaman, J., Stieglitz, M., Burns, D., 2004. Are big basins just the sum of small catchments? Hydrol. Process. 18, 3195–3206. doi: 10.1002/hyp.5739

Slater, A.G., Lawrence, D.M., 2013. Diagnosing Present and Future Permafrost from Climate Models. J. Clim. 26, 5608–5623. doi: 10.1175/JCLI-D-12-00341.1

Smith, K., 2018. Snow Accumulation in the Niaqunguk (Apex) River Watershed near Iqaluit, Nunavut, Canada. Carleton, Ottawa, Canada.

Smith, L.C., Pavelsky, T.M., MacDonald, G.M., Shiklomanov, A.I., Lammers, R.B., 2007. Rising minimum daily flows in northern Eurasian rivers: A growing influence of groundwater in the high-latitude hydrologic cycle. Geophys. Res. Biogeosciences 112, n/a-n/a. doi: 10.1029/2006JG000327

Spence, C., Woo, M., 2003. Hydrology of subarctic Canadian shield: soil-filled valleys. J. Hydrol. 279, 151–166. doi: 10.1016/S0022-1694(03)00175-6

Squires, C.A., 1984. The late Foxe deglaciation of the Burton Bay area southeastern Baffin Island, N.W.T. University of Windsor, Windsor, ontario.

St Amour, N.A., Gibson, J.J., Edwards, T.W.D., Prowse, T.D., Pietroniro, A., 2005. Isotopic time-series partitioning of streamflow components in wetland-dominated catchments,

lower Liard River basin, Northwest Territories, Canada. Hydrol. Process. 19, 3357–3381. doi: 10.1002/hyp.5975

St. Jacques, J.-M., Sauchyn, D.J., 2009. Increasing winter baseflow and mean annual streamflow from possible permafrost thawing in the Northwest Territories, Canada. Geophys. Res. Lett. 36. doi: 10.1029/2008GL035822

Stewart, K.A., Lamoureux, S.F., 2011. Connections between River Runoff and Limnological Conditions in Adjacent High Arctic Lakes: Cape Bounty, Melville Island, Nunavut. ARCTIC 64. doi: 10.14430/arctic4097

Tetzlaff, D., Birkel, C., Dick, J., Geris, J., Soulsby, C., 2014. Storage dynamics in hydropedological units control hillslope connectivity, runoff generation, and the evolution of catchment transit time distributions. Water Resour. Res. 50, 969–985. doi: 10.1002/2013WR014147

Tetzlaff, D., Buttle, J., Carey, S.K., McGuire, K., Laudon, H., Soulsby, C., 2015. Tracer-based assessment of flow paths, storage and runoff generation in northern catchments. Hydrol. Process. 29, 3475–3490. doi: 10.1002/hyp.10412

Tetzlaff, D., Piovano, T., Ala-Aho, P., Smith, A., Carey, S.K., Marsh, P., Wookey, P.A., Street, L.E., Soulsby, C., 2018. Using stable isotopes to estimate travel times in a data-sparse Arctic catchment: Challenges and possible solutions. Hydrol. Process. 32, 1936–1952. doi: 10.1002/hyp.13146

Therneau, T.M., Atkinson, B., 2014. mvpart: Multivariate partitioning. R package version 1.6-1.

Thiel, G.D., 2016. Investigating seasonal hydrology and its relationship with microbiological indicators in the Apex River watershed (Iqaluit, Nunavut). Queen's University, Kingston, Ontario.

Throckmorton, H.M., Newman, B.D., Heikoop, J.M., Perkins, G.B., Feng, X., Graham, D.E., O'Malley, D., Vesselinov, V.V., Young, J., Wullschleger, S.D., Wilson, C.J., 2016. Active layer hydrology in an arctic tundra ecosystem: quantifying water sources and cycling using water stable isotopes: Active Layer Hydrology in the Arctic Coastal Plain. Hydrol. Process. 30, 4972–4986. doi: 10.1002/hyp.10883

Tiwari, T., Lidman, F., Laudon, H., Lidberg, W., Ågren, A.M., 2017. GIS-based prediction of stream chemistry using landscape composition, wet areas, and hydrological flow pathways: Modeling Biogeochemistry. J. Geophys. Res. Biogeosciences 122, 65–79. doi: 10.1002/2016JG003399

Tremblay, T., Unpublished. Detailed surficial geology map for area northeast of Iqaluit.

Tromp-van Meerveld, H.J., McDonnell, J.J., 2006a. Threshold relations in subsurface stormflow: 2. The fill and spill hypothesis: THRESHOLD FLOW RELATIONS, 2. Water Resour. Res. 42, n/a-n/a. doi: 10.1029/2004WR003800

Tromp-van Meerveld, H.J., McDonnell, J.J., 2006b. Threshold relations in subsurface stormflow: 2. The fill and spill hypothesis. Water Resour. Res. 42, W02411. doi: 10.1029/2004WR003800

U. S. Department of the Interior Bureau of Reclamation, 2001. Water measurement manual, 3ed. U.S. Department of the Interior, Bureau de Reclamation, Washington, DC.

van Meerveld, H.J., Seibert, J., Peters, N.E., 2015. Hillslope-riparian-stream connectivity and flow directions at the Panola Mountain Research Watershed: Hillslope-Riparian-Stream Connectivity and Flow Directions at Panola. Hydrol. Process. 29, 3556–3574. doi: 10.1002/hyp.10508

Vonk, J.E., Tank, S.E., Mann, P.J., Spencer, R.G.M., Treat, C.C., Striegl, R.G., Abbott, B.W., Wickland, K.P., 2015. Biodegradability of dissolved organic carbon in permafrost soils and aquatic systems: a meta-analysis. Biogeosciences 12, 6915–6930. doi: 10.5194/bg-12-6915-2015

Walsh, J.E., Overland, J.E., Groisman, P.Y., Rudolf, B., 2011. Ongoing Climate Change in the Arctic. AMBIO 40, 6–16. doi: 10.1007/s13280-011-0211-z

Walvoord, M.A., Kurylyk, B.L., 2016. Hydrologic Impacts of Thawing Permafrost—A Review. Vadose Zone J. 15. doi: 10.2136/vzj2016.01.0010

Walvoord, M.A., Striegl, R.G., 2007. Increased groundwater to stream discharge from permafrost thawing in the Yukon River basin: Potential impacts on lateral export of carbon and nitrogen. Geophys. Res. Lett. 34. doi: 10.1029/2007GL030216

Water Office Canada, 2019. Historical Daily Discharge, Apex River at Apex (10UH002). Environment Canada. Retrieved from: https://wateroffice.ec.gc.ca/report/historical_e.html?stn=10UH002 (Jan. 2019)

Williams, T.J., Quinton, W.L., Baltzer, J.L., 2013. Linear disturbances on discontinuous permafrost: implications for thaw-induced changes to land cover and drainage patterns. Environ. Res. Lett. 8, 025006. doi: 10.1088/1748-9326/8/2/025006

Woo, M., 2012. Permafrost Hydrology. Springer Berlin Heidelberg, Berlin, Heidelberg.

Woo, M., Mielko, C., 2007. An integrated framework of lake-stream connectivity for a semi-arid, subarctic environment. Hydrol. Process. 21, 2668–2674. doi: 10.1002/hyp.6789

Woo, M., Steer, P., 1983. Slope hydrology as influenced by thawing of the active layer, Resolute, NWT. Can. J. Earth Sci. 20, 978–986. http://dx.doi.org/10.1139/e83-087

Woo, M.-K., 1980. Hydrology of a small lake in the candadian high Arctic. Arct. Alp. Res. 12, 227–235. doi: 10.1080/00040851.1980.12004181

Woo, M.-K., Kane, D.L., Carey, S.K., Yang, D., 2008. Progress in permafrost hydrology in the new millennium. Permafr. Periglac. Process. 19, 237–254. doi: 10.1002/ppp.613

Woo, M.-K., Steer, P., 1982. Occurrence of surface flow on arctic slopes, southwestern Cornwallis Island. Can. J. Earth Sci. 19, 2368–2377. doi: 10.1139/e82-206

Woo, M.-K., Thorne, R., 2006. Snowmelt contribution to discharge from a large mountainous catchment in subarctic Canada. Hydrol. Process. 20, 2129–2139. doi: 10.1002/hyp.6205

Wright, N., Hayashi, M., Quinton, W.L., 2009. Spatial and temporal variations in active layer thawing and their implication on runoff generation in peat-covered permafrost terrain. Water Resour. Res. 45, W05414. doi: 10.1029/2008WR006880

Wrona, F.J., Johansson, M., Culp, J.M., Jenkins, A., Mård, J., Myers-Smith, I.H., Prowse, T.D., Vincent, W.F., Wookey, P.A., 2016. Transitions in Arctic ecosystems: Ecological implications of a changing hydrological regime. J. Geophys. Res. Biogeosciences 121, 650–674. doi: 10.1002/2015JG003133

Young, K.L., Woo, M., Edlund, S.A., 1997. Influence of Local Topography, Soils, and Vegetation on Microclimate and Hydrology at a High Arctic Site, Ellesmere Island, Canada. Arct. Alp. Res. 29, 270. doi: 10.2307/1552141

Annexe A - Components of the self-made pressure sensor/logger

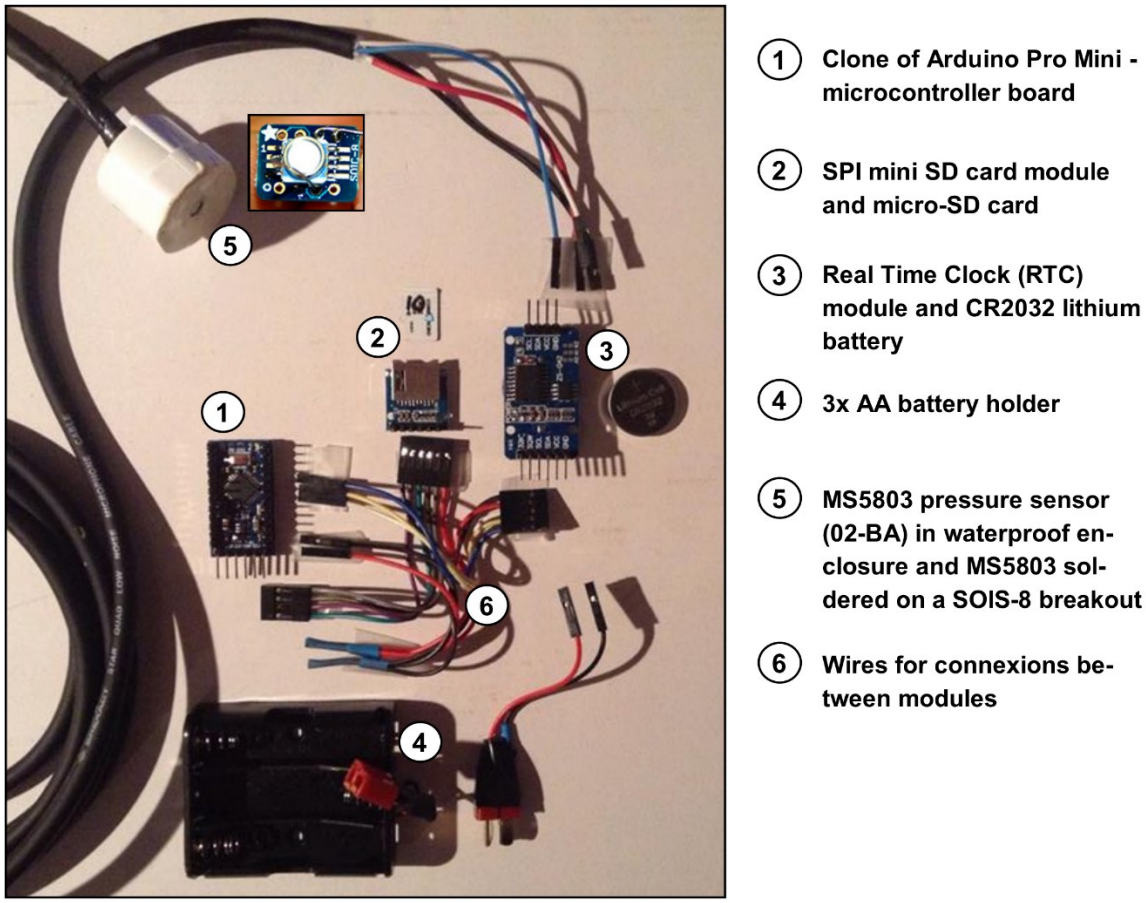

Figure A1. Components used to construct self-made pressure sensor / logger units. MS5803 pressure sensors as a accuracy of ±0.5 mbar and is manufactured by TE connectivity, Schaffhausen, Switzerland. More details on the construction of the MS5803 pressor sensor - board and on the Arduino mini data logger are provided on The Cave Pearl Project (https://thecavepearlproject.org/2014/03/27/adding-a-ms5803-02-high-resolution-pressure-sensor/ and https://thecavepearlproject.org/2016/10/27/diy-arduino-promini-data-logger-2016-build-update/)

Annexe B - Water levels and ratings curves

In appendix B, the raw and smoothed water levels at each of the 19 gauged sites. The rating curves, relation type and R^2 are also shown. Smoothing of water levels were performed using loess regression with span parameters of 0.03 or 0.04, which correspond to the proportion of time series data taking into account to predict the smoothed value. Significance of rating curves were varying between 0.93 and 0.99 and amount of discharge measurements used to derive the stage - discharge relationships varying between 3 and 10. Grey shading area around rating curves indicate the 0.95 confidence interval.

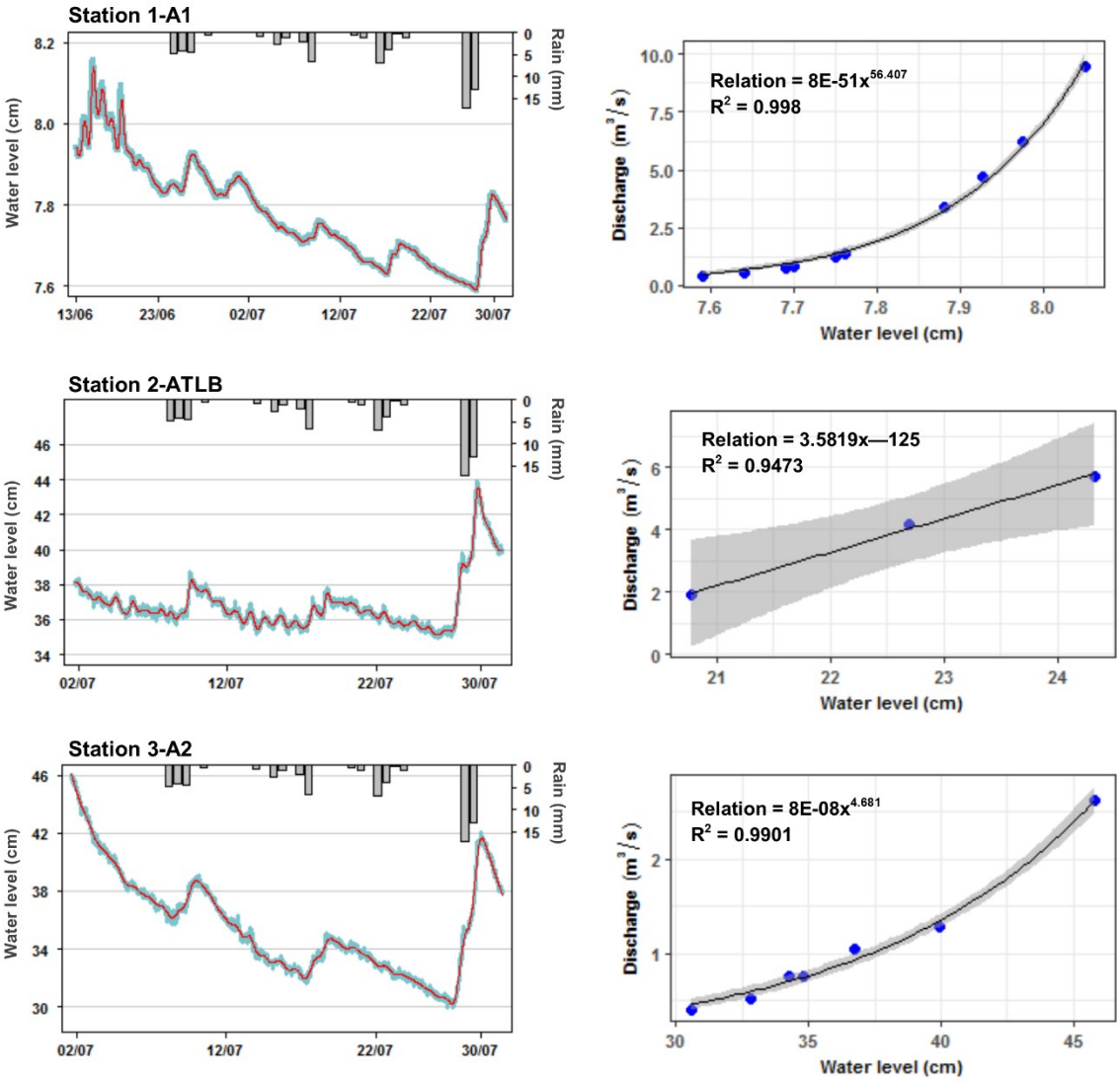

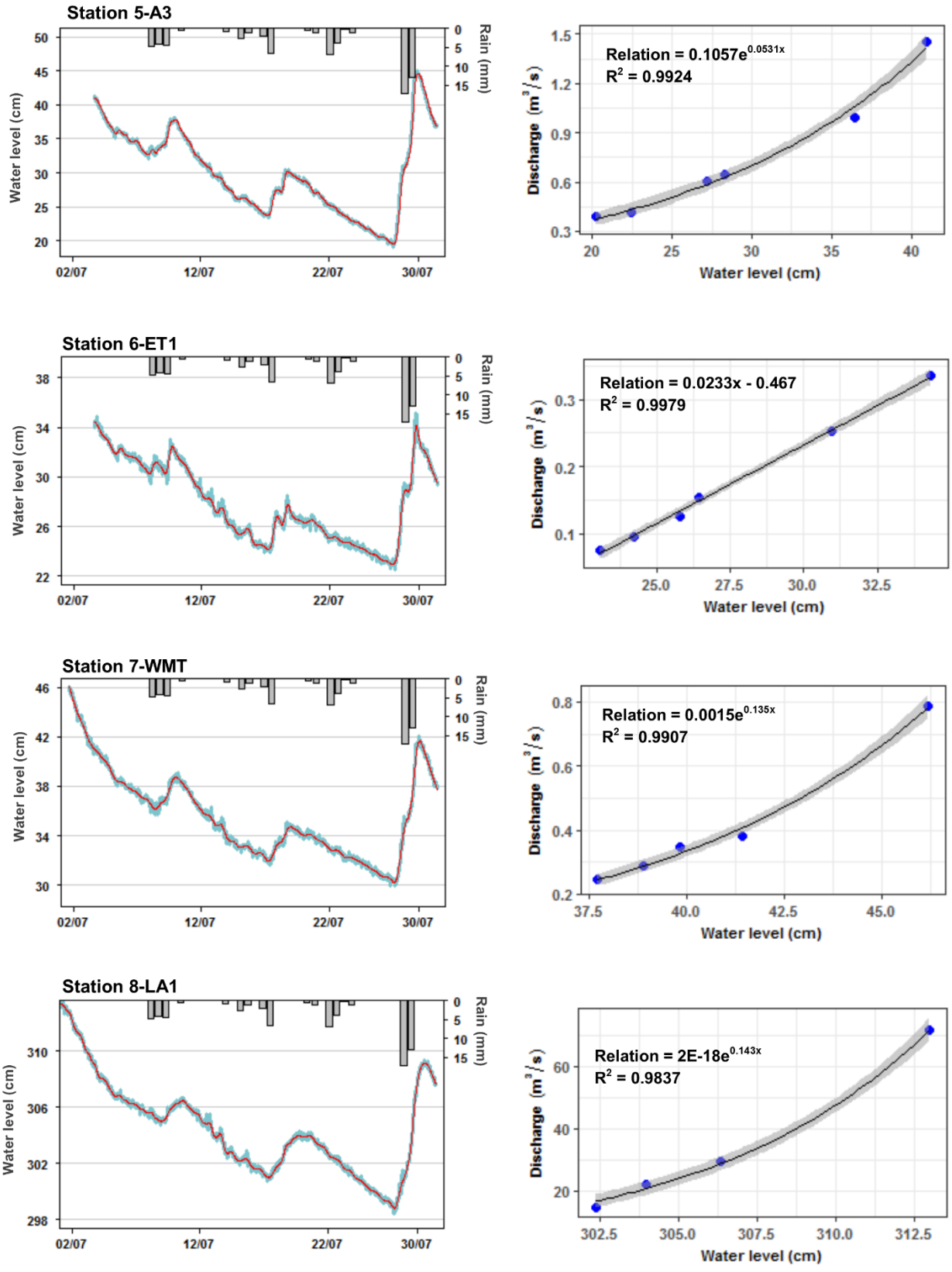
Station 5-A3
Water level (cm)
Rain (mm)
02/07
12/07
22/07
30/07
Relation = 0.1057e^0.0531x
R² = 0.9924
Discharge (m³/s)
Water level (cm)
Station 6-ET1
Relation = 0.0233x - 0.467
R² = 0.9979
Station 7-WMT
Relation = 0.0015e^0.135x
R² = 0.9907
Station 8-LA1
Relation = 2E-18e^0.143x
R² = 0.9837

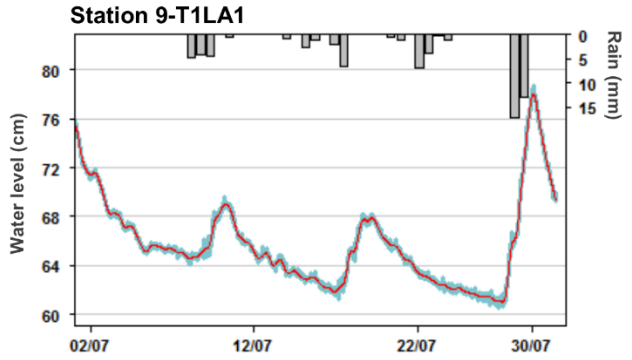
Station 9-T1LA1
Water level (cm)
Rain (mm)
02/07
12/07
22/07
30/07

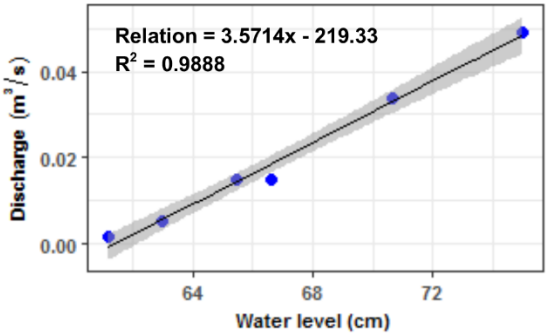
Relation = 3.5714x - 219.33
R² = 0.9888
Discharge (m³/s)
Water level (cm)

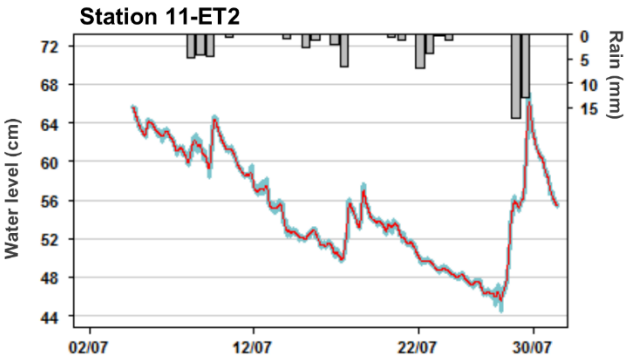
Station 11-ET2
Water level (cm)
Rain (mm)
02/07
12/07
22/07
30/07

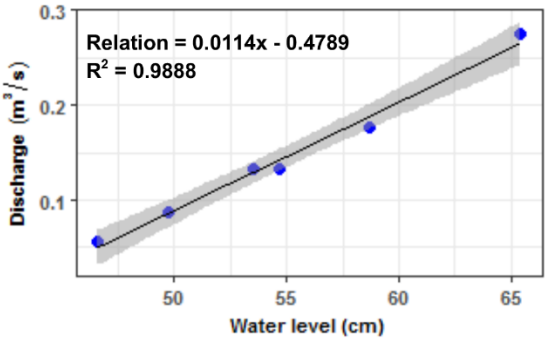
Relation = 0.0114x - 0.4789
R² = 0.9888
Discharge (m³/s)
Water level (cm)

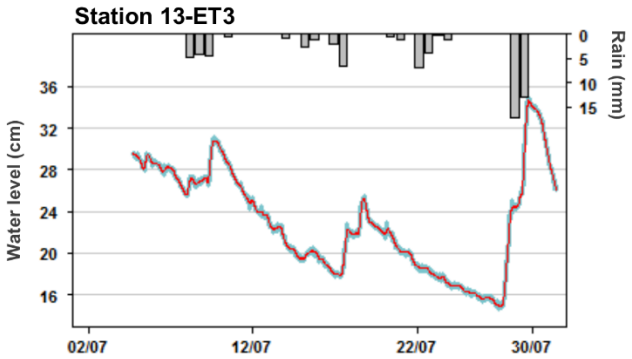
Station 13-ET3
Water level (cm)
Rain (mm)
02/07
12/07
22/07
30/07

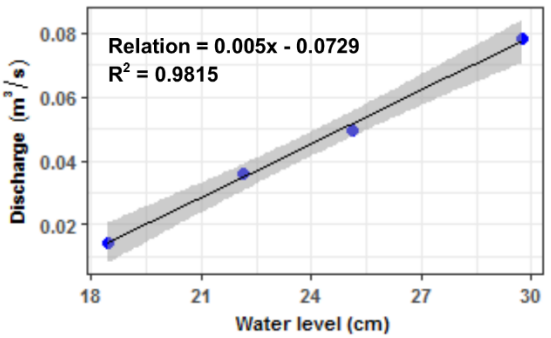
Relation = 0.005x - 0.0729
R² = 0.9815
Discharge (m³/s)
Water level (cm)

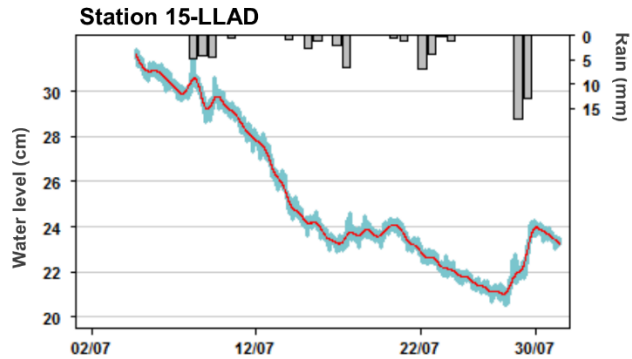
Station 15-LLAD
Water level (cm)
Rain (mm)
02/07
12/07
22/07
30/07

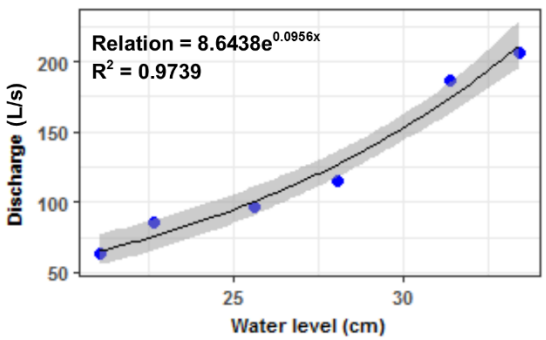
Relation = 8.6438e^0.0956x
R² = 0.9739
Discharge (L/s)
Water level (cm)

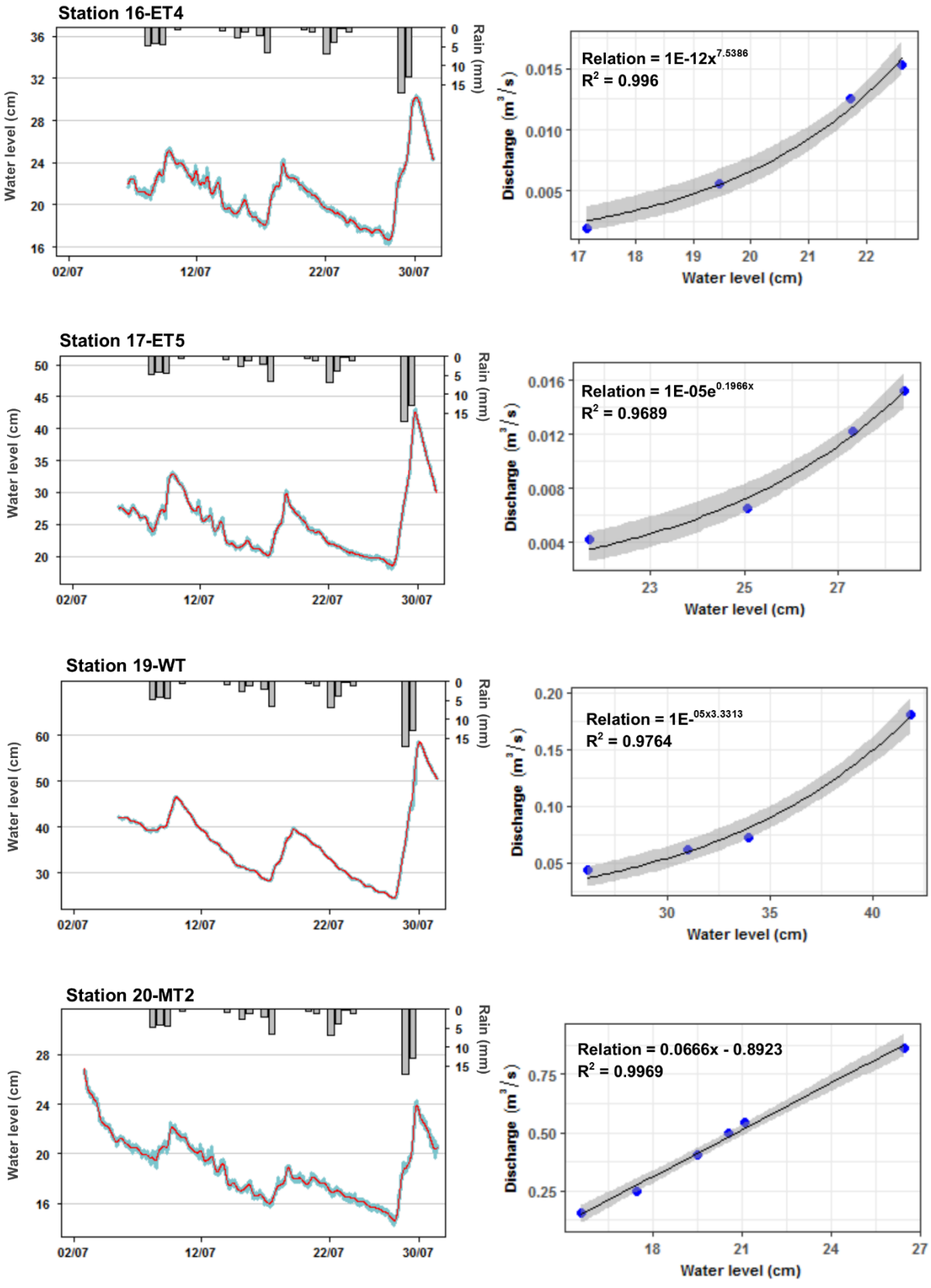
Station 16-ET4
Water level (cm)
Rain (mm)
02/07
12/07
22/07
30/07
Relation = 1E-12x^7.5386
R² = 0.996
Discharge (m³/s)
Water level (cm)
Station 17-ET5
Relation = 1E-05e^0.1966x
R² = 0.9689
Station 19-WT
Relation = 1E-05x3.3313
R² = 0.9764
Station 20-MT2
Relation = 0.0666x - 0.8923
R² = 0.9969

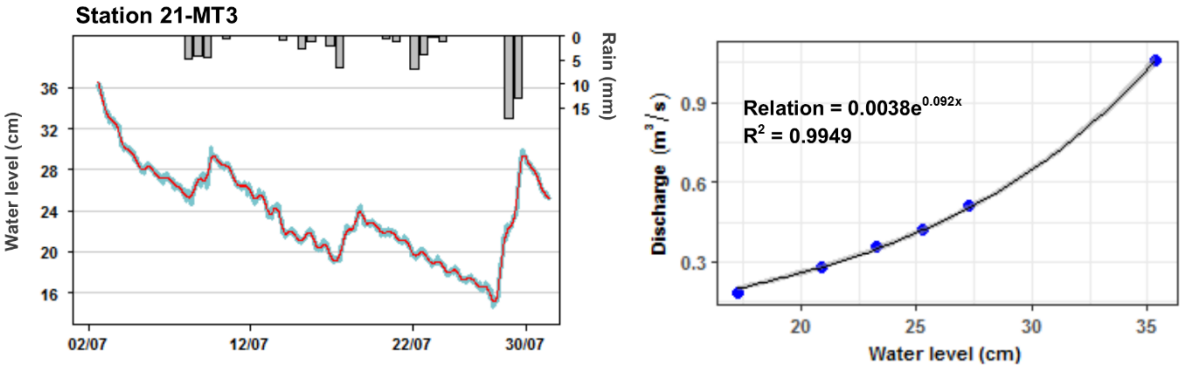
Station 21-MT3
Water level (cm)
Rain (mm)
02/07
12/07
22/07
30/07
Relation = 0.0038e^0.092x
R² = 0.9949
Discharge (m³/s)
Water level (cm)

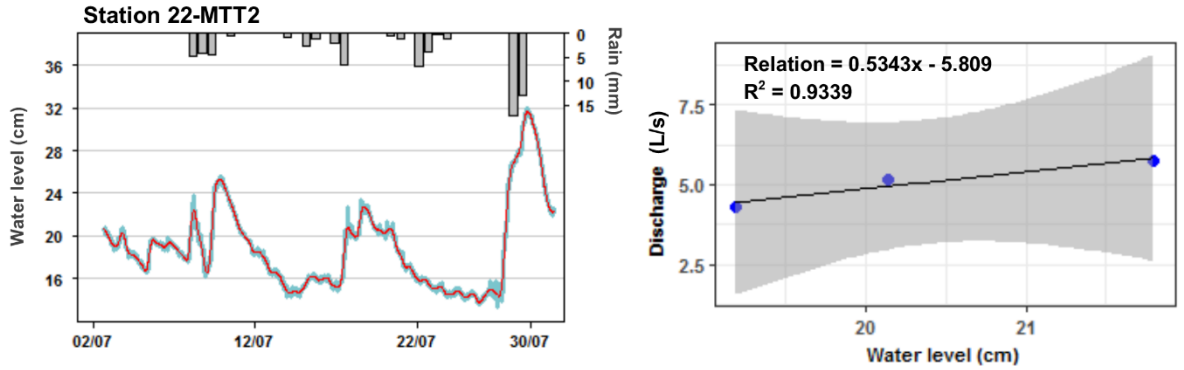
Station 22-MTT2
Water level (cm)
Rain (mm)
02/07
12/07
22/07
30/07
Relation = 0.5343x - 5.809
R² = 0.9339
Discharge (L/s)
Water level (cm)

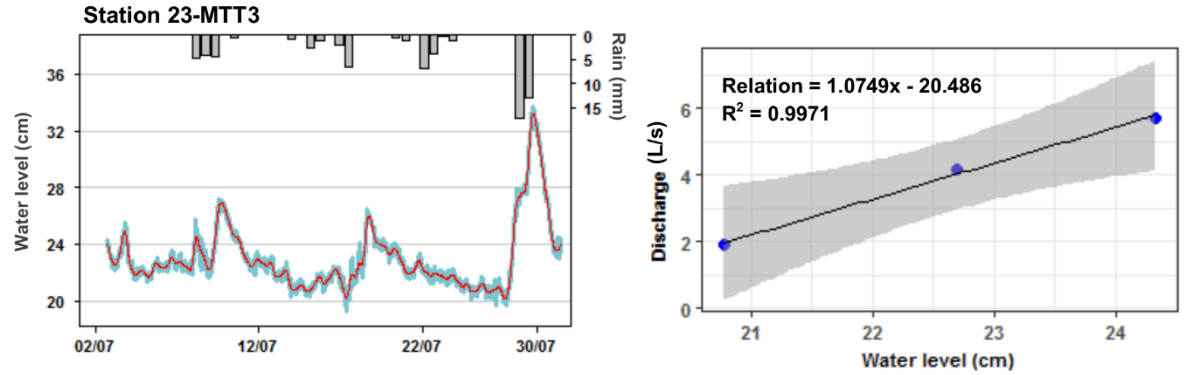
Station 23-MTT3
Water level (cm)
Rain (mm)
02/07
12/07
22/07
30/07
Relation = 1.0749x - 20.486
R² = 0.9971
Discharge (L/s)
Water level (cm)

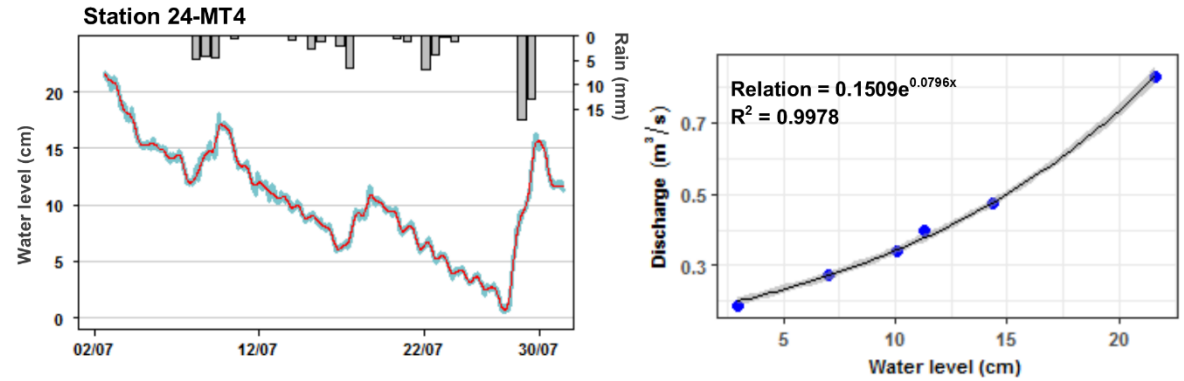
Station 24-MT4
Water level (cm)
Rain (mm)
02/07
12/07
22/07
30/07
Relation = 0.1509e^0.0796x
R² = 0.9978
Discharge (m³/s)
Water level (cm)

Annexe C - Decisions tree for the snow distribution landscape classification

Decision rules from Smith et al. (2016).

The four terrain variables used for the landscape classification were; slope (β), both perspectives of topographic openness at a 25 m radius (O+25 and O-25) and wind shelter index at a 30 m distance (W30). These rules defined three final snow classes: Scour, Drift, and other areas.

Scour was the shallowest class, defined by exposure to wind from all directions – this was selected with the rule: O+25 ≥ 90 °. The spatial pattern of Scours closely matches the distribution of bare rock on ridges and hilltops observed in the field. This class also covers the centres of large lakes, which are usually scoured during winter.

The deepest snow class was named Drift, and is aggregated from 2 subclasses: Catchment and Sheltered Slope. The first subclass was Catchment, defined by topographic enclosure (O-25 > 90 °), which accounts for snow settling in locally enclosed terrain, a phenomenon referred to as the "diffusion effect" by Ohara (2014). The second sub-class is Sheltered Slope. This was aggregated from a Slope subclass, defined by β > 9 ° following Essery and Pomeroy (2004) and Pomeroy (1997), and a Sheltered class, defined by W30 > 0.

The final class corresponds to other areas not assigned to Scour or Drift. These areas are mildly exposed to the wind and act as a source area for blowing snow. Observations in the field suggested that most of the NRW falls under this snow accumulation regime.

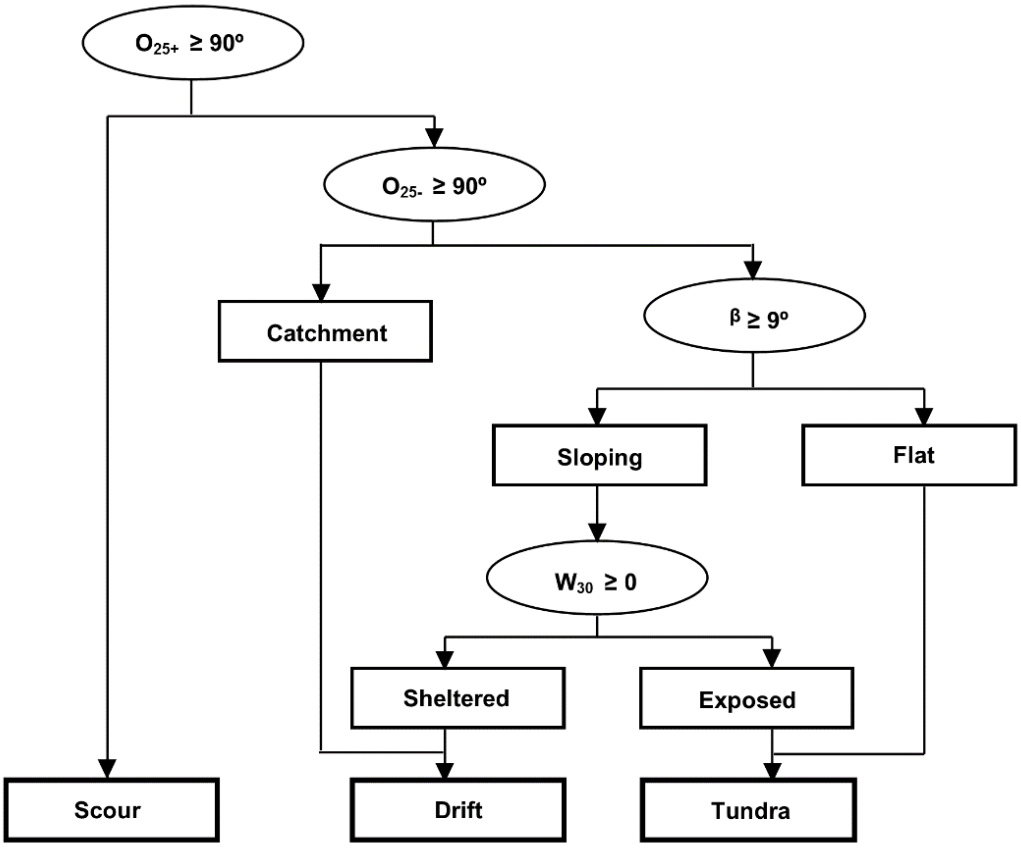

Figure C1: Decision tree for snow distribution classification from landscape characteristics.

Annexe D - Modelling spatial patterns using Asymmetric Eigenfunction Maps (AEM)

Finally, to identify the patterns of similarities or dissimilarities in chemistry among sites we used Asymmetric Eigenvector Maps (AEM). This method allows to compute spatial variables, called AEM eigenfunctions, that represent different patterns of positive or negative correlation among the sites (Blanchet et al., 2008a). The eigenfunctions can be used as explanatory variables in canonical analysis (i.e, RDA, variation partitioning) to investigate which spatial structures better explain the patterns of the response variables under study (Legendre and Legendre, 2012). The computation of AEM eigenfunction required three distinct computation procedures; (i) the generation of a connectivity network, (ii) the matrix representation of the connectivity network and (iii) algebraic computation of eigenvectors.

D1. Generation of connectivity network

The slope gradient is the first processes controlling the movement of water. If water can be lost (i.e., evaporation, hyporheic exchange) or stored (i.e., lake or pond disconnection) along a stream network. However water flows will never be occurred from downstream to upstream, or a least over a significant reach distance. Asymmetric Eigenvector Maps (AEM) is an eigenfunctions based analysis adapted to study such physical structure influenced by a direction process (i.e., flow upstream to downstream). The first step of the AEM analysis is to build a connectivity network among measurements sites (Figure 1). Computation examples will be conducted on a simplified connection network (Figure 1b).

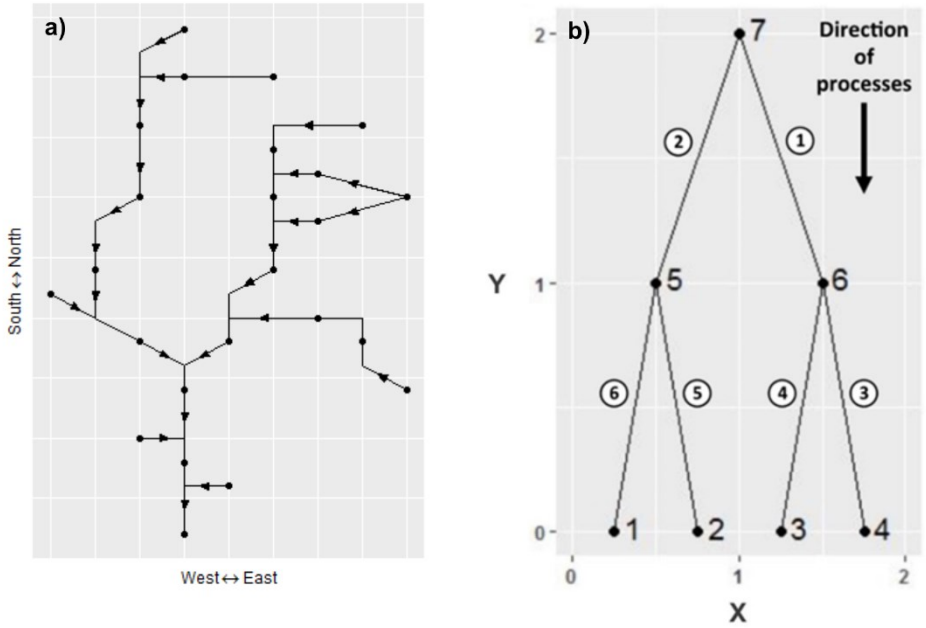

Figure D1: Schematic connexion diagrams showing the possible connexions between sites for a) the sampling sites across the hydrological network of the Niaqunguk River, based on the surface on the flow directions, thus an edge from one site to his surrounding neighbours is only created if they are located downstream and b) for a simplified example of connexions network. Sites and edges between sites are numbered for the next step of the method.

Network consist of edges representing possible connexion between sites. The directionality of connexions in our network is taking into account, by only modelling connexions from upslope and higher site to site located at lower distance upslope (Y) and surface elevation (Z). To simplify the mathematical and visual explanations of the method, examples will be conducted on a simplified connexion network (Figure 1b). For the simplified example, the piezometer 7, located the highest on the Y axis, serve as the origin site, in that sense where all network sites connect to this origin through at least one possible path in the network. In other examples, where multiple sites would be located at similar distance along the Y axis and that lower sites would not be connected to all of these upslope sites, a new origin site (0) can be created to model upslope connectivity through all the networks.

D2. Matrix representation of connectivity network

The network can be coded into two matrixes (i.e., Site-by-edge, From-to) to compute the AEM eigenfunctions and to test the spatial correlation modelled by these variables (Table

D1 and D2). The Site-by-edge matrix is a binary matrix, where the row are the sites of the network and the columns represent the edges number. Values 1 and 0 represent respectively the presence or the absence of connection between sites. The From-to matrix is two columns representing the departure and arrival sites of an edge, this matrix has the same number of rows as the edges in the network. The directionality in the connexions network is represented in both matrixes. Generation of the AEM site-by-edge matrices was done with the function buil.binary() of the R package adespatial (Blanchet et al., 2015).

Table D1: Site-by-edge matrix

		Edges					
		1	**2**	**3**	**4**	**5**	**6**
Sites	**1**	0	1	0	0	1	0
	2	0	1	0	0	0	1
	3	1	0	0	1	0	0
	4	1	0	1	0	0	0
	5	0	1	0	0	0	0
	6	1	0	0	0	0	0
	7	0	0	0	0	0	0

Table D2: From-to matrix

From	To
7	6
7	5
6	4
6	3
5	1
5	2

D3. Computation of Eigenvectors

Three techniques (i.e., PCA, PCoA and SVD) can be used to decompose the site-by-edge matrix (matrix E) into eigenfunctions. The three forms of decomposition produce equivalent AEM spatial eigenfunctions (Legendre et Legendre, 2012). For PCA and SVD methods it's beforehand necessary to centre by columns the matrix E, to produce the matrix Ec. The centring operation change the coordinates of the objects based on a new origin point (0,0).

The centring result from subtracting the column means from the values x in the corresponding columns:

$$Site\ by\ link\ (E) = \begin{bmatrix} x_{11} & x_{12} & x_{1k} \\ x_{21} & x_{22} & x_{2k} \\ x_{i1} & x_{32} & x_{ik} \end{bmatrix} \quad E_c = [x_{ik} - \overline{x_k}\,] = \begin{bmatrix} z_{11} & z_{12} & z_{1k} \\ z_{21} & z_{22} & z_{2k} \\ z_{i1} & z_{32} & z_{ik} \end{bmatrix} \tag{1}$$

$$\begin{bmatrix} 0 & 1 & 0 & 0 & 1 & 0 \\ 0 & 1 & 0 & 0 & 0 & 1 \\ 1 & 0 & 0 & 1 & 0 & 0 \\ 1 & 0 & 1 & 0 & 0 & 0 \\ 0 & 1 & 0 & 0 & 0 & 0 \\ 1 & 0 & 0 & 0 & 0 & 0 \\ 0 & 0 & 0 & 0 & 0 & 0 \end{bmatrix} = \begin{bmatrix} -0.43 & 0.57 & -0.14 & -0.14 & 0.86 & -0.14 \\ -0.43 & 0.57 & -0.14 & -0.14 & -0.14 & 0.86 \\ 0.57 & -0.43 & -0.14 & 0.86 & -0.14 & -0.14 \\ 0.57 & -0.43 & 0.86 & -0.14 & -0.14 & -0.14 \\ -0.43 & 0.57 & -0.14 & -0.14 & -0.14 & -0.14 \\ 0.57 & -0.43 & -0.14 & -0.14 & -0.14 & -0.14 \\ -0.43 & -0.43 & -0.14 & -0.14 & -0.14 & -0.14 \end{bmatrix}$$

The principal component analysis (PCA) allow to compute the relations between objects (in the present example: rows) and descriptors (columns) based on the new created variable, called principal component. The computation of the principal component required a series of operations; starting from the covariance matrix S:

$$\mathrm{S} = \frac{1}{n-1}\, E'_c\, E_c = \begin{bmatrix} 0.29 & -0.21 & 0.10 & 0.10 & -0.07 & -0.07 \\ -0.21 & 0.29 & -0.07 & -0.07 & 0.10 & 0.10 \\ 0.10 & -0.07 & 0.14 & -0.02 & -0.02 & -0.02 \\ 0.10 & -0.07 & -0.02 & 0.14 & -0.02 & -0.02 \\ -0.07 & 0.10 & -0.02 & -0.02 & 0.14 & -0.02 \\ -0.07 & 0.10 & -0.02 & -0.02 & -0.02 & 0.14 \end{bmatrix} \tag{2}$$

it's then possible to compute the eigenvalues (λ):

$$|S - \lambda_k I| = \begin{bmatrix} 0.29 & -0.21 & 0.10 & 0.10 & -0.07 & -0.07 \\ -0.21 & 0.29 & -0.07 & -0.07 & 0.10 & 0.10 \\ 0.10 & -0.07 & 0.14 & -0.02 & -0.02 & -0.02 \\ 0.10 & -0.07 & -0.02 & 0.14 & -0.02 & -0.02 \\ -0.07 & 0.10 & -0.02 & -0.02 & 0.14 & -0.02 \\ -0.07 & 0.10 & -0.02 & -0.02 & -0.02 & 0.14 \end{bmatrix} - \begin{bmatrix} \lambda_1 & 0 & 0 & 0 & 0 & 0 \\ 0 & \lambda_2 & 0 & 0 & 0 & 0 \\ 0 & 0 & \lambda_3 & 0 & 0 & 0 \\ 0 & 0 & 0 & \lambda_4 & 0 & 0 \\ 0 & 0 & 0 & 0 & \lambda_5 & 0 \\ 0 & 0 & 0 & 0 & 0 & \lambda_6 \end{bmatrix} \tag{3}$$

$$\lambda_1 = 0.62 \quad \lambda_2 = 0.17 \quad \lambda_3 = 0.17 \quad \lambda_4 = 0.11 \quad \lambda_5 = 0.04 \quad \lambda_6 = 0.04$$

and the normalized (i.e. scaled to unit length) eigenvectors (U):

$$(S - \lambda_k I)u_k = 0 = \begin{bmatrix} 0.63 & 0.00 & 0.00 & -0.50 & 0.33 & 0.50 \\ -0.63 & 0.00 & 0.00 & -0.50 & -0.33 & 0.50 \\ 0.23 & -0.70 & -0.11 & -0.35 & -0.44 & -0.35 \\ 0.23 & 0.70 & 0.11 & -0.35 & -0.44 & -0.35 \\ -0.23 & 0.11 & -0.70 & -0.35 & 0.44 & -0.35 \\ -0.23 & 0.11 & 0.70 & -0.35 & 0.44 & -0.35 \end{bmatrix} \quad (4)$$

Each eigenvector u_k are computing using corresponding eigenvalue λ_k .The objects principal component matrix (F) is equal to the product between E_c and the eigenvectors matrix U_i;

$$F = E_c U = \begin{bmatrix} -0.72 & 0.18 & 1.13 & 0.45 & -0.37 & 0.27 \\ -0.72 & -0.18 & -1.13 & 0.45 & -0.37 & 0.27 \\ 0.72 & -1.13 & 0.18 & 0.45 & 0.37 & 0.27 \\ 0.72 & 1.13 & -0.18 & 0.45 & 0.37 & 0.27 \\ -0.53 & 0.00 & 0.00 & -0.27 & 1.02 & -0.93 \\ 0.53 & 0.00 & 0.00 & -0.27 & -1.02 & -0.93 \\ 0.00 & 0.00 & 0.00 & -1.29 & 0.00 & 0.77 \end{bmatrix} \quad (5)$$

The principal component in Q-mode (rows are the object) represents the relation between the objects or in the present example the sites, for which positive and negative site values are representing different spatial patterns. Note that it's also possible the compute identical eigenfunctions obtained through PCA using the rescaled eigenvector matrix produced by a Principal Coordinates Analysis (PCoA).

Equivalent but not identical eigenfunctions can also be computed from a Singular Value Decomposition (SVD) of the matrix E_c. Computation of eigenfunction through the SVD method for matrix E_c decomposition operates according to this algorithm:

$$E_c(nxp) = V(nxk) * D\ (kxk) * U'(kxp) \quad (6)$$

$$\begin{bmatrix} -0.43 & 0.57 & -0.14 & -0.14 & 0.86 & -0.14 \\ -0.43 & 0.57 & -0.14 & -0.14 & -0.14 & 0.86 \\ 0.57 & -0.43 & -0.14 & 0.86 & -0.14 & -0.14 \\ 0.57 & -0.43 & 0.86 & -0.14 & -0.14 & -0.14 \\ -0.43 & 0.57 & -0.14 & -0.14 & -0.14 & -0.14 \\ 0.57 & -0.43 & -0.14 & -0.14 & -0.14 & -0.14 \\ -0.43 & -0.43 & -0.14 & -0.14 & -0.14 & -0.14 \end{bmatrix} = \begin{bmatrix} -0.44 & 0.11 & 0.70 & 0.28 & -0.23 & 0.17 \\ -0.44 & -0.11 & -0.70 & 0.28 & -0.23 & 0.17 \\ 0.44 & -0.70 & 0.11 & 0.28 & 0.23 & 0.17 \\ 0.44 & 0.70 & -0.11 & 0.28 & 0.23 & 0.17 \\ -0.33 & 0.00 & 0.00 & -0.16 & 0.63 & -0.57 \\ 0.33 & 0.00 & 0.00 & -0.16 & -0.63 & -0.57 \\ 0.00 & 0.00 & 0.00 & -0.79 & 0.00 & 0.48 \end{bmatrix} *$$

$$\begin{bmatrix} 1.93 & 0.00 & 0.00 & 0.00 & 0.00 & 0.00 \\ 0.00 & 1.00 & 0.00 & 0.00 & 0.00 & 0.00 \\ 0.00 & 0.00 & 1.00 & 0.00 & 0.00 & 0.00 \\ 0.00 & 0.00 & 0.00 & 0.79 & 0.00 & 0.00 \\ 0.00 & 0.00 & 0.00 & 0.00 & 0.52 & 0.00 \\ 0.00 & 0.00 & 0.00 & 0.00 & 0.00 & 0.48 \end{bmatrix} * \begin{bmatrix} 0.63 & 0.00 & 0.00 & 0.50 & -0.33 & -0.50 \\ -0.63 & 0.00 & 0.00 & 0.50 & 0.33 & -0.50 \\ 0.23 & 0.70 & -0.11 & 0.35 & 0.44 & 0.35 \\ 0.23 & -0.70 & 0.11 & 0.35 & 0.44 & 0.35 \\ -0.23 & 0.11 & 0.70 & 0.35 & -0.44 & 0.35 \\ -0.23 & -0.11 & 0.70 & 0.35 & -0.44 & 0.35 \end{bmatrix}$$

Where E_c is the centred site-by-link (where n < p), U' and V are orthonormal matrices (i.e., matrices containing column vectors that are normalized and orthogonal to one another), k is the minimum number of rows (n) or column (p) of the rectangular matrix E_{center} (n < p so k = n), D is a diagonal matrix containing singular values (Legendre and Legendre, 2012). Matrix V contain n eigenvectors (e.g., AEM eigenfunctions) and each vector can be used as spatial explanatory variable for further analysis of the water level variation. Produced eigenfunction by PCA or SVD can be used interchangeably as the explanatory matrix in the next step of the analysis because they only differ by the scaling of their vectors. Bubble maps can be used for visual representation of the spatial structure of computed eigenfunctions (vectors 1 to 6 of matrix F and V) (Figure 2). Black and white points, as well as the size of point in bubble maps can be used to represent patterns of positive or negative spatial correlation among sites. Principal component analysis were performed with the function *rda()* from the R package *vegan* (Oksanen et al., 2017), Principal Coordinates Analysis can be accomplished using the function *dudi.pco()* of the *ade4* package (Chessel and Dufour, 2004) and Singular value decomposition were performed with the function *svd()* of the *base* package (R Core Team, 2016).

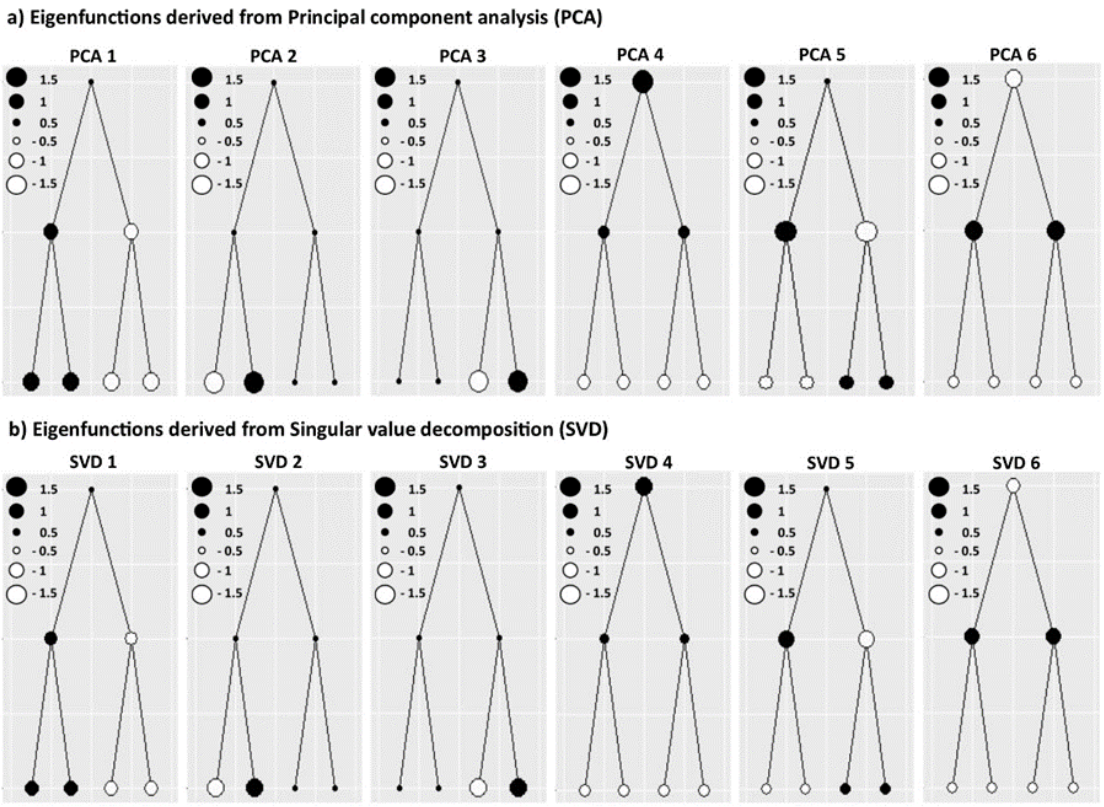

Figure D2: Maps of Eigenfunctions derived from a) Principal component analysis (PCA) and b) Singular value decomposition (SVD). The sets of eigenfunction are equivalent and only differ by the scaling their values.

D4. Moran's I coefficients

Morans's I coefficient allow to investigate the spatial correlation (Moran's spatial correlation's statistic) among sites in a 2-dimension spatial structure. The equation of Moran's coefficients involves the computation of a distance matrix (D) among sites for which weights can be applied to produce a weighting matrix (W) and simulate resistance between sites. Moran's formula is an adapted version of the Pearson correlation coefficient, using the similarity or covariance between sites (h, i) and the maximum-likelihood estimator of the sample variance (i) (Legendre et Legendre, 2012). Values of Moran's I coefficient can be compared to an expected I value under the hypothesis of absence of spatial correlation ($-\frac{1}{n-1}$). Higher values are associated with positive spatial correlation, while lower I coefficient values to negative correlations (Blanchet et al., 2008b). Moran's I coefficients are a more global

measurement and sensitive to extreme values, it's well adapted to determine if eigenfunction are globally modelling positive or negative spatial correlation in the connexion network. Moran's I coefficient can be computed for each eigenfunctions (vectors) derived from the site-by-edges matrix of a connexion diagram.

$$I = \frac{\frac{1}{W}\sum_{h=1}^{n}\sum_{i=1}^{n} w_{hi}(y_h-\bar{y})(y_i-\bar{y})}{\frac{1}{n}\sum_{i=1}^{n}(y_i-\bar{y})^2} \quad (7)$$

y_h and y_i are the are the values of the eigenfunction at sites h and i. w_{hi} is the weights that can be applied on the connexion between h and i. n is the number of sites where y was measured. W is the sum of element w_{hi}, here no weights have been applied ($w_{hi} = 0$) between sites, instead we used the From-to matrix to compute the Moran's coefficient based only on the similarity between connected sites. For the present example, Moran's I coefficient of eigenfunctions 1 to 4 are associated to positive spatial correlation, whereas eigenfunctions 5 and 6 are modelling negative spatial correlation since there values are lower than the expected Moran's value (i.e., 0.17) with absence of correlation (Figure 3). Moran's I coefficients were computed with the function *moran.I.multi()* of the R package *AEM* (Blanchet et al., 2015).

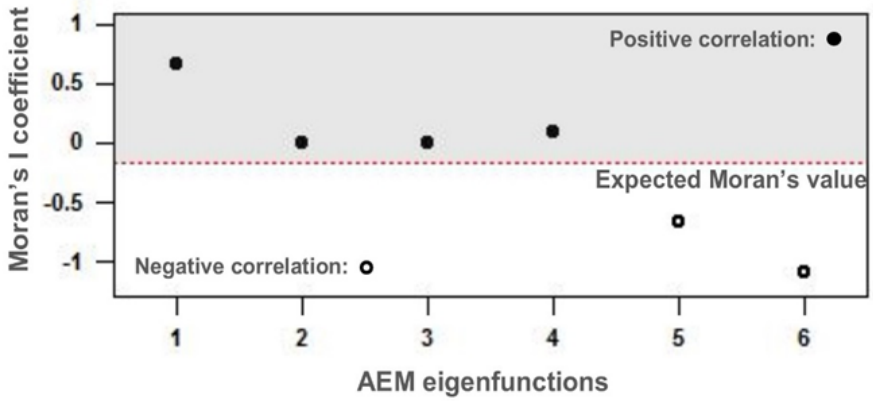

Figure D3: Plots of the expected Moran's I coefficient computed for each eigenfunction. The dashed red line represent the expected Moran's value under the hypothesis of absence of spatial correlation ($-\frac{1}{n-1}$). AEM eigenfunctions with Moran's coefficient higher than the Moran's value are associated to a positive spatial correlation, while eigenfunctions with Moran's coefficient lower than the expected value to negative spatial correlation.

D5. Canonical analysis

The last stage of our analytical procedure was to use the produced eigenfunctions as well as landscape indexes computed for each site, as explanatory variables in canonical analysis to investigate the variance of the variable under study (here: water chemistry at each sampling sites). Prior to canonical analysis, we used the forward selection procedure, using cutoff level of $alpha = 0.05$, to select only significant explanatory variables (i.e., landscape indexes) and therefore create a more parsimonious model to explain the studied variable (Blanchet et al., 2008a) all AEM eigenfunction were used. The forward selection is based on the total explained variance (adjusted canonical R^2_a) and the statistical significance ($alpha$), tested using permutations (i.e., 999 permutations), of the model of explanatory variables after the stepwise addition of variables. For our purpose (i.e., description) the primary interest is to correctly estimate the parameters of the model; the effect of collinearity between added variables must then be minimized. Collinearity is not a problem for eigenfunctions since they are derived from SVD and are uncorrelated one to another. We assessed the possible collinearity between environmental proxies by computing the variance inflation factors (VIF) for each explanatory variable, which is done by the regression of variable i, in turn, on all the other variables in the group. Variables with high VIF (>5) were removed from the analysis.

Here we studied the water chemical (i.e., SpC, DOC, $\delta^{18}O$, Mg^{2+}) variation among 24 sampling sites. Simple redundancy analysis (RDA) can be first used to investigate the proportion of chemical variance explained by the AEM eigenfunctions based on the asymmetric relation between the response variables (Y) and the explanatory variables (X) matrixes. RDA allow to find those components of Y which are linear combinations of X and represent as much variance of Y as possible (Legendre and Legendre, 2012). RDA analysis involves two computational steps; (i) multivariate linear regression of Y on X to produce a matrix of fitted values ($\hat{Y}$);

$$\hat{Y} = X\,[X'X]^{-1}X'Y \tag{9}$$

Here $[X'X]^{-1}X'Y$ result in a matrix of regression coefficients, which are the same as those obtained from multiple regressions computed in separate runs for each column of Y. Fitted values $\hat{Y}$ are therefore computed from the product between the regression coefficient and the explanatory variables matrix (X). The second step, (ii) consist on a principal component analysis (PCA) of matrix $\hat{Y}$. PCA of matrix $\hat{Y}$ produced eigenvalues and eigenvectors (equations 3 and 4 respectively) from which its possible to compute the ordination object or sites fitted scores (equation 5). The sites ordination scores result from the combination of explanatory variables and are equivalent to the fitted values of a multiple linear regression. The strength of the linear relationship between Y and X (i.e., canonical R^2 or multivariate redundancy statistic and the adjusted form R^2_a) and the statistical significance of the regression model can be tested using these following equations (Legendre et al., 2011);

$$R^2_{x|y} = \frac{SS\,(\hat{Y})}{SS\,(Y)} \tag{10}$$

where $R^2_{x|y}$ is the multivariate statistic and indication the proportion of Y variation explained by the regression on X, $SS\,(\hat{Y})$ is the total sum of square (or sum of squared deviations from the means) of and SS(Y) is the total sum of squares of Y. The adjusted multivariate redundancy statistic (or adjusted canonical R^2_a) is obtained from the classical Ezekiel (1930) formula:

$$R^2_a = 1 - (1 - R^2_{x|y})\,\frac{(n-1)}{(n-m-1)} \tag{11}$$

where m is the number of explanatory variables in X or, more precisely, the rank of the variance-covariance matrix of X. Since the WLV matrix wasn't standardized prior to RDA to preserve the effect of absence of water levels variation, we performed permutation tests to determine the statistical significance of the RDA's model. Permutation test uses a modified version of the F-statistic for overall significance, by removing the amount of response variables of the non- standardize matrix Y. The resulting equation is:

$$F = \frac{R^2_{x|y}/m}{(1-R^2_{x|y})/(n-m-1)} \quad (12)$$

The produced F statistic from the division of the sum of all canonical eigenvalues ($R^2_{x|y}$) by the residual sum of square ($1 - R^2_{x|y}$) allow to determine if the linear relationship between the response matrix and the explanatory matrix is significant (i.e., rejection of H_0). n and m are respectively the number of object and the number of explanatory variables. To evaluate the individual contribution (R^2) of each environmental proxy (m) containing in matrix X, we performed m separated canonical analysis.

Since landscape indexes give some insights of the processes controlling the chemical patterns among sampling sites (from the degrees of spatial correlation) they can be used as second set of explanatory variables (W) to investigate a which scale the landscape index 1 (X) is explaining the chemical variation matrix (Y). This is done by partitioning the variation (i.e., variation partitioning) into the matrix X and W. Starting from a Venn diagram (Figure 5) summarizing the component of the variation partitioning, there is the steps involves to determine the variation of Y commonly explained by X and W (Legendre and Legendre, 2012, p.571).

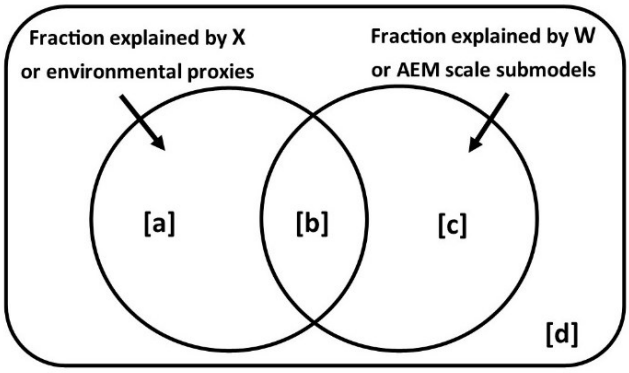

Figure D4: Example of a Venn diagram showing the different fraction of variance a responses variable or matrix computed in variation partitioning.

The global $[a + b + c]$ and individual ($[a + b], [b + c]$) fractions of explained variance (R^2_a) are first obtain from the regression of Y on the matrix X and W. (ii) The fraction [a] and [b] are simply derived from the following subtractions, using the R^2_a values;

$$[a] = [a + b + c] - [b + c] \qquad and \qquad [c] = [a + b + c] - [a + b] \tag{13}$$

and correspond to the fraction of Y variance uniquely explained by each of the selected landscape indexes. The fraction [b] is the intersection between X and W or common fraction of Y variance explained by the two set of variables. Fraction [b] is also found by the subtraction of R_a^2 values;

$$[b] = [a + b] + [b + c] - [a + b + c] \quad or \quad [a + b] - [a] \quad or \quad [b + c] - [c] \tag{14}$$

Important fraction [b] can be used to identify the proportion explained by the the first landscape index, however fraction [b] cannot be tested for significance. [b] is the unexplained variance obtained from one minus the global fraction of explained variance. Canonical redundancy analysis (RDA) were performed with the function rda() and variation partitioning with the function varpart(), both from the R package vegan (Oksanen et al., 2017).

Annexe E - Watershed scale maps of the computed landscape indices

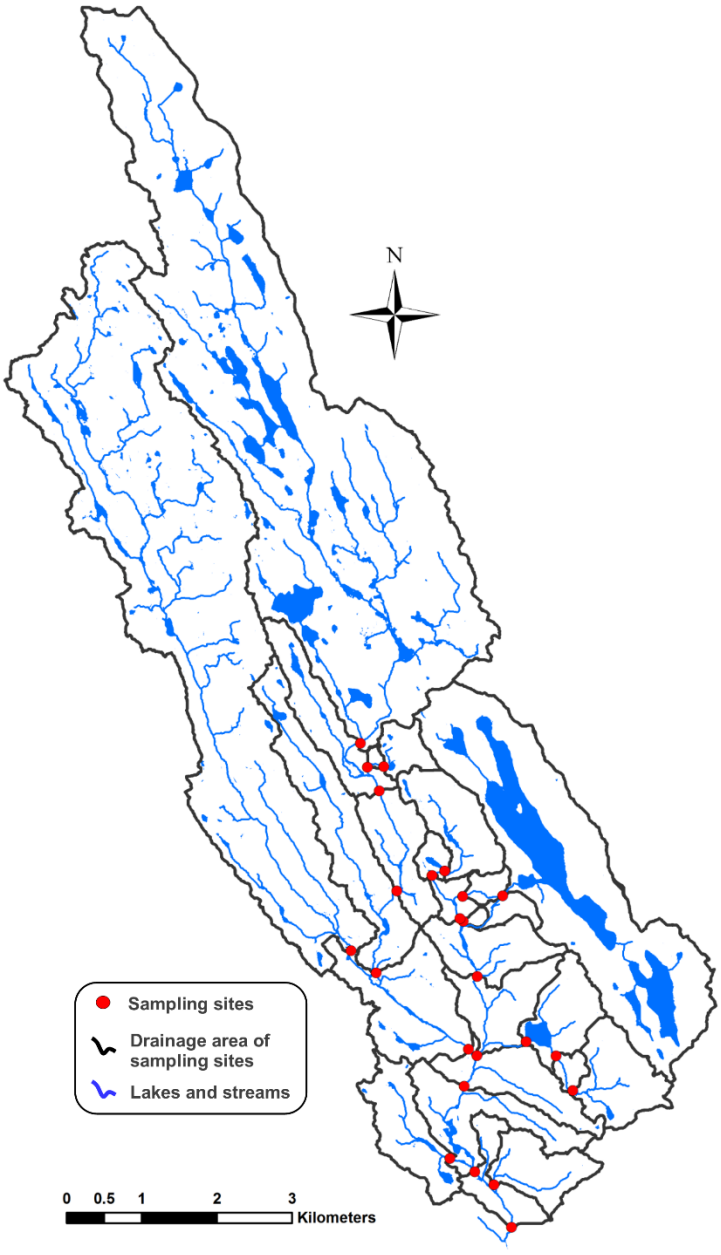

Figure E1 : Drainage area, streams and lake areas used to compute the drainage area (DA), proportion or lake areas (LAKE) and drainage density (DD) indexes.

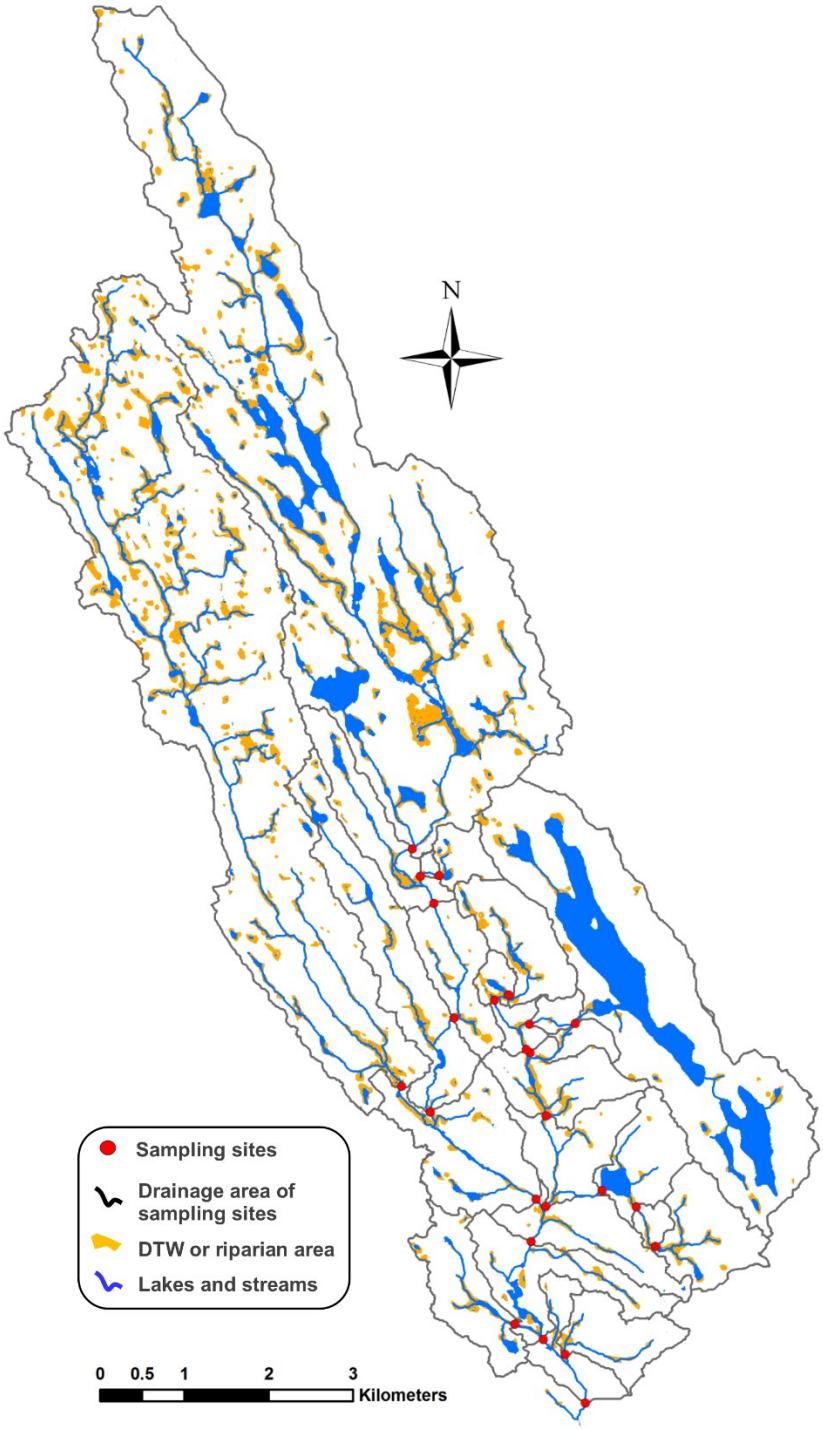

Figure E2 : Computed DTW areas representing the extend of the riparian areas within the drained area of each sampling site.

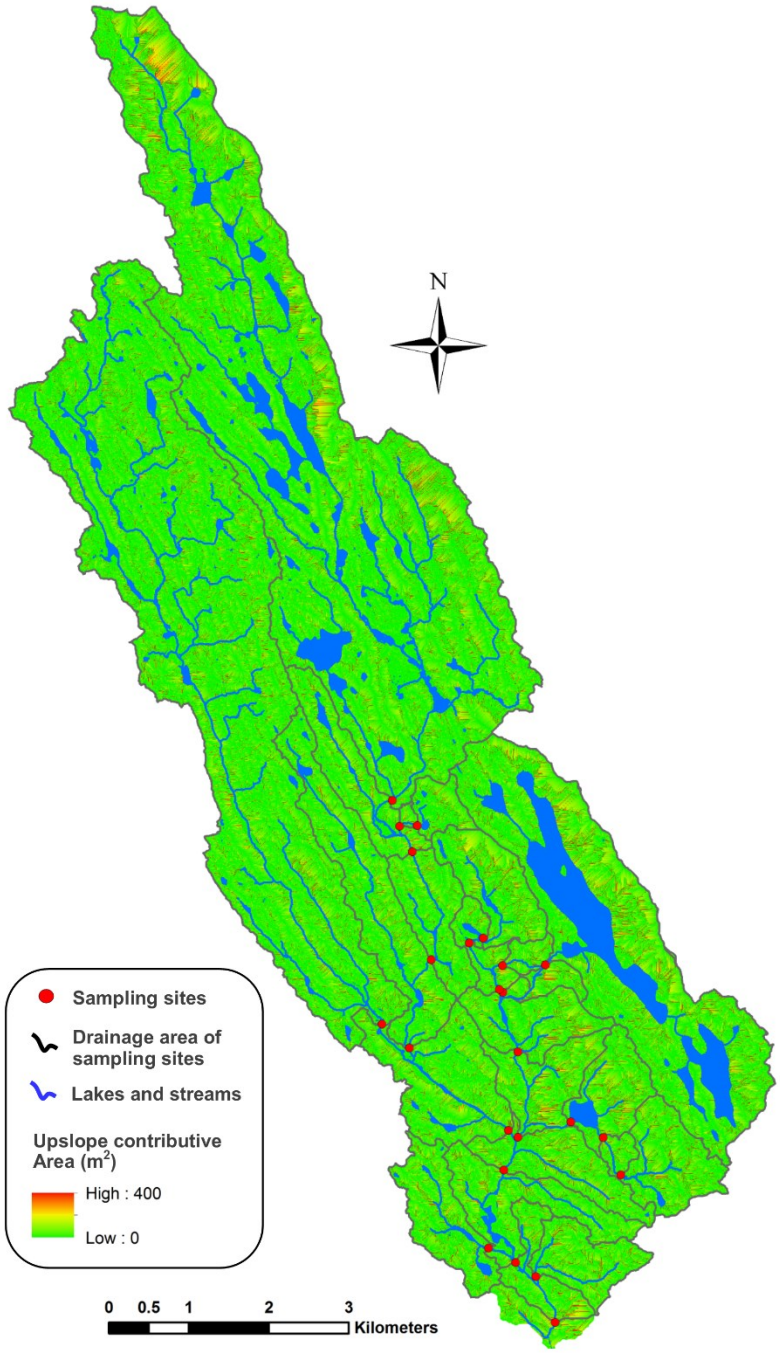

Figure E3 : Upslope contributive area (UCA) model used to compute the average UCA value within the riparian area of each sampled site.

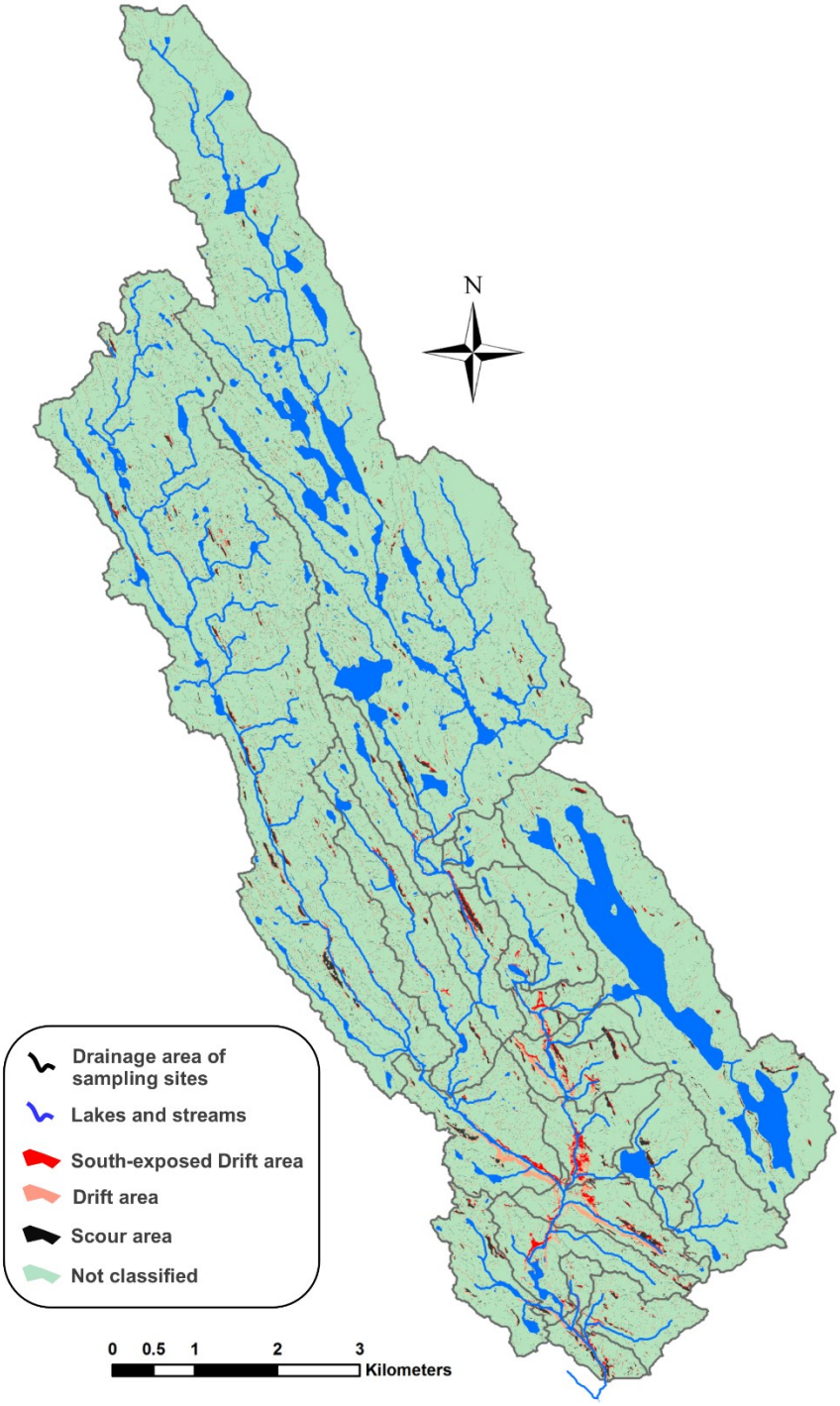

Figure E4 : Results of the landscape classification for snow distribution within the Niaqunguk watershed used to compute the South-Exposed drift areas.